EXPERIMENTAL INVESTIGATION OF R134A FLOW IN A 1.65 MM COPPER MINITUBE

BİLGEHAN TEKİN

FEBRUARY 2011

EXPERIMENTAL INVESTIGATION OF R134A FLOW IN A 1.65 MM COPPER MINITUBE

A THESIS SUBMITTED TO
THE GRADUATE SCHOOL OF NATURAL AND APPLIED SCIENCES
OF
MIDDLE EAST TECHNICAL UNIVERSITY

BY

BİLGEHAN TEKİN

IN PARTIAL FULFILLMENT OF THE REQUIREMENTS
FOR
THE DEGREE OF MASTER OF SCIENCE
IN
MECHANICAL ENGINEERING

FEBRUARY 2011

Approval of the thesis:

EXPERIMENTAL INVESTIGATION OF R134A FLOW IN A 1.65 MM COPPER MINITUBE

Submitted by **BİLGEHAN TEKİN** in partial fulfillment of the requirements for the degree of **Master of Science in Mechanical Engineering Department, Middle East Technical University** by,

Prof. Dr. Canan Özgen
Dean, Graduate School of **Natural and Applied Sciences** _____

Prof. Dr. Suha Oral
Head of Department, **Mechanical Engineering** _____

Assoc. Prof. Dr. Almıla Güvenç Yazıcıoğlu
Supervisor, **Mechanical Engineering Dept., METU** _____

Prof. Dr. Sadık Kakaç
Co-Supervisor, **Mechanical Engineering Dept., TOBB ETU** _____

Examining Committee Members:

Prof. Dr. Rüknettin Oskay
Mechanical Engineering Dept., METU _____

Assoc. Prof. Dr. Almıla Güvenç Yazıcıoğlu
Mechanical Engineering Dept., METU _____

Prof. Dr. Sadık Kakaç
Mechanical Engineering Dept., TOBB ETU _____

Assoc. Prof. Dr. Derek Baker
Mechanical Engineering Dept., METU _____

Dr. Hüsnü Kerpiççi
Research & Development Expert, Arçelik _____

Date: **04.02.2011**

I hereby declare that all information in this document has been obtained and presented in accordance with academic rules and ethical conduct. I also declare that, as required by these rules and conduct, I have fully cited and referenced all material and results that are not original to this work.

Name, Last name : Bilgehan Tekin

Signature :

ABSTRACT

EXPERIMENTAL INVESTIGATION OF R134A FLOW IN A 1.65 MM COPPER MINITUBE

Tekin, Bilgehan

M.Sc., Department of Mechanical Engineering

Supervisor : Assoc. Prof. Dr. Almıla G. Yazıcıoğlu

Co-supervisor : Prof. Dr. Sadık Kakaç

February 2011, 154 pages

This thesis investigates the refrigerant (R-134a) flow in a minitube experimentally. The small scale heat transfer is a relatively new research area and has been in favor since the end of 1970's. Refrigerant flow in mini- and microscale media is a potential enhancement factor for refrigeration technology in the future. For the forthcoming developments and progresses, experimental studies are invaluable in terms of having an insight and contributing to the establishment of infrastructure in the field in addition to leading the numerical and theoretical approaches. The studies in the literature show that low mass flow rate and constant wall temperature approach in minitubes and minichannels were not among the main areas of interest. Therefore, an experimental set-up was prepared in order to perform experiments of two-phase refrigerant flow in a 1.65 mm diameter copper minitube with the constant wall temperature approach. The design, preparation, and modifications of the experimental set-up are explained in this thesis. Two-phase flow and quality arrangements were done by pre-heating the refrigerant at saturation pressure and the constant wall temperature was achieved by a secondary cycle with water and ethylene glycol mixture as the working fluid. The heat transfer coefficient and the pressure drop for the two-phase flow with varying quality values and saturation temperatures of the refrigerant were calculated and compared with the results available in literature.

Keywords: Minichannels, forced convection heat transfer, R134a, two-phase flow, experimental study.

ÖZ

1.65 MM'LİK BİR MİNİBORUDA R134A AKIŞININ DENEYSEL OLARAK İNCELENMESİ

Tekin, Bilgehan
Yüksek Lisans, Makina Mühendisliği Bölümü
Tez Yöneticisi : Doç. Dr. Almıla G. Yazıcıoğlu
Ortak Tez Yöneticisi : Prof. Dr. Sadık Kakaç

Şubat 2011, 154 Sayfa

Bu tez bir miniboruda soğutkan (R-134a) akışını deneysel olarak incelemektedir. Küçük ölçeklerdeki ısı transferi göreceli olarak yeni bir araştırma alanıdır ve 1970'lerin sonlarından bu yana revaçtadır. Mini ve mikro ölçeklerdeki soğutkan akışı soğutma teknolojisinin geleceği için potansiyel bir iyileştirme faktörüdür. Yaklaşan belli gelişme ve ilerlemeler için, nümerik ve teorik çalışmalara öncülük etmesinin yanı sıra konunun iç yüzünün anlaşılması ve alandaki altyapının kurulumuna katkıda bulunulması konularında deneysel çalışmalar çok değerlidir. Literatürdeki çalışmalar göstermektedir ki miniboru ve minikanallardaki düşük debi ve sabit duvar sıcaklığı yaklaşımı genel ilgi alanları arasında değildir. Bu sebeple, 1.65 mm çaplı bakır miniborudaki iki fazlı soğutkan akışının sabit duvar sıcaklığı yaklaşımıyla deneylerinin yapılması için bir deney düzeneği hazırlanmıştır. Deney düzeneğinin tasarımı, hazırlığı ve yapılan değişiklikleri bu tezde açıklanmaktadır. İki fazlı akış ve kuruluk dereceleri ayarlamaları doyma basıncındaki soğutkanın ön ısıtıcıyla ısıtılmasıyla olmuş, sabit duvar sıcaklığı yaklaşımı su etilen glikol karışımı kullanılan ikincil bir çevrimle sağlanmıştır. Soğutkanın değişen kuruluk dereceleri ve doyma sıcaklıkları için iki fazlı akışta ısı transfer katsayısı ve basınç düşmesi hesaplanmış ve literatürdeki sonuçlarla karşılaştırılmıştır.

Anahtar kelimeler: Minikanallar, zorlanmış konveksiyonla ısı transferi, R134a, iki fazlı akış, deneysel çalışma.

To My Parents

ACKNOWLEDGEMENTS

The author wants to express his sincere gratitude and appreciation to his supervisor Assoc. Prof. Dr. Almıla G. Yazıcıoğlu and co-supervisor Prof. Dr. Sadık Kakaç for their guidance, advices, constructive criticism, encouragements and perception throughout the research.

The author would also like to thank Dr. Hüsnü Kerpiççi, Mr. Aydın Çelik and Mr. Yiğit Ata Ağartan for their support, suggestions and comments.

The technical assistance of Mr. Mustafa Yalçın and Mr. Fikri Çavuşoğlu are gratefully acknowledged.

This study was supported by The Scientific and Technological Research Council of Turkey (TÜBİTAK) Project No. 107M504, in which Arçelik provided technical and informative support as a project partner.

TABLE OF CONTENTS

ABSTRACT iv
ÖZ v
ACKNOWLEDGEMENTS vii
TABLE OF CONTENTS viii
LIST OF TABLES xii
LIST OF FIGURES xv
LIST OF SYMBOLS xviii
CHAPTERS
1. INTRODUCTION 1
1.1 DOMESTIC COOLING AND EVAPORATORS 1
1.2 MICRO- AND MINICHANNEL HEAT TRANSFER 3
1.3 MOTIVATION AND OBJECTIVES 17
2. EXPERIMENTAL SET-UP 19
2.1 MAIN THEORY OF THE INVESTIGATION 19
2.2 DESIGN OF THE SET-UP 22
2.2.1 Constant Wall Temperature 26
2.2.2 Counter Flow Heat Exchanger 26
2.3 EQUIPMENT 26
2.4 PREPARATION OF THE SET-UP 29
2.4.1 Structural Frame 30
2.4.2 Data Acquisition 32
2.4.3 Refrigerant (R-134a) Cycle 34
2.4.4 Water (Water + Ethylene Glycol Mixture) Cycle 42
2.4.5 Test Section 46
2.4.6 The Leakage and Preliminary Tests for the Initial Design 48
2.4.6.1 The Leakage Tests 48
2.4.6.2 Data Acquisition Process and Preliminary Tests 49
2.5 MODIFICATIONS 52

2.5.1 Ring and Bumper Design for the Glass Tube 53
2.5.2 Leakage Tests for the Glass Tube..... 56
2.5.3 Copper Tube as a Replacement for Glass Tube..... 58
2.6 CALIBRATIONS..... 60
2.6.1 RTD and Thermocouple Calibrations 61
2.6.2 Transducer Calibrations 61
2.6.3 Heater Loss Calibrations 63
2.6.4 Test Section Loss Calibrations 67
3. TWO-PHASE FLOW EXPERIMENTS 75
3.1 APPROACH..... 75
3.2 CONDITIONS 76
3.3 FLOW ORDER 80
3.4 DATA ANALYSIS..... 82
3.5 CALCULATIONS 83
3.5.1 Experimental Calculations..... 84
3.5.2 Calculations with Correlations in Literature..... 86
3.5.2.1 Güngör and Winterton Correlation..... 87
3.5.2.2 Chen Correlation 88
3.5.2.3 Bertsch Correlation 89
4. EXPERIMENTAL RESULTS AND DISCUSSION 91
4.1 HEAT TRANSFER COEFFICIENT 92
4.1.1 Constant Quality Results of the Experiments 92
4.1.2 Constant Mass Flux Results of the Experiments 95
4.1.3 Comparison with Literature 99
4.2 PRESSURE DROP..... 107
5. CONCLUSIONS 110
5.1 SUMMARY AND CONCLUSIONS 110
5.2 SUGGESTIONS FOR FUTURE WORK..... 111
REFERENCES 112
APPENDICES 117
A. THE SPECIFICATIONS OF THE DEVICES IN THE EXPERIMENTAL SET-UP 117
A.1 Refrigerated Circulating Bath..... 117
A.2 Digital Gear Pump System 118

A.3 Micro Flow-meter 119
A.4 Glass Tube 120
A.5 Compact Pressure Transducer 120
A.6 RTD Probe 121
A.7 Thermocouple Wire 121
A.8 Rotameter 122
A.9 Differential Pressure Transducer 122
A.10 DC Power Supply 123
A.11 Data Acquisition System 124
B. SKETCH OF THE EXPERIMENTAL SET-UP IN PRELIMINARY DESIGN 125
C. CONNECTIONS OF EXPERIMENTAL SET-UP IN PRELIMINARY DESIGN 126
D. THE TECHNICAL DRAWINGS OF THE PARTS IN THE TEST SECTION 129
D.1 Technical drawing for the flange 129
D.2 Technical drawing for the shell 130
D.3 Technical drawings of the Ring and the Bumper 131
E. THE CALIBRATION TABLES AND GRAPHS FOR MEASUREMENT DEVICES 132
E.1 A sample calibration curve for a calibrated RTD 132
E.2 The calibration results for the CPTs 133
E.3 The calibration curve for the CPT 1 134
E.4 The calibration curve for the CPT 2 134
E.5 The calibration results for the DPT 135
E.6 The calibration curve for the DPT 135
F. THE WATER ETHYLENE GLYCOL 1:1 VOLUMETRIC MIXTURE PROPERTIES 136
F.1 Specific Gravity of the mixture 136
F.2 Specific Heat of the mixture 137
F.3 Dynamic Viscosity of the mixture 138
F.4 Conductivity of the mixture 139
G. THE REFRIGERANT (R-134A) PROPERTIES 140
G.1 Viscosity (liquid) of the refrigerant 140

G.2 Viscosity (gas) of the refrigerant 141
G.3 Conductivity (liquid) of the refrigerant 142
G.4 Conductivity (gas) of the refrigerant 143
G.5 Prandtl number (liquid) of the refrigerant 144
G.6 Prandtl number (gas) of the refrigerant 145
G.7 Surface tension of the refrigerant 146
G.8 Specific heat (liquid) of the refrigerant 147
H. THE RESULTS FOR A TWO-PHASE EXPERIMENT 149
H.1 The Geometry of Both Sides 149
H.2 Test Conditions for the Experiment 150
H.3 Refrigerant Experiment States 151
H.4 Water side properties 151
H.5 Refrigerant Experimental Calculations 152
H.6 Refrigerant Calculations of the Correlations in the Literature 153
H.7 Experimental Results and Results of the Correlations in the Literature 154

LIST OF TABLES

TABLES

Table 1 The states for the calibrations of pre-heater 65
Table 2 The pre-heater calibration curve values 66
Table 3 Water side geometrical constraints 69
Table 4 Viscous heating experimental values 70
Table 5 The water side geometry for heat loss calculations 73
Table 6 The results for the maximum heat loss to the surroundings..... 74
Table 7 The refrigerant conditions for the test section in two-phase flow 77
Table 8 The average refrigerant parameters for the two-phase experiments 78
Table 9 The water side parameters range for two-phase flow experiments..... 78
Table 10 The pre-heater and the test section heat transfer rates for two-phase experiments 79
Table 11 Flow order part 1: from computer start-up to refrigerant pump start-up 80
Table 12 Flow order part 2: from refrigerant pump start-up until the end..... 81
Table 13 The refrigerant side geometry in the test section..... 83
Table 14 Heat transfer coefficient dependence on saturation pressure for constant refrigerant quality..... 93
Table 15 Heat transfer coefficient dependence on mass flux for constant refrigerant quality 94
Table 16 Heat transfer coefficient dependence on saturation pressure for constant refrigerant mass flux 96
Table 17 Heat transfer coefficient dependence on quality for constant refrigerant mass flux 98
Table 18 Comparison of experimental results for the heat transfer coefficient for constant quality and varying mass flux..... 99
Table 19 Comparison of experimental results for the heat transfer coefficient for varying quality..... 102
Table 20 Comparison of experimental results with Tibiriçá [28] in terms of quality dependence..... 103

Table 21 Comparison of experimental results with Shiferaw [23] in terms of quality dependence 105
Table 22 Dependence of pressure drop on mass flux for constant quality 107
Table 23 Dependence of pressure drop on quality for constant refrigerant mass flux 109
Table C.1: The necessary pipes for the set-up connections 126
Table C.2: Elbows and T-connections 126
Table C.3: Refrigerant (R-134a) cycle connectors and pipes 127
Table C.4: Water cycle connectors and pipes 128
Table E.1: The calibration results for the compact pressure transducers 133
Table E.2: The calibration results for the differential pressure transducer 135
Table F.1: Specific gravity dependence on temperature for the water – ethylene glycol mixture 136
Table F.2: Specific heat dependence on temperature for the water – ethylene glycol mixture 137
Table F.3: Dynamic viscosity dependence on temperature for the water – ethylene glycol mixture 138
Table F.4: Conductivity dependence on temperature for the water – ethylene glycol mixture 139
Table G.1: Viscosity (liquid) dependence on saturation pressure for R-134a ... 140
Table G.2: Viscosity (vapor) dependence on saturation pressure for R-134a... 141
Table G.3: Conductivity (liquid) dependence on saturation pressure for R-134a 142
Table G.4: Conductivity (vapor) dependence on saturation pressure for R-134a 143
Table G.5: Pr (liquid) dependence on saturation pressure for R-134a 144
Table G.6: Pr (vapor) dependence on saturation pressure for R-134a 145
Table G.7: Surface tension dependence on saturation pressure for R-134a 146
Table G.8: Specific heat (liquid) dependence on saturation pressure for R-134a 147
Table H.1: The geometries of both sides 149
Table H.2: Test conditions for the experiment 150
Table H.3: Refrigerant experiment states 151
Table H.4: Water side properties 151

Table H.5: Refrigerant experimental calculations 152
Table H.6: Calculations of correlations in the literature 153
Table H.7: Experimental results and the results of the correlations in literature
..... 154

LIST OF FIGURES

FIGURES

Figure 1 Conventional Mechanical Refrigeration System 2
Figure 2 Schematic view of the set-up at the first design 24
Figure 3 Schematic view of the set-up at preliminary design with states 29
Figure 4 Schematic view of the set-up at preparation stage 30
Figure 5 Technical drawing of structural frame 32
Figure 6 The photos of data logger 32
Figure 7 The photo of thermocouple plug panels 34
Figure 8 The refrigerant bath and the coil heat exchanger 36
Figure 9 The refrigerant cycle (bath section) 37
Figure 10 The refrigerant cycle (the pump and the flowmeter before by-pass line added) 38
Figure 11 The photo of flowmeter and by-pass line 39
Figure 12 The pre-heater before and after winding 40
Figure 13 The control box and the power transducer of the pre-heater 41
Figure 14 The water cycle 45
Figure 15 The photo of the test section at the initial preparation 47
Figure 16 The photo of the set-up after the preliminary tests 52
Figure 17 The schematic view of the set-up in the actual experiments 53
Figure 18 The adapter parts for glass - copper transition 54
Figure 19 The adapter parts mounted on the cycle 55
Figure 20 The test section after the shell was closed with bolts and silicone 56
Figure 21 The exit of the test section with solidified glue at the adapter 57
Figure 22 The test section with copper tube 58
Figure 23 Test section with copper tube after insulation 59
Figure 24 The pre-heater section of refrigerant cycle as control volume 64
Figure 25 The calibration curve of the pre-heater 67
Figure 26 Viscous heating versus Reynolds number 71
Figure 27 Heat transfer coefficient versus saturation pressure for constant refrigerant quality 93

Figure 28 Heat transfer coefficient versus mass flux for constant refrigerant quality 95
Figure 29 Heat transfer coefficient versus saturation pressure for constant refrigerant mass flux 96
Figure 30 Heat transfer coefficient versus quality for constant refrigerant mass flux 98
Figure 31 Experimental results and results of correlations in the literature for heat transfer coefficient versus mass flux, x = 18% 100
Figure 32 Heat transfer coefficient ratio versus mass flux, x = 18% 101
Figure 33 Experimental results and results of correlations in the literature for the heat transfer coefficient versus quality 102
Figure 34 Heat transfer coefficient versus quality for current experiments and results of Tibiriçá [28] 104
Figure 35 Heat transfer coefficient versus quality for the current experiments and those of Shiferaw [23], G = 200 kg/m^{2}s 106
Figure 36 Pressure drop versus mass flux for constant refrigerant quality 108
Figure 37 Pressure drop versus quality for the constant refrigerant mass flux, G = 200 kg/m^{2}s 109
Figure B.1 Sketch of the experimental set-up in the preliminary design 125
Figure D.1 Technical drawing of the flange 129
Figure D.2 Technical drawing of the shell 130
Figure D.3 Technical drawings of the ring and the bumper 131
Figure E.1 A sample calibration curve for an RTD 132
Figure E.2 The calibration curve for the compact pressure transducer 1 134
Figure E.3 The calibration curve for the compact pressure transducer 2 134
Figure E.4 The calibration curve for the differential pressure transducer 135
Figure F.1 Specific gravity versus temperature for the water – ethylene glycol mixture 136
Figure F.2 Specific heat versus temperature for the water – ethylene glycol mixture 137
Figure F.3 Dynamic viscosity versus temperature for the water – ethylene glycol mixture 138
Figure F.4 Conductivity versus temperature for the water – ethylene glycol mixture 139

Figure G.1: Viscosity (liquid) versus saturation pressure for R-134a 141
Figure G.2: Viscosity (vapor) versus saturation pressure for R-134a 142
Figure G.3: Conductivity (liquid) versus saturation pressure for R-134a..... 143
Figure G.4: Conductivity (vapor) versus saturation pressure for R-134a 144
Figure G.5: Pr (liquid) versus saturation pressure for R-134a 145
Figure G.6: Pr (vapor) versus saturation pressure for R-134a..... 146
Figure G.7: Surface tension versus saturation pressure for R-134a 147
Figure G.8: Specific heat (liquid) versus saturation pressure for R-134a..... 148

LIST OF SYMBOLS

A ..... inner surface area of the copper tube, m^2
Al ..... aluminum
Bo ..... boiling number
Br ..... Brinkman number
Co ..... confinement number
c_p ..... specific heat, kJ/kgK
D_h ..... hydraulic diameter, m
E ..... enhancement factor
F ..... correction factor
Fo ..... boiling enhancement factor
G ..... mass flux, kg/m^2s
g ..... gravitational acceleration, 9.81 m^2/s
$\bar{h}$ ..... average convective heat transfer coefficient of R134a, W/m^2K
h ..... enthalpy, kJ/kg
I ..... current, mA
i ..... latent heat, kJ/kg
k ..... thermal conductivity, W/mK
L ..... Length of the test section, m
M ..... moleculer weight, kg/kmol
Nu ..... Nusselt number
$\dot{m}$ ..... mass flow rate, kg/s
p ..... pressure, Pa
Pr ..... Prandtl number
$\dot{Q}$ ..... heat transfer rate, W
q" ..... heat flux, W/m^2
r ..... radius, m
Re ..... Reynolds Number
S ..... suppression factor
T ..... temperature, K
t ..... thickness, m

U ..... Overall heat transfer coefficient, W/m^2K

$\dot{V}$ ..... volumetric flow rate, m^3/s

X_{tt} ..... Lockhart-Martinelli parameter

x ..... quality

Greek letters

Δ ..... difference

μ ..... dynamic viscosity

ρ ..... density

σ ..... surface tension

θ_b ..... wall superheat

Subscripts

c ..... copper

cb ..... convective boiling

conv ..... convection

H ..... pre-heater

he ..... pre-heater exit

hi ..... pre-heater inlet

i ..... tube inner

ins ..... insulation

l ..... liquid

LM ..... logarithmic mean

nb ..... nucleate boiling

o ..... tube outer

p ..... pool boiling

R ..... refrigerant

r ..... reduced

re ..... refrigerant test exit

ri ..... refrigerant test inlet

s ..... saturation

si ..... shell inner

so ..... shell outer

TP ..... two-phase

V.....viscous heating
w..... test section wall
W..... water
W,loss.....water side loss to the surroundings
we..... water test exit
wi..... water test inlet

CHAPTER 1

INTRODUCTION

1.1 DOMESTIC COOLING AND EVAPORATORS

In the present era, the demand and the need for energy are soaring with the increase of civilization. Therefore, careful use of energy resources and increase in the efficiency of energy transfer are worth and needed to be considered. In the energy field, heat transfer is one of the main areas. There are several fields where heat transfer takes place and/or is used with different aspects and subjects in daily life, in industrial applications to name a few.

Among the areas of heat transfer, cooling is a significant concept for a wide range of applications. For almost all fields of industrial applications and domestic appliances, it has a great importance either directly or indirectly. For instance; in refrigerators, cooling is the main purpose to protect the food and beverages inside, while in automobiles, for better performance of engine and for the engine parts not to be worn or damaged, cooling has an indirect but important effect. When the domestic cooling is taken into consideration, refrigerators and air conditioners are the main devices used. They differ in terms of the aim, mechanism of the cooling and the energy consumption rate. Refrigerators compose more than 13% of total electricity consumption in households [1], which is an important factor for the thesis in terms of the motivation; and will be explained in the forthcoming parts. In this thesis, evaporator of a refrigerator, specifically, alternatives for the tubing within, is the subject of interest.

For a household refrigerator, the cooling process takes place in a refrigeration cycle. Figure 1 shows conventional vapor compression refrigeration cycle [2]. In the evaporator part, heat is absorbed from refrigerator food compartment; and the low pressure, low temperature liquid refrigerant is evaporated at a relatively constant pressure and temperature.

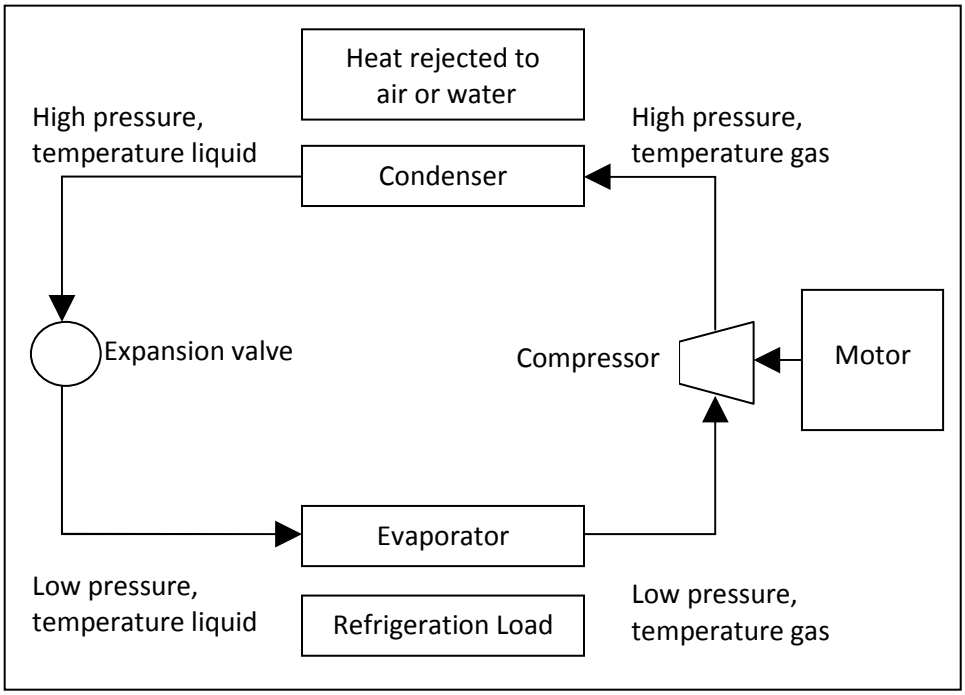

Figure 1: Conventional Mechanical Refrigeration System

In the conventional refrigerators, the evaporator is composed of circular tubes usually made from copper and these tubes are conventional (macroscale) channels [3]. In this thesis using minitubes instead of conventional channels in the evaporator is investigated experimentally by designing and building a new experimental set-up with the constant wall temperature approach for the two-phase flow of refrigerant-134a (R-134a) in a minitube (circular) with a diameter of 1.65 mm.

1.2 MICRO- AND MINICHANNEL HEAT TRANSFER

Heat transfer in small scales is one of the relatively new fields that has been attracting researchers' interest. There are different approaches for the naming of small scale tubes and channels. According to Kandlikar [3]; when tubes or channels have hydraulic diameter (D_h) larger than 3 mm, they are called conventional channels, while minichannels have 3 mm > D_h > 200 μm, and microchannels have 200 μm > D_h > 10 μm. This thesis is based on Kandlikar's categorization, but in some studies, as well as the industry, the ranges given above were not considered the same by the authors and they called all small channels microchannels. In order not to change the original terminology; when studies from literature are presented, the authors' naming for the channels is used in this text.

For the last three decades, micro- and mini-scale heat transfer studies have been increasingly popular. One of the very first studies was conducted by Tuckerman and Pease [4]. They experimentally studied microchannel water flow for cooling the CPU of a computer and showed that heat transfer increases in microchannels, compared to macrochannels. This study attracted the interest of many researchers to examine the heat transfer at mini- and micro-scales. Moreover, the fact that the correlations for the conventional channels were not valid for the mini- and micro-channels led to an instant necessity for new studies about this subject.

As mentioned in the Introduction, and as it is known from basic principles of thermodynamics, there is two-phase flow in the evaporators. In the refrigerators, refrigerants are used because they have lower boiling temperatures and high heat capacities. The facts that heat transfer and heat transfer coefficient are much larger for two-phase flow than for single-phase flow and that small scale heat transfer is greater than large scale (conventional) heat transfer directed the studies to be focused on refrigerant flow boiling in mini- and microchannels.

Heat transfer for a flowing fluid in an internal flow is characterized by several variables. These are mainly the bulk fluid temperature and pressure, mass flow

rate / fluid velocity (Reynolds number), geometry (channel height, width and length / tube diameter and length), channel port number (single- / multi-channel), flow type (laminar / turbulent), flow phase (single- / two-phase), boundary conditions (constant wall temperature / constant heat flux), pressure drop (friction factor), heat transfer coefficient (Nusselt number).

Several researches about the effects of the above mentioned variables on the heat transfer for minichannels, flow boiling of refrigerants, and both have been performed. The previous studies and their results directed the idea of the current experimental set-up and presented the necessity of this field. Among hundreds of invaluable scientific studies, some were examined and they are mentioned in the forthcoming section in the relation about the present thesis.

For a single-phase internal flow, the flow regime is an important parameter for heat transfer performance. There are two main flow regimes, designated by the Reynolds number (Re), which are laminar and turbulent flow. Reynolds number is a dimensionless quantity, which may be thought of as the ratio of the inertial forces in the fluid to the viscous forces. For internal flow in conventional channels, flows with $Re < 2300$ are designated as laminar. Although many text books inform that when $Re > 2300$, the flow is called turbulent; there is actually no sharp transition. Instead, there is a flow regime which is neither laminar nor turbulent, and it is called transition flow. Choi et al. [5] made a research on dry nitrogen flow in microchannels, about the effect of flow regime on heat transfer in microchannels. The authors compared the flow regime effect on heat transfer for long micro-tubes with diameter between 3 – 81 μm and proposed a correlation for Nusselt number (Nu) as a function of Re for laminar flow. They concluded that laminar flow had better performance in heat transfer than turbulent flow. Moreover, Harms et al. [6] studied the thermal and hydraulic properties of the flow of deionized water for two micro-channel configurations (single- and multi-channels) theoretically and experimentally and found the critical Reynolds number as 1500. They also concluded that the laminar flow was better in terms of heat transfer performance than turbulent flow similar to Choi et al. [5].

Flow geometry also has an important effect on the internal flow in mini- and microchannels. The tubes are mainly considered as circular and non-circular, in terms of the cross sectional shape. Non-circular tubes are traditionally called channels in text books. These channels can have various shapes; triangular, rectangular, square, wide parallel channels with small gaps in between, to name a few. One other parameter to be considered about the flow geometry is the number of ports in which fluid flows. When there is one tube / channel, it is called a single channel; on the other hand, the flow can be divided into several ports (multi-port microchannels) to increase the wetted perimeter and decrease the hydraulic diameter. Since the beginning of the research of internal flow in mini- and microchannels, several studies have been done about the effect of flow geometry on the heat transfer performance and pressure drop. Jung and Kwak [7] observed water flow in 5 parallel rectangular microchannels with 3 different hydraulic diameters. The authors kept the channel length constant and evaluated the friction factor. They observed that the values were close to the theoretical values for macroscopic correlations, whereas the Nusselt number relation deviated and was strongly dependent on Reynolds number. Therefore, the authors offered a new correlation instead of using constant value of Nusselt number for laminar developed flow as in macroscale tubes and channels. Moreover it was shown that the heat transfer coefficient was linearly dependent on the wall temperature and fluid properties; such as viscosity, which affects the heat transfer mechanism significantly. Park and Punch [8] concentrated on single-phase flow in microchannels experimentally. The aim was to investigate the friction factor and heat transfer in arrays of microchannels for different hydraulic diameters ranging from 106 μm to 307 μm for low Reynolds number ($69<Re<800$) values. The friction factor results matched the correlations for conventional channels whereas the Nusselt number values deviated significantly. As a result, the authors proposed a correlation including Nusselt, Reynolds, Prandtl (Pr), and Brinkman (Br) numbers. Brinkman number is a dimensionless number that relates the heat conduction from a wall to a flowing viscous fluid.

Besides the flow regime and flow geometry, many studies on the single- and two-phase flow have been performed. Heat transfer in two-phase flow is known to be

superior compared to single-phase flow. Studies were focused on the effect of different parameters on two-phase mini- and microchannel flow.

Kandlikar [9] reviewed the previous studies on mini- and microchannel heat transfer and pressure drop. The comparison of the mentioned channels with the conventional-sized channels/tubes was handled and flow boiling characteristics were considered. Also, the author pointed to the fact that the configuration – one or multi ports – had an important effect on heat transfer and pressure drop. His study focused on relevant geometries, fluids, and heat/mass fluxes. He concluded that for multi-port channels, large pressure drop fluctuations occurred and also stated that heat transfer correlations for mini- and microchannels could be better predicted from the macroscale correlations as a first estimate. Moreover, he mentioned that the deviations in heat transfer and pressure drop of single and multichannels were caused by the fluctuations and flow instabilities. Although this article is relatively older (2002) than the others, it is beneficial to have an insight on the differences between single- and multiport channels and micro- and macroscale flows. In addition, an organized literature review is beneficial when comparing the current study with those in the literature.

Qu and Mudawar [10] investigated the boiling heat transfer of water flowing in parallel microchannels. The cross-section of each channel was 231 μm × 713 μm and there were 21 channels in total. For different inlet and boundary conditions, they performed experiments and concluded that contrary to macroscale flow, the heat transfer tended to decrease with increasing equilibrium quality. Several available correlations from literature were analyzed and it was found that none of them succeeded in predicting the experimental results, since most of their ranges of operation did not include the experimental conditions.

Saitoh et al. [11] performed experiments with three small diameter tubes (0.51, 1.12, and 3.1 mm inner diameter) using R-134a as the working fluid, which is also used in the current research. The authors examined the local heat transfer coefficient and pressure drop for all three tubes for different heat and mass fluxes, evaporating temperatures, and inlet qualities. The main goal for the experiments was to investigate the effect of tube diameter on heat transfer for

two-phase flow conditions. They concluded from the experiment that as the diameter gets smaller, the forced convective evaporation reduces, which means that the experimental heat transfer coefficient increases with increasing heat flux, but was not affected with the increasing mass flux. In addition, a dry-out in the lower quality region has been observed as the tube diameter decreased. On the other hand, after calculating the frictional pressure drop with the homogeneous model and the Lockhart-Martinelli correlation, and comparing with the experimental results, the authors realized that as diameter decreases, one can better predict the frictional pressure drop by using the homogeneous model rather than by the Lockhart-Martinelli correlation.

Bertsch et al. [12] worked with refrigerants and performed experiments in copper microchannel cold plate evaporators. In addition to R-134a, the authors used R-245fa as the working fluid. For two different arrays of microchannels with hydraulic diameters of 1.09 and 0.54 mm and with an aspect ratio of 2.5 for both, they measured heat transfer coefficient for different quality, saturation temperature, mass flux, and heat flux values. After their experiments, the authors concluded that the heat transfer coefficient was highly dependent on heat flux and quality while it was not affected much by saturation temperature and mass flux in the range of interest. Also, they concluded that in the flow boiling regime, R-134a was superior in heat transfer than R-245fa. Moreover, as the mass flux increases, the dominance of nucleate boiling increases for higher heat fluxes. The dependence of heat transfer coefficient on quality was also examined and the outcome was that the heat transfer coefficient strongly depends on the quality and there was a rapid decrease in the coefficient for qualities above 0.5. The highest value of heat transfer coefficient was seen for the quality values between 0.1 and 0.5 depending on the geometry and flow conditions. On the other hand, it has been reported that the smaller the hydraulic diameter, the higher the heat transfer coefficient, however small the difference. The authors also compared their results with several correlations in the literature and found that only a few are applicable for these microchannels and with errors as well.

Revellin and Thome [13] studied the flow-boiling regimes experimentally and they used an optical measurement method. Their test tubes were glass tubes, 0.5 and

0.8 mm in diameter. The authors carried out the experiments with R-134a and R-245fa at different saturation temperatures and pressures. The experiments showed four different flow patterns with their transitions. The interesting result was that for R-134a, neither macroscale correlations nor the microscale correlations for air/water flows were close to the results. Inlet sub-cooled temperatures and the saturation pressures did not significantly affect the performance. Also the different channels' results were not much different from each other except the flow patterns. The main difference recorded was that for R-134a, flow regime transitions were more affected by the mass flux than for R-245fa, which indicates that mass flux is an important issue to handle in two-phase flow in mini- and microchannels.

Bertsch et al. [14] also worked with refrigerant R-134a as the working fluid with similar conditions and the same aspect ratio in their previous work [12]. The authors examined a microchannel evaporator with 17 parallel channels of hydraulic diameter 1.089 mm (this time they did not consider any other channels with different hydraulic diameter) and found that the heat transfer coefficient reaches the largest value for the quality of 0.2 for all the experiments. Also, they realized that the heat transfer coefficient decreased rapidly after the maximum value with the increasing quality. In these experiments, one new outcome was that the effect of saturation pressure on the heat transfer coefficient was negligible. Moreover, it was reported that different from other microchannel studies, the heat transfer coefficient increased dramatically not only with the increasing heat flux but also with the increasing mass flux.

Yan and Lin [15] investigated evaporation heat transfer coefficient and pressure drop in a small pipe. These authors also used R-134a as the working fluid. The diameter of the pipe was 2 mm, which is close to the test pipe diameter in the current study, and is valuable to understand how the results deviate from the larger pipe heat transfer conditions. The authors found that for the small pipe mentioned above, the evaporation heat transfer coefficient is about 30-80% higher with the increasing heat flux and mass flux than that for conventional pipes; however the pressure drop was also larger. They also offered correlations for the heat transfer coefficient and friction factor.

Liu et al. [16] performed a numerical study of heat transfer in microchannels. They were interested in 2-D modeling of the water flow in a 100 μm hydraulic diameter microchannel for low Reynolds number flows and localized heat flux conditions. They focused on the viscosity and thermal conductivity variation and their effects on the heat transfer. It was revealed that the heat transfer increased with the viscosity variation with temperature, while the axial conduction resulting from the thermal conductivity variation seemed to be negligible except for very low Reynolds number cases. In their study, the significant outcomes were that the velocity field and the temperature distribution were coupled, the velocity field was distorted with the property variations, and the cross-flow introduced in the numerical approach affected the convection in a non-negligible manner.

Liu and Garimella [17] made experiments with water flowing inside microchannels. There were two different channels with dimensions of 275 x 636 and 406 x 1063 μm^2. The authors tried different water inlet temperatures with a variety of mass fluxes and different heat fluxes with a maximum value of 129 W/cm^2. They also tried two-phase flow but only with a maximum exit quality of 0.2. After the experiments, they calculated the convective heat transfer coefficient and compared the values with the results of correlations for macrochannels. As in the previous studies, the outcome is that the correlations worked for the subcooled region, but not for the saturated flow boiling regions. Then, the authors offered an analytical solution for the flow boiling region, which matched well with the experiments.

Agostini et al. [18] studied the flow boiling of R-134a in minichannels experimentally. The authors used 11 parallel rectangular multichannel straight aluminum drawn tubes with a hydraulic diameter of 2.01 mm. The working conditions were in the ranges of: 90 – 295 kg/m^2s for mass flux and 6.0 – 31.6 kW/m^2 for heat flux. The saturation pressures for the experiments were 405 and 608 kPa. The cooling at the inlet was varied from 1 K to 17 K. They concluded that although dry-out occurred for low quality values, heat transfer for the minichannels was greater than the heat transfer for conventional channels in the literature.

Djordjevic et al. [19] examined the evaporation heat transfer of ammonia and R-134a experimentally in a gasketed plate heat exchanger with Chevron-type plates. Saturation temperatures were between 268 – 283 K for ammonia and 265 – 283 K for R-134a. The second fluid used in the heat exchanger was a water – ethylene glycol mixture, which is also the secondary fluid used in the current experiments. In the heat exchanger, parallel flow resulted in a better performance than counter flow, contrary to the expectations of the authors. Comparisons with the literature gave a good match in terms of heat transfer coefficient even if the results for flow arrangements are against, and some correlations from the literature were adapted to the heat exchanger used in the experiments.

De Rossi et al. [20] carried out flow boiling heat transfer and pressure drop experiments for R-134a with a saturation temperature between -8.8 and 19.9ºC. The tube they selected was 6 mm in diameter and stainless steel. Their working mass flux and heat flux values were variable. After the experiments, they were able to comment on how these variables affected the heat transfer coefficient and pressure drop. They concluded that the heat transfer coefficient increased with the increasing quality, heat flux, and mass flux, but the saturation pressure affected the heat transfer coefficient only for low qualities. The pressure drop also increased with the increasing mass flux and decreasing saturation pressure.

Ong and Thome [21] performed experiments on flow boiling inside a 1.030 mm diameter channel. They chose three different refrigerants; R-134a, R-236fa, and R-245fa. They collected data for flow boiling heat transfer and flow pattern visualization. Similar to the other researchers, they conducted experiments with different heat and mass fluxes and concluded that for the saturated flow boiling heat transfer, the local heat transfer coefficient showed strong dependence on heat and mass flux but no significant dependence on the subcooled residuals. The authors mentioned that the changes due to these dependencies in heat transfer matched well with the flow transitions and added that the forced convection and nucleate boiling in microchannels was still unclear and should be studied further.

Choi et al. [22] used 2000 mm long, 1.5 and 3.0 mm diameter horizontal stainless steel minitubes in their study. They examined the flow boiling heat transfer of R-22, R-134a, and CO_2 in minichannels flow. They evaluated the heat transfer coefficient for laminar flow with 10 – 40 kW/m^2 heat flux, 200 – 600 kg/m^{2}s mass flux, and 0 – 1.0 quality variations. They varied heat flux values for different experiments and investigated the constant heat flux performance. For different fluids, the results for average heat transfer coefficient ratios, which are the ratios of the average heat transfer coefficients of the fluid to that of R-22, were 1.0, 0.8, and 2.0 for R-22, R-134a, and CO_2, respectively. In conclusion, they developed a new correlation for heat transfer coefficient in flow boiling heat transfer in minitubes.

Shiferaw et al. [23] compared the flow boiling heat transfer results of flow in 1.1 mm inner diameter stainless steel tube with the results of three region flow model. The fluid used in the experiments was R134a. The parameters changed were mass flux (100 – 600 kg/m^{2}s), heat flux (16 – 150 kW/m^2) and saturation pressure (6 – 12 bars). According to the results of the experiments; at quality values below 50% and low heat and mass fluxes, heat transfer coefficient changes with the heat flux and saturation pressure, but not with the quality, contrary to many previous studies. Mass flux effect seemed to be negligible on heat transfer coefficient. For the high heat flux and above 50% quality values, heat transfer coefficient does not change with heat flux and decreases with the increasing quality value, which was considered to be caused by dry-out. At low pressure values, the three region model had a good match with the experimental results, whereas it was not valid for the dry-out regions.

Matkovic et al. [24] took the condensation of R134a and R32 in 0.96 mm diameter stainless steel minichannel into consideration and calculated the local heat transfer coefficient by measuring the local heat flux and saturation temperature and pressure. In the experiments, the mass flux was varied from 100 to 1200 kg/m^{2}s and the saturation temperature was 40°C. The experimental results came out to be consistent with the results from the condensation equations derived for conventional channels. It has been concluded that for the minichannel condensers, on condition that there is relatively high velocity flow

inside circular cross-sectional minichannel, the correlations for the conventional channels are applicable.

Revellin et al. [25] studied the critical heat flux, which is an important subject in boiling, in mini- and microchannels. They compared the methods used in the literature to find the best match to the critical heat flux in small scale flow. The database they established consisted of the experimental investigation on 9 different fluids including R134a. They proposed the best correlations and methods for water and non-water based fluids among the ones they compared.

In et al. [26] observed the flow boiling of R134a and R123 experimentally in circular stainless steel microtubes with an inner diameter of 0.19 mm. They varied some parameters in the experiments, which were heat flux, mass flux, quality, and saturation pressure. Heat flux values were 10, 15 and 20 kW/m^2, mass fluxes were 314, 392 and 470 kg/m^2s, saturation pressures were 158 and 208 kPa for R123, 900 and 1100 kPa for R134a, and quality was between 0.2 and 0.85. For the two-phase heat transfer in R123 flow, nucleate boiling ran out at low quality values and the evaporation of liquid layers around augmented bubbles were dominant. On the other hand, for the two-phase heat transfer in R134a flow, up to larger quality values, nucleate boiling was dominant in flow boiling and for large quality values two-phase forced convection heat transfer was dominant. The results for R134a were similar to the macrochannel characteristics except the nucleate boiling development and small forced convection area. At the low and medium (about 0.5) quality values, heat transfer coefficient highly depended on heat flux and saturation pressure whereas mass flux and quality did not have an important effect on it. On the other hand, at high quality values, while heat flux and saturation pressure effects on heat transfer coefficient were negligible, mass flux had significant effects.

Park et al. [27] acquired new experimental results for critical heat flux values for the flow of three refrigerants (R134a, R236fa, R245fa) in two different copper multi-port microchannels. One of the test sections was composed of 20 parallel rectangular channels, 467 μm wide and 4052 μm deep. The other test section was composed of 29 channels, 199 μm wide and 756 μm deep. Microchannels

were 30 mm long and they were heated up with electrical resistances along a 20 mm length at the mid-section. For the varying mass flux values from 100 kg/m^{2}s to 4000 kg/m^{2}s, critical heat fluxes were measured to be from 37 W/cm^2 to 342 W/cm^2. Critical heat flux increased with increasing mass flux, and at high velocities (high mass fluxes) the increase was observed to be less. In the 4052 µm deep channels, the critical heat flux partly increased with the inlet cooling, but as the cross-sectional area of inlet cooling decreased; it was observed that the effect on the critical heat flux also decreased. Depending on the flow condition and the channel dimensions, the critical heat flux was inversely proportional to the increasing saturation temperature. When the experimental results were compared with the correlations, there was a good match with the ones for circular tubes using effective diameter and mass velocity.

Tibiriça et al. [28] researched the flow boiling heat transfer of R134a and R245fa in a 2.3 mm inner diameter stainless steel tube experimentally and also displayed the characterization of flow model. They gathered the experimental data for the flows in the ranges of 50 – 700 kg/m^{2}s mass flux, 5 – 55 kW/m^2 heat flux and 0.05 – 0.99 quality values. The calculated heat transfer coefficients were between 1 – 14 kW/m^{2}K. They concluded that heat transfer coefficient strongly depends on the heat flux, mass flux and quality.

Raja et al. [29] tested the flow boiling of a mixture composed of three refrigerants – R-134a, R290 and R600a with mixing ratios of 91%, 4.068%, and 4.932% (in terms of mass), respectively – in two different, 9.52 and 12.7 mm diameter, horizontal tubes. They applied heat flux values of 2 – 8 kW/m^2 to find the behavior of heat transfer coefficient under constant heat flux approach. The inlet temperature of the refrigerant was between -9 – 5°C and mass flow rate was in the range of 3 – 5 g/s. The heat transfer coefficient values came out to vary in the range from 500 to 2200 W/m^{2}K in two tubes. They compared the results for both tubes and found that the heat transfer coefficient in the 9.52 mm tube is 10 % – 45 % (for different flow rates) larger than the 12.7 mm tube. Moreover, they made a comparison of heat transfer performance for refrigerant mixture and pure R134a. When the pressure was constant along the flow, the mixture gave better performance throughout the boiling, whereas for constant inlet temperature, it

was larger only for high qualities. In the experiments, the authors also discussed the boiling mechanisms in terms of flow patterns and used Kattan – Thome – Favrat maps to verify the flow type in boiling. They concluded that for the boiling of this refrigerant mixture, nucleate boiling was dominant even at high qualities with low heat and mass flux values. Also, when there was constant pressure and flow rate; heat transfer coefficient significantly depended on heat flux.

Ding et al. [30] concentrated on the frictional pressure drop in two-phase flow of a R410a-oil mixture. They selected 5 mm outside diameter internal spiral grooved microfin tube to arrange the flow which had 5°C saturation temperature, 200 – 400 kg/m^{2}s mass flux, 7.46 – 14.92 kW/m^2 heat flux, 0.1 – 0.8 quality at the inlet, and 0 – 5 % oil concentration. They revealed that the pressure drop made a peak at a quality between 0.7 and 0.8 and it was larger for larger mass flux values. In addition, the presence of oil in the refrigerant increased the pressure drop and this effect increased with increasing quality values because of the larger concentration of oil inside the mixture. The authors considered the increase in pressure drop by comparing with the zero oil condition, and calculated an enhancement factor to be between 1.0 and 2.2 when compared with the pure refrigerant. They offered a new correlation with the experimental results using the local thermodynamics properties of the mixture.

Chen et al. [31] conducted an experiment to examine the two-phase heat transfer and flow pattern for R134a flow in two ducts. The ducts were narrow, with 1.0 and 2.0 mm gaps and they were placed horizontally. The authors determined the effects of geometry (duct gap), saturation conditions and quality, heat and mass flux, on evaporation heat transfer coefficient. These affecting parameters were between 5 and 15 kW/m^2 for heat flux, 0.05 and 0.95 for quality, 5 and 15°C for saturation temperature, and 300 and 500 kg/m^{2}s for mass flux (for 2.0 mm duct), 500 and 700 kg/m^{2}s for mass flux (for 1.0 mm duct). The results displayed that heat transfer coefficient was directly proportional (almost linear) with the quality and at higher mass fluxes the proportionality got steeper. In addition, heat transfer coefficient increased with increasing heat flux and saturation temperature and it was larger for the 1.0 mm duct. Yet, these were less effective on this narrow duct at small heat flux and large mass flux values. The authors also

visualized the flow patterns by taking pictures and proposed a correlation for heat transfer coefficient in two-phase flow of narrow ducts.

Saisorn et al. [32] also studied two-phase R134a flow experimentally in a minichannel. Their channel was 1.75 mm in diameter (circular), 600 mm long, horizontal, and made of stainless steel. The results for both flow pattern and heat transfer coefficient were obtained for the mass flux values from 200 to 1000 kg/m^2, heat flux values from 1 to 83 kW/m^2 and at 8, 10, and 13 bar saturation pressures. They calculated the heat transfer coefficient in terms of these varying parameters and commented that the higher the heat flux, the more was the heat transfer coefficient, while mass flux and quality did not affect the results significantly. On the other hand, increasing saturation pressure decreased the heat transfer coefficient. Moreover, the authors examined five flow patterns for flow-boiling.

Consolini and Thome [33] attracted attention to the fact that although there is a common belief and consensus on the higher heat dissipation of micro-channel flow boiling, the characteristics of this small scale heat transfer still need to be investigated further. Thus, they studied flow boiling heat transfer of the refrigerants R134a, R236fa and R245fa in two different microchannels which had diameters of 510 and 790 μm with mass fluxes changing in the range of 300 – 2000 kg/m^2s and with a maximum heat flux of 200 kW/m^2. For the two refrigerants, R134a and R236fa; heat transfer coefficient depended on the heat flux as well as the fluid properties at not only low qualities but also high qualities, where as a flow mode, annular flow dominates the flow. Although the third refrigerant, R245fa, showed a similar behavior as the other refrigerants at low quality values; at high values, it was independent from heat flux and α-x plane curves kept increasing for higher qualities.

In light of the literature review presented above, the following general conclusions can be made:

The saturation pressure has no significant effect on the two-phase heat transfer. Although for some studies, the increasing saturation pressure increased the heat

transfer coefficient drastically, the general consensus was on the negligible effect on the boiling heat transfer.

The quality change in the two-phase flow was agreed upon for almost all studies in terms of increasing heat transfer up to moderate quality values, 30 – 50 %. The change of the heat transfer coefficient for high quality values was concluded in two ways: continuous increase and decrease after a peak. The studies were mostly experimental studies and the changes would have occurred due to the experiment conditions.

Some of the authors in the literature proposed correlations for the numerical and experiments studies they performed. These correlations are valuable in terms of comparison and establishing the infrastructure. On the other hand, it should be noted that the correlations based on the results of these studies would be valid only for the ranges of the experiments.

The pressure drop for two-phase flow was mentioned to increase in comparison with the pure liquid flow and it can be commented that a trade-off between the heat transfer and pressure drop can be expected.

The heat transfer coefficient of two-phase flow of any fluid is considerably larger in comparison with the single-phase flow. The problems of dry-out, flow arrangement – vertical and horizontal flow –, the need for high heat flux, which is the general tendency for the studies to achieve high qualities, could be made as an inference from the studies.

1.3 MOTIVATION AND OBJECTIVES

As it can be observed from the studies in literature, some of which were presented in the previous section, small scale heat transfer and especially flow boiling heat transfer in mini- and microchannels is a field that attracts the attention of many researchers. The results and comments show that despite the fact that there are several invaluable researches and papers in this area, there is still need for further investigations. The experimental, numerical, and theoretical infrastructure about the mini- and microscale heat transfer is being established in the present era. Among these three main approaches, experimental studies are a must to increase the understanding, and they lead the numerical and theoretical studies.

There are basically two approaches used as models in boundary conditions which are constant wall temperature and constant heat flux approaches. For the two-phase flow boiling heat transfer in mini- and microchannels, the literature shows that the studies were focused on mainly the constant heat flux approach. It is needed to support and extend the constant wall temperature approach, which is observed in common household refrigerators. On the other hand, when the mini- and microchannels are compared, because of the difficult manufacturing and establishment procedures, high pressure drop and no limitation in terms of space, the microchannel applications would not be practical in refrigerators. Therefore, minichannels in refrigerators would be a better solution in terms of increasing heat transfer rate and keeping the pressure drop in a reasonable amount.

The refrigerant flow in small scale has been widely investigated by several scientists. Because of the low boiling points of the refrigerants, two-phase flow studies are also performed to reveal the phase change effect. These studies are mainly at high pressures because of the fact that the saturation temperatures of the refrigerants come closer to the room conditions at relatively high pressures (over 6 – 7 bars). The refrigerants in refrigerators have lower values of saturation temperatures and pressures, so there is lack of research on the two-phase

refrigerant flow in mini- and microchannels at relatively low pressures and temperatures.

When these three aspects; the value of experimental study, the need for constant wall temperature approach, and the need for low pressure studies are considered, in addition to the results of the studies in the literature about two-phase heat transfer in small-scale media, which show that there is a remarkable enhancement of heat transfer in small scales; the motivation of this thesis emerges.

The aim of this thesis is to establish an experimental set-up for investigating the small scale heat transfer for two-phase refrigerant flow in 1.65 mm copper tube. The process and progress of the experimental set-up installation is presented and the design, installation and calibration of the devices, preliminary experiments, and their results are given.

The following chapter is about the construction of the “Experimental Set-up”, the preliminary tests and the calibrations of the measurement devices. Chapter 3 focuses on “Two-Phase Flow Experiments” in terms of data analyses and calculations. The results of the experiments and the comparison with the available studies and correlations in the literature are given in Chapter 4, “Experimental Results and Discussion”. The final chapter, Chapter 5 “Conclusions”, concludes the thesis by summarizing the work, commenting on the conclusions, and making suggestions on the future work.

CHAPTER 2

EXPERIMENTAL SET-UP

The aim of this study is to establish an experimental set-up to investigate the two-phase flow of R134a in 1.65 mm copper tube. The process of the set-up installation – design of the set-up, equipment used, preparation for the set-up, calibrations made –, preliminary test and modifications done are given in this section.

The flow in the experiments is internal laminar flow at steady-state conditions. The tube used is circular, so the flow can be considered as laminar flow through a pipe. The experimental results and calculations of the correlations in the literature are done in the forthcoming Chapter, yet the main theory in terms of Thermodynamics, Heat Transfer and both General and Particular Laws is presented in thie following section.

2.1 MAIN THEORY OF THE INVESTIGATION

Heat transfer is defined as the energy transfer study which takes place in the presence of a temperature difference. There are General Laws – physical laws independent of the medium – and Particular Laws – that depend on the medium – that govern the heat transfer study. These laws are very significant for engineers in all stages of a heat exchange device from design to operation [34].

General Laws for heat transfer are [34]

- the law of conservation of mass
- the first law of thermodynamics

- the second law of thermodynamics
- Newton's second law of motion

Some particular laws about heat transfer are [34]

- Fourier's law of heat conduction
- Newton's law of cooling
- Stefan – Boltzmann's law of radiation
- Newton's law of viscosity, and so on.

The general forms of the General and Particular Laws for a Control Volume are [34]:

The law of conservation of mass:

$$\frac{\partial}{\partial t}\int_{C.V.}\rho\, dv = -\int_{C.S.}\rho\vec{V}\cdot\hat{n}\ dA \tag{1}$$

The first law of Thermodynamics:

$$\frac{\partial}{\partial t}\int_{C.V.}\rho\left(u+\frac{1}{2}V^2\right)dv + \int_{C.S.}\rho\left(u+\frac{1}{2}V^2\right)\vec{V}\cdot\hat{n}\ dA = \dot{Q}_{C.S.} - \dot{W}_{C.S.} + \frac{\partial}{\partial t}\int_{C.V.}\rho\,\vec{f}\cdot\ \vec{V}\,dv \tag{2}$$

The second law of Thermodynamics:

$$\frac{\partial}{\partial t}\int_{C.V.}s\rho\, dv + \int_{C.S.}s\rho\,\vec{V}\cdot\hat{n}\ dA \geq \int_{C.S.}\frac{1}{T}\frac{\delta Q}{dT} \tag{3}$$

Newton's second law of motion:

$$\vec{F} = \frac{\partial}{\partial t}\int_{C.V.}\rho\vec{V}\, dv + \int_{C.S.}\vec{V}\,\rho\vec{V}\cdot\hat{n}\ dA \tag{4}$$

Fourier's law of heat conduction:

$$\vec{q} = -k\,\vec{\nabla}T \tag{5}$$

Newton's law of cooling:

$$q_n = h(T_W - T_\infty) \tag{6}$$

Stefan – Boltzmann's law of radiation:

$$q_{bb}^r = \sigma T^4 \tag{7}$$

In the interest of this experimental study, the flow is steady, laminar, tubular flow with one-inlet and one-exit in the continuum regime. The laminar flow is caused by the low flow rate, which is to be explained in the forthcoming sections. The verification of the continuum concept is given in the calculations. Radiation heat transfer is neglected since conduction and convection dominates the heat transfer process. Therefore the equations mentioned above are simplified due to the conditions and such assumptions. The simplified versions of the equations are:

The law of conservation of mass (Continuity equation):

$$\dot{m} = \dot{m}_i = \dot{m}_e \tag{8}$$

The first law of Thermodynamics:

$$\dot{m}(h_e - h_i) = \dot{Q}_{C.S.} \tag{9}$$

The second law of Thermodynamics:

$$\dot{S}_{gen} = \dot{m}(s_e - s_i) - \frac{\dot{Q}_{C.S.}}{T} \tag{10}$$

Logarithmic Mean Temperature Difference (LMTD) Method:

$$\dot{Q}_{C.S.} = UA\ F\ \Delta T_{LM} \tag{11}$$

Overall Heat Transfer Coefficient:

$$UA = \left[\frac{1}{hA} + \frac{\ln\left(r_o/r_i\right)}{2\pi kL}\right]^{-1} \tag{12}$$

Pressure Drop (applicable only for single-phase flow):

$$\Delta P = 4f\frac{L}{d_i}\frac{\rho {u_m}^2}{2} \tag{13}$$

The main goal in this study is to estimate the heat transfer coefficient and measure the pressure drop for the two-phase flow experimentally and compare them with the available studies in the literature. Single-phase laminar flow inside a circular tube is very-well known since it can be solved analytically; on the other hand, it is not same for the two-phase flow. The studies in the literature show that the efforts on the two-phase flow are focused on numerical and experimental ways to establish a database and construct an infrastructure in this field.

2.2 DESIGN OF THE SET-UP

The set-up is designed to perform two-phase R134a flow experiments. The necessity of constant wall temperature approach led the design to have two cycles. Thus, two cycles and a heat exchanger at the evaporation part of the R134a flow design was done to achieve this goal. These are provided in two sub-sections “Constant Wall Temperature” and “Heat Exchanger”. In this part the general design of the set-up is given.

In the early design of the experimental set-up, the test section was decided to be a glass tube with 1.8 mm internal, 3.0 mm external diameter. With the glass tube, there could be flow visualization in addition to the experiments. The process about the change is given in the “Preparation” part.

For the two cycles, due to the fact that fluids are needed to be conditioned; vessels to be considered as reservoirs had to be present to set the fluid temperature at the designated values. Therefore, two refrigerated circulating baths – one for each cycle – were put on the set-up to maintain the desired temperatures.

To circulate the fluids in the system, pumps were used. The aims of the pumps are to sustain the constant pressure and provide a constant flow rate – with lowest oscillations possible – at steady-state conditions.

Two-phase flow experiments are the main goal, so the quality of the refrigerant at the test section must be known. Therefore, a pre-heater was placed just before the test section to specify and acquire the quality value.

Data acquisition is a must and it can also be considered the most important part of experimental studies. The flow rates of the fluids that are cooled / heated in the circulating bath and pumped to system by pumps are to be measured. The importance of the measurement is significant not only to measure the flow rate but also to arrange it to the specified values in the experiments. A micro-flowmeter is selected since the flow rates are relatively much smaller for the primary cycle if refrigerant cycle is considered as the primary cycle of the system. For the secondary cycle of the system, two rotameters are placed in the design to measure the flow rates at the test section and the by-pass. In addition to the flow rates, the properties of the fluids along the flow at the system pressure and temperature readings must be recorded. These values are needed for both the arrangement of the devices to get the desired test points and designation of the states at the specified locations.

These mentioned parts in the design are located in a schematic of the set-up, which is presented in Figure 2. The outer cycle in the figure is the refrigerant cycle and the inner cycle is the water cycle. The fluid used in the secondary cycle had been thought to be water in the preliminary design but then it was changed to a mixture to decrease the freezing point. This mixture is composed of water and ethylene glycol.

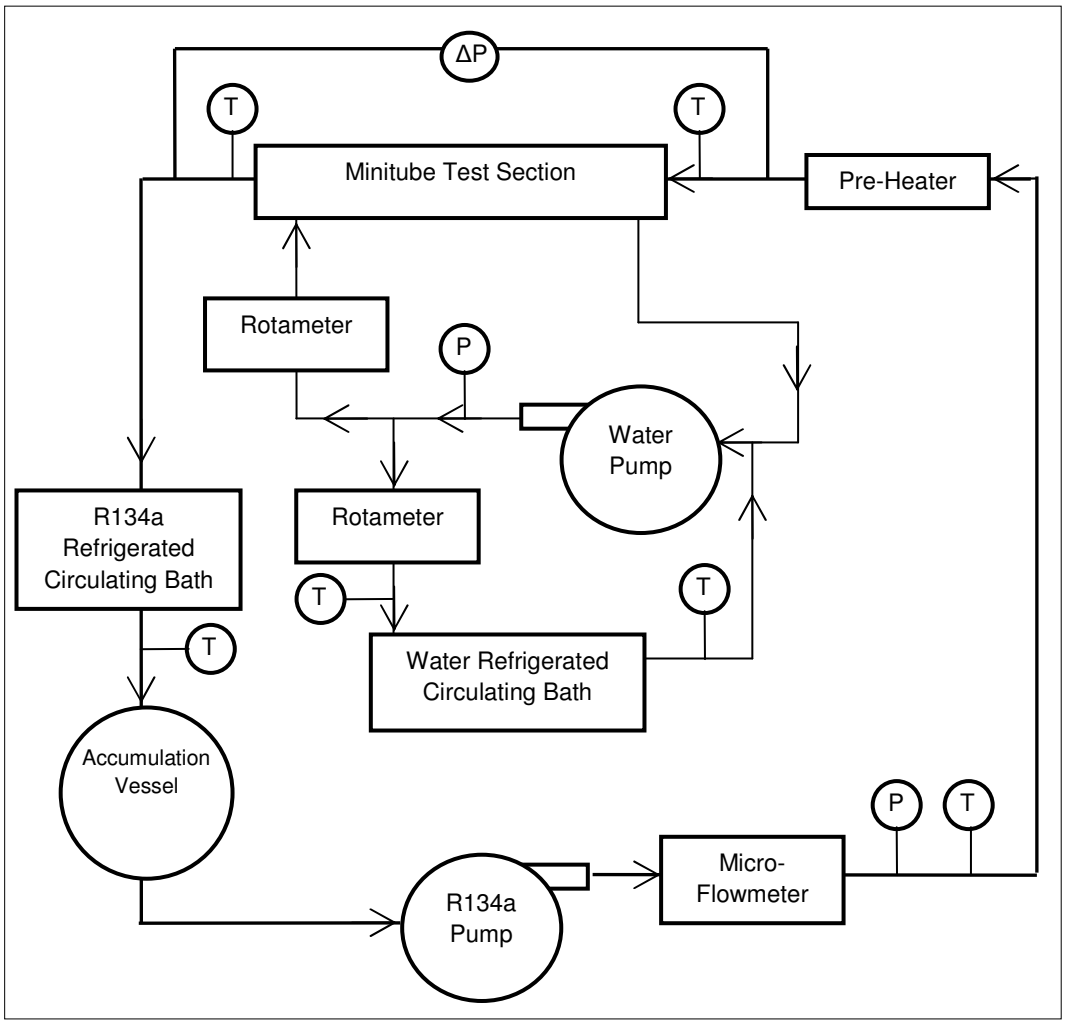

Figure 2: Schematic view of the set-up at the first design

In the refrigerant cycle starting from the test section exit, refrigerant flows through the circulating bath to specify the temperature. After the circulating bath, the temperature at the exit is measured and then there is an accumulation vessel. This vessel is added to the system to assure the liquid phase of refrigerant before the pump because pumps operate much more efficiently in liquid phase than in two-phase or vapor phase. After the vessel, there comes the pump to circulate the refrigerant inside the system and maintain the steady state conditions in terms of pressure. The flow rate is measured after the pump by a micro-flowmeter. The flowmeter should be capable of reading low flow rates, which is one of the main objectives in the experiments. When the flow leaves the

flowmeter, the temperature and the pressure of the refrigerant are to be measured. The reason behind this concept is to determine the state after all the devices before the pre-heater. Since the state is must be known at least by two independent properties, the flow must be in single-phase at this location to find the state correctly. When the state information is acquired, the refrigerant should be heated up to two-phase for evaporation experiments. There is a pre-heater placed for this purpose. The name is selected as pre-heater because the refrigerant is heated just before it enters the test section. The given heat input from the pre-heater to the refrigerant is also measured to determine the state at the inlet of the test section. The test section will be described in the “Counter Flow Heat Exchanger” section.

The water-ethylene glycol cycle is the second cycle of the system. For simplicity, it is called water cycle / side throughout the thesis. After the test section for the water side, the fluid comes to the pump. It is pumped and the pressure is measured at the exit of the pump section. Then the flow is divided into two parts. One of the divided parts goes to test section whereas the other line goes back to pump. The reason is to decrease the back pressure effect that can occur in the tubes or in the test section due to the small diameter. This effect may cause the pump to operate at very high temperatures and burn-out may occur. After the division of the flow, the by-pass side – the part that goes back to pump inlet – starts with a rotameter, which is placed to measure the volumetric flow rate sent back to the pump. Then the flow is directed to the refrigerated circulating bath of the secondary cycle. The temperature is measured both at the inlet and exit of the bath. The temperature is arranged in the bath and then the flow goes to the junction at the inlet of the pump where it mixes with the flow coming from the test section. The other part after the division of the flow flows into another rotameter which measures the volumetric flow rate that goes to the test section. The water flow at the test section is presented in the “Counter Flow Heat Exchanger” section.

2.2.1 Constant Wall Temperature

Constant wall temperature approach is provided by adding a secondary cycle to the set-up and flowing another fluid inside this cycle. The aim is to achieve constant wall temperature at the test section. It is decided to circulate water, which has a high heat capacity – capable of transferring large amounts of heat in small temperature differences – and make the flow as fast as possible to increase the mass flow to decrease the temperature difference. The verification of the constant wall temperature is needed during the experiments and for this purpose it is decided to measure the temperature of the wall at the test section from several locations.

2.2.1 Counter Flow Heat Exchanger

The test section is designed preliminarily as a heat exchanger with counter flow arrangement. The flow arrangement was selected due to the fact that the correction factor for the counter flow is 1 (highest value) for phase change on one-side and it also has higher effectiveness than parallel flow. For the two-phase flow, counter or parallel flow has no difference, but it is decided to prepare in this configuration for forthcoming experiments with both single- and two-phase flow. The heat exchanger is considered as a shell-and-tube heat exchanger with refrigerant flow on the tube side and water flow on the shell side. Since the flow of refrigerant is on the tube side, it is advantageous in terms of the heat loss considerations to the surroundings. The net heat transfer rate from water is the actual transfer rate to the refrigerant. To calculate the heat transfer coefficient and pressure drop, the temperatures at the inlet and exit of the test section for both fluids and the pressure difference between the inlet and exit of the refrigerant side are measured.

2.3 EQUIPMENT

After the design of the experimental set-up, the devices that are to be used are specified and obtained. These devices are selected in terms of the needs for the experimental conditions in addition to the economical sufficiency.

As given in the schematic view and mentioned in the design part, a circulating bath [35], pump [36], and micro-flowmeter [37] are selected for the refrigerant cycle. The accumulation vessel is provided by Arçelik, the company participating in the project as the technical supporting partner. For the pre-heater part, heat-rolled strips were the first design selection. Then the design has been changed due to the possible problems that may occur in these strips since the geometry is cylindrical. Therefore, an electric resistance heater was decided to be the pre-heater of the set-up and a control box that can both manually and automatically control the heater power input was added to the set-up. This control box was designed and produced by Yenel Ltd. in Teknokent, METU. The test tube was 1.8 mm inner diameter glass tube in the first design [38] and then it has been changed to 1.65 mm inner diameter copper tube, which is already present in the laboratory of the department. For the pressure measurement at the flowmeter exit of the refrigerant cycle, a pressure transducer is used [39]. For the temperature measurements, both RTD (Resistance Temperature Detector) probes and thermocouples are used. An RTD is much more sensitive compared to thermocouples, so it is used for critical temperature measurements, which are mainly to determine the state of the refrigerant. On the other hand, there were two types of RTDs used in the set-up: one has a probe with 0.093" (2.36 mm) diameter [40] and the other with 1.8 mm. The RTD with the smaller probe is more sensitive so it was used in the flowmeter exit location. The larger RTD is used to measure the temperature of the refrigerant at the exit of the bath. Also several thermocouple measurements are desired along this cycle to verify the RTD readings. T type thermocouples [41] are selected.

For the water side, a pump, two rotameters, and a circulating bath functioning like a reservoir are needed. The pump was a 373 W water pump. The refrigerated circulating bath is the same as that at the refrigerant side [35]. Since the flow at the water side is designed to be single-phase (liquid) flow, rotameters instead of flowmeters are used [42]. The temperature and pressure measurements are also similar to the refrigerant cycle. The temperatures at the inlet and exit of the bath are measured. The sensitiveness for these points does not have a high importance so the thicker RTDs are used, which are the same as the primary

cycle [40]. The pressure is read by an identical pressure transducer [39] at the exit of the pump. Thermocouple readings at the water side are also planned, with the same type.

At the test section, the temperature readings are important for both cycles at both inlet and exit. The measurements at these points are done by RTDs to have more accurate results. The critical side is the refrigerant side so the thinner probe RTDs are used on this side while the thicker probe RTDs are for the water inlet and exit readings. The pressure drop along the refrigerant flow is another consideration for the experimental design; thus, a differential pressure transducer is purchased [43]. The pressure drop for the water side is not of interest. Moreover, the variation of the wall temperature at the test section is needed to be measured and thermocouples are to be used for this purpose at several locations along the refrigerant tube.

For the pressure transducers, DC voltage input is needed so there is a need for a DC Power Supply [44]. The output of temperature and pressure readings and the input of pre-heater power values are in terms of voltage and current in volts (millivolts) and amperes (milliamperes). Since these must be converted into the necessary units with proper calibrations, it was decided to gather the experimental data by means of a data acquisition system [45] and transfer them into a computer interface.

The specifications of these devices mentioned above are given in Appendix A. These devices are to be connected and mounted on the set-up by tubes, pipes, and connectors. In the preliminary design, the set-up is drawn in Key-Creator technical drawing program and length, material, and diameter of the pipes and tubes; diameter, type, and material of the connectors; and junction and connection points are determined. This design, which is given as a schematic in Figure 3, as a sketch in Appendix B, and as tables for connection parts in Appendix C, was altered during and after the preparation of the set-up.

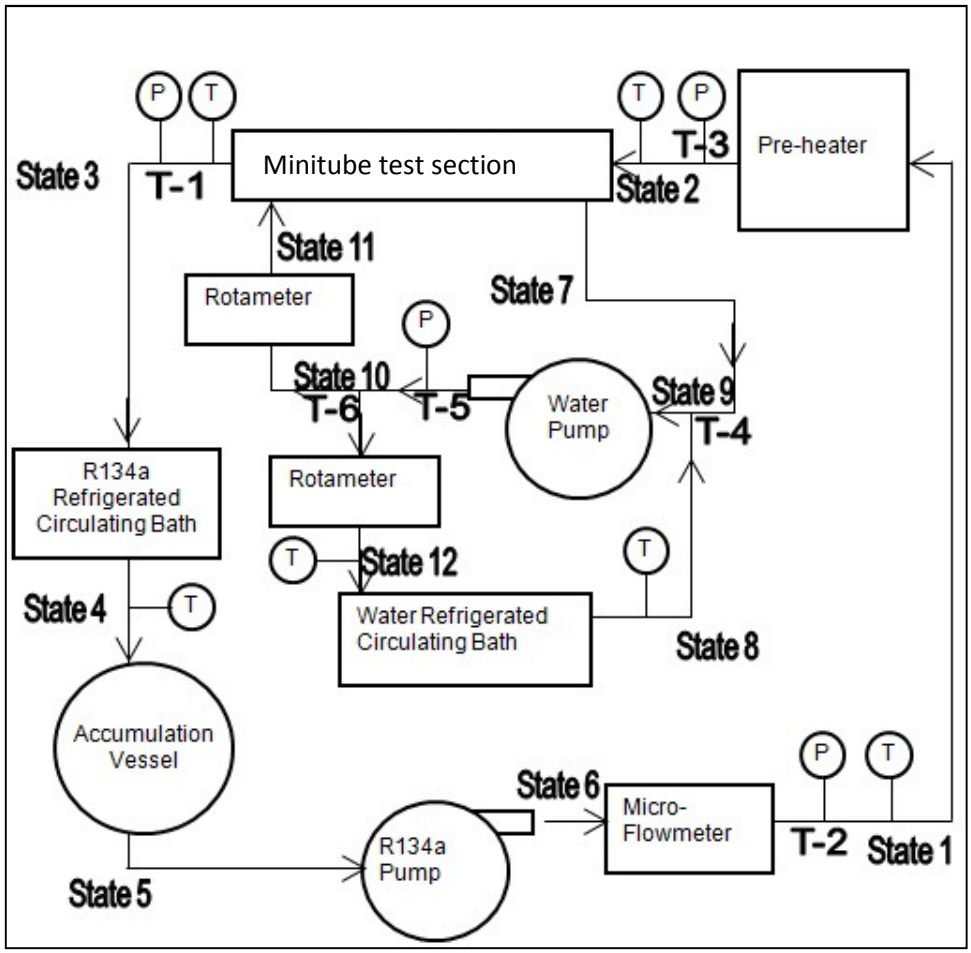

Figure 3: Schematic view of the set-up at preliminary design with states

2.4 PREPARATION OF THE SET-UP

The set-up was prepared with the devices acquired. In this section, the preparation and establishment of the set-up according to the initial design with some changes in the water cycle are explained and the schematic view of the experimental set-up is given in Figure 4.

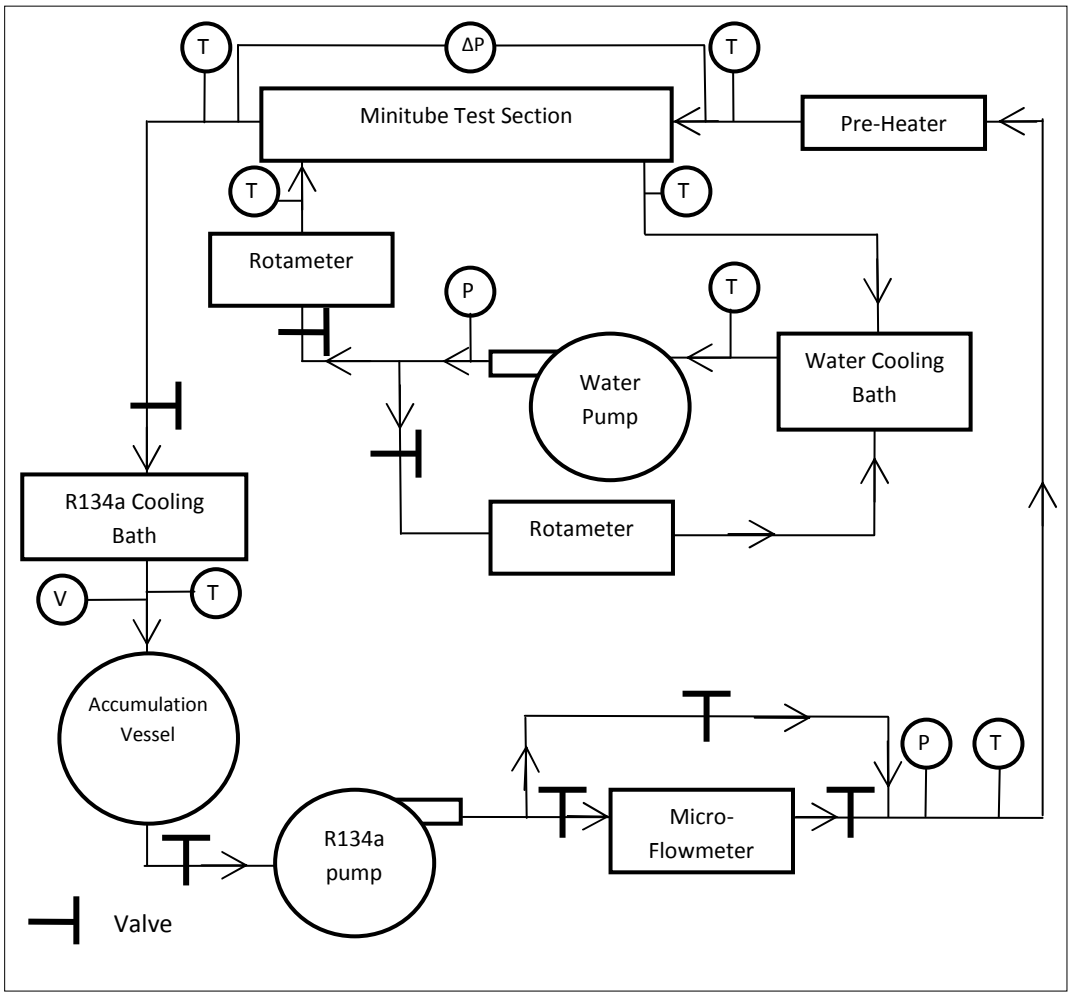

Figure 4: Schematic view of the set-up at the preparation stage

2.4.1 Structural Frame

Before starting the establishment of experimental set-up, a structural frame was designed to hold the devices and the system together and in an order. The technical drawing of this frame is given in Figure 5.

For the frame, 40 mm L brackets were used. In accordance with the technical drawing, this frame was prepared in METU Mechanical Engineering Department's Machine Shop with the permission and support of the professors in charge. When dimensions of the frame were decided, the subjects like ease of working, mobility, strength, and space necessity were considered. Since there

are two cycles in the set-up – R134a cycle and water (water + ethylene glycol mixture) cycle – and since they coincide with each other only at the test section, two horizontal parts on the frame were designed. Devices on the R134a cycle and the test section were placed on the upper part and devices on water cycle were placed on the lower part. Also, the test section was fixed to the vertical part placed on the upper part. The points that were taken into consideration in the preparation of the dimensions of the frame are: (a) Length: there should be enough space to fit into for the devices that forms both cycles separately. (b) Width: It should be suitable to be transported if there is a need to change the laboratory. (c) Height: There should be enough distance for the devices to function properly and the test section should be mounted and/or changed easily and properly. Moreover, 4 wheels were welded to the bottom of the frame, which gives the ease and opportunity to move, transport and/or arrange the devices and set-up itself in short or long term.

After the manufacturing of the structural frame that forms the general structure of the experimental set-up, 3 pieces of hardboard were placed on the frame to put the devices on. These hardboards, one placed vertically and two horizontally – for upper and lower parts,,were 18 mm thick, 2210 mm long, and 800 mm, 640 mm, and 590 mm wide, respectively. They were selected in order to maintain the entirety of the setup in addition to meet the requirements of the strength to carry the loads of the devices and other components, the resistance to low temperatures, the ease of machining and assembly, and to be esthetic as much as it can be.

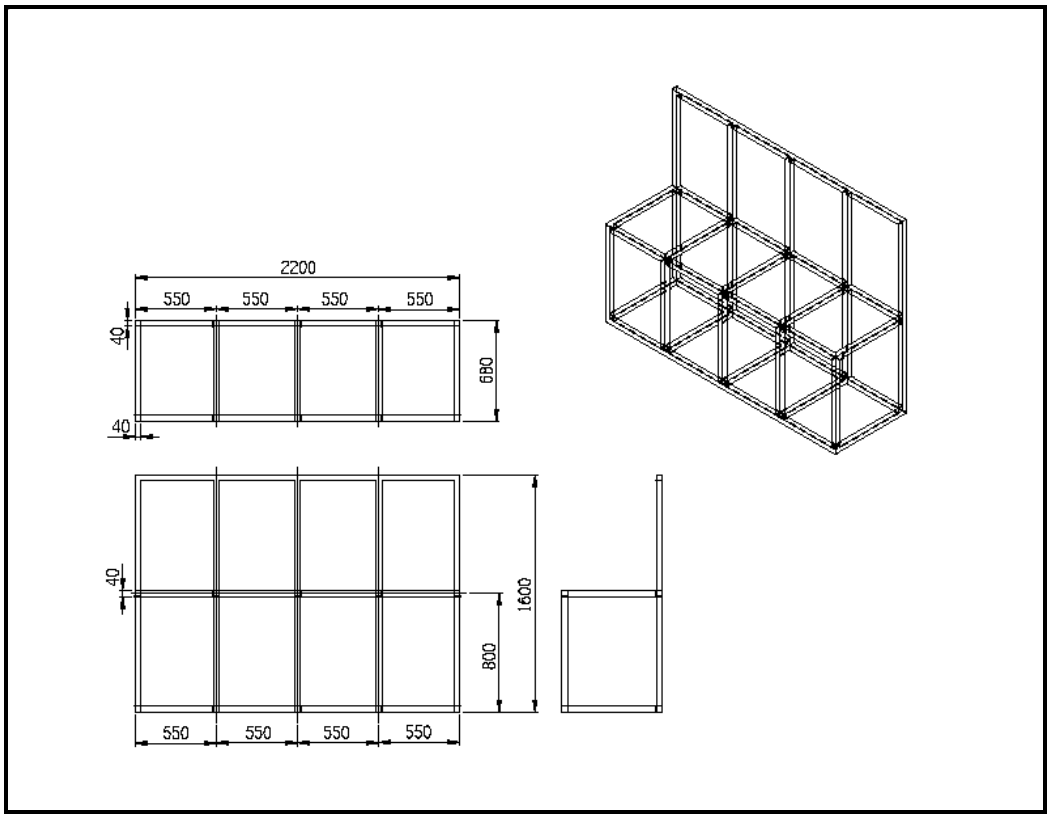

Figure 5: Technical drawing of the structural frame

2.4.2 Data Acquisition

Figure 6: The photos of the data logger

Before moving on to the fluid cycles and set-up placement, the data acquisition unit and cards, and the data acquisition process will be described. Initially 2 data

acquisition cards were purchased. On each of these cards 20 voltage and 2 current readings can be performed by the slots. In total, out of 40 voltage and 4 current slots, 43 of them were filled in the first preparation of the set-up. All of the voltage slots were used for temperature readings. Among the 40 temperature readings, 32 were used for thermocouples, and 7 were used for RTDs. The last slot was used as a reference for RTD readings and its end was embedded in a brass block. During this initial establishment process, 3 of 4 current reading capacities were used and one of them remained empty for the pre-heater control box and/or other pressure readings that could be added to the system. 2 of the 3 slots used were for compact pressure transducers and the other one was for the differential pressure transducer. The photos of the data logger are given in Figure 6.

For the temperature readings at the test section, as mentioned in the previous section, temperature measurements with thermocouples at the surface of the tube in which refrigerant flows were planned. After the installation of the experimental set-up, various tubes/channels are desired to be tested. When the thermocouples are fixed at the surface of the tubes/channels, they will obviously be shortened by cutting at the time of the change of the test tube/channel. To prevent this shortening effect to cause any change in data acquisition unit, connector plugs were decided to be used. These were for T-type thermocouples [46] and 20 of them with 2 “10 Circuit T-type Standard Panel”s were acquired, which can be seen in Figure 7 .

In the forthcoming parts, calibrations, placement in the setup, installations, data acquisition processes, and the aims of the use of the RTDs, the thermocouples, and the pressure transducers are presented in detail when the establishment of the experimental set-up is mentioned.

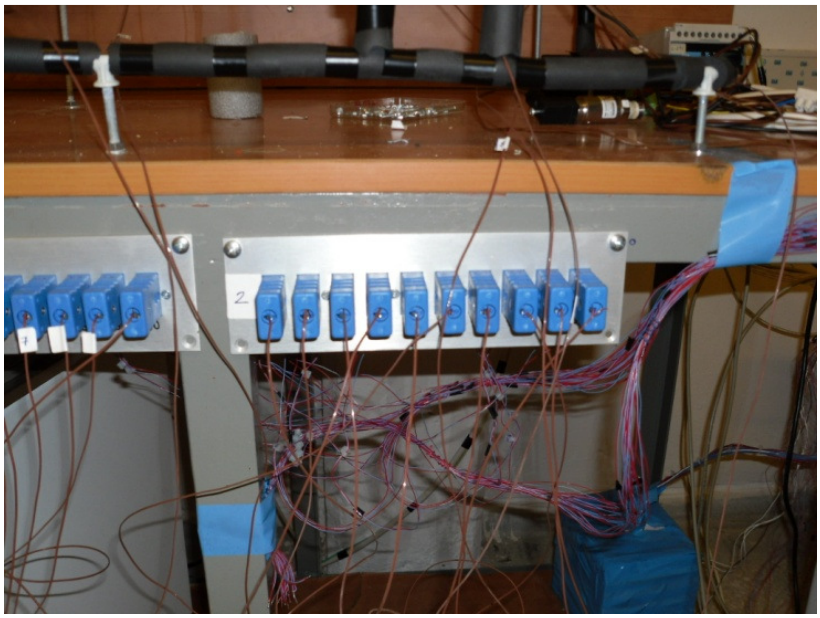

Figure 7: The photo of thermocouple plug panels

2.4.3 Refrigerant (R-134a) Cycle

For the refrigerant cycle, the upper horizontal part of the frame structure was selected. In the refrigerant cycle, 1/4” (1/4 inches, 6.35 mm) outside diameter copper tubes are used to connect the devices and form the cycle. The material of the tubes was copper due to the fact that it does not react with the refrigerant flowing inside and it can resist low temperatures and high pressures. The test section, which is also part of refrigerant cycle and placed on the upper horizontal part of the frame, is explained in the “Test Section” part. In this sub-section, the preparation of the refrigerant cycle from the exit of the test section to the inlet of test section is presented.

As it is seen in Figure 3, at the test exit of the refrigerant cycle, the temperature should be measured. For this purpose, a thin RTD and a thermocouple were placed there. The RTD probe was added to the cycle by a pipe tee, which is also made of copper and welded by oxygen welding to the copper tubes forming the cycle. RTD probe was put along the flow to read the temperature value from the

fluid whereas the thermocouple was fixed with aluminum tape on the outer wall of the copper tube, thus it read the temperature at the surface not at the fluid flow.

At the refrigerant cycle, refrigerated circulating baths came after the test section and temperature measurements. Since the volume of the bath (7 liters) was very large and the refrigerant coming from the test section was predicted to be two-phase or superheated vapor, keeping the vapor-phase refrigerant inside the bath was considered to be impossible due to the possible leakage problems from the hatch of the bath. Instead, it was decided to prepare a helical coil of the copper tube to act like a heat exchanger inside the bath. To cool the refrigerant flowing inside this helical coil, it was needed to fill the bath with another fluid – in liquid phase –, thus bath would cool this fluid, and it would cool the refrigerant. The helical coil was prepared longer than it had been planned because of the possible risks of not cooling the refrigerant enough. It was prepared in the department's laboratory, so any modifications could be made easily and quickly. To provide the cooling of the refrigerant, deionized water and ethylene glycol mixture was put inside the bath. Under normal conditions, deionized water has a freezing point of 0ºC and ethylene glycol has a freezing point of -11.3ºC. However the mixture of these two fluids has a lower freezing point. The bath has a minimum critical temperature of -44ºC, a minimum operation temperature of -40ºC, and in the experimental conditions the refrigerant was considered to have minimum saturation pressure as atmospheric pressure at which the saturation temperature is -26.3ºC. Therefore, the freezing point of the mixture inside the bath should be below -40ºC not to freeze, which may cause a decrease in performance or worse, failure in the bath. Thus, 66% ethylene glycol, 34% deionized water mixture (volume basis), which has freezing point between -45ºC and -50ºC [47], was prepared as the bath fluid. The bath and the upper part of the coil heat exchanger are given in Figure 8.

Figure 8: The refrigerant bath and the coil heat exchanger

At the exit of the bath, necessary connections were made to measure the temperature with both an RTD and a thermocouple, similar to the exit of the test section. The temperature measurement at this point is very important in terms of knowing the state of the refrigerant and being able to adjust the temperature to get the desired values at the other points of the cycle. Therefore, it is invaluable for the experiments to continue successfully.

The refrigerant is highly evaporative and at vapor state at room conditions, in addition to the fact that it can mix with air easily. A charge valve was needed to prevent this mixture with air and fill the refrigerant side with that fluid. The valve connection was made by pipe tee with welding. The coolest part of the cycle is the flow inside the bath; therefore, the charge valve was placed at the exit of the bath just after the RTD. During the experiments, it is desired to know the state of the refrigerant at specified points, and for the initial flow the phase is an important parameter to be adjusted. To see whether the fluid is in liquid-phase or not, a sight glass was added to the system. It was also beneficial to achieve the cooling in the bath in terms of condensation performance after the refrigerant being

charged inside the bath. The sight glass had both side threaded joints and it was fastened with an internally threaded joint to the copper tube on which a countersink has been made to fit the sight glass and prevent leakage. On the other hand; an accumulation vessel was put between RTD and charge valve. The aim of the use of this vessel was to accumulate the refrigerant cooled in the bath and provide only liquid flow back to the system. In addition to the sight glass, in a manner of speaking, they acted as double-check.

It is important to cool and condense the refrigerant inside the bath so the smaller the volume at the first charge, the faster is the liquid refrigerant. To make the volume smaller, two on/off valves were put at the inlet and exit of the bath after the RTD, accumulation vessel, charge valve, and sight glass. The reason of the selection of the placement was to cool the charged refrigerant, to see the condensate and to decide the start of the circulation. These valves also had threaded joints and placed to the cycle with internally threaded joints and countersink made copper tubes like the sight glass. The section of the refrigerant cycle from the on/off valve at the inlet of the bath to the on/off valve after the sight glass is given in Figure 9.

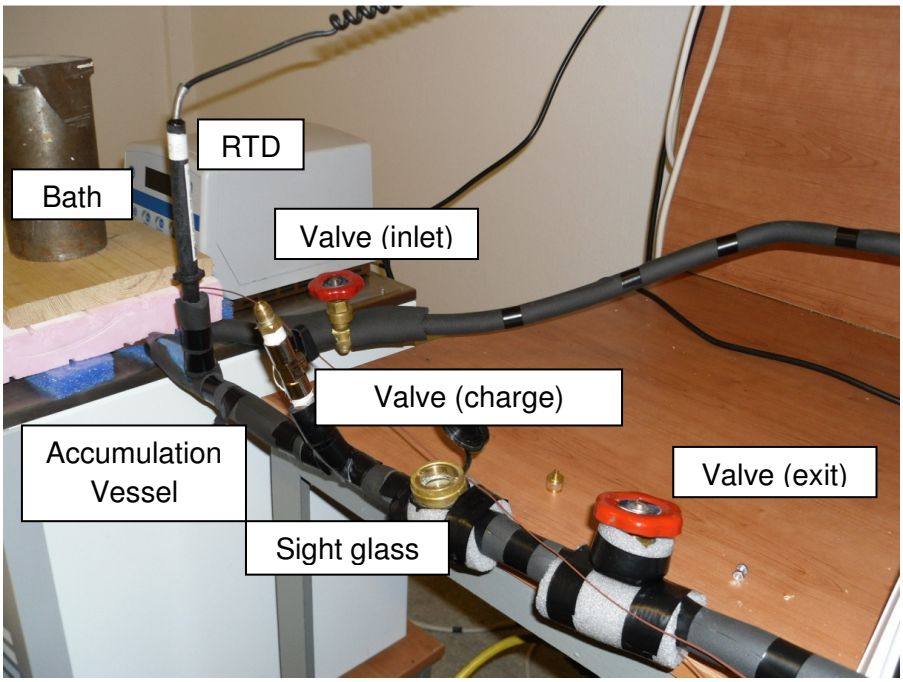

Figure 9: The refrigerant cycle (bath section)

After the sight glass and on/off valve, there comes the gear pump and the micro-flowmeter in the refrigerant cycle. The pump was placed after the bath exit and the accumulation vessel to make sure the phase of the fluid coming in was liquid. It was declared to operate in both phases but it gave better performance in single fluid phase and also there was the risk for the gears to wear out because the material of the gears was not steel, instead it was thermoplastic material PPS, Polyphenylene Sulphide, which has a tendency to wear out in two-phase flow. The gear pump system was embedded into the system serially and the connections were made by threaded joints. In order not to have problems with pump in terms of suction and discharge, mounting straight piping at the inlet and the exit was taken into consideration. The pump operated at different rotation speeds and it gave the opportunity to change the mass flow rate without changing the valve openings, and, without increasing the back pressure effect on the pump, which heats it up and decreases the operating life.

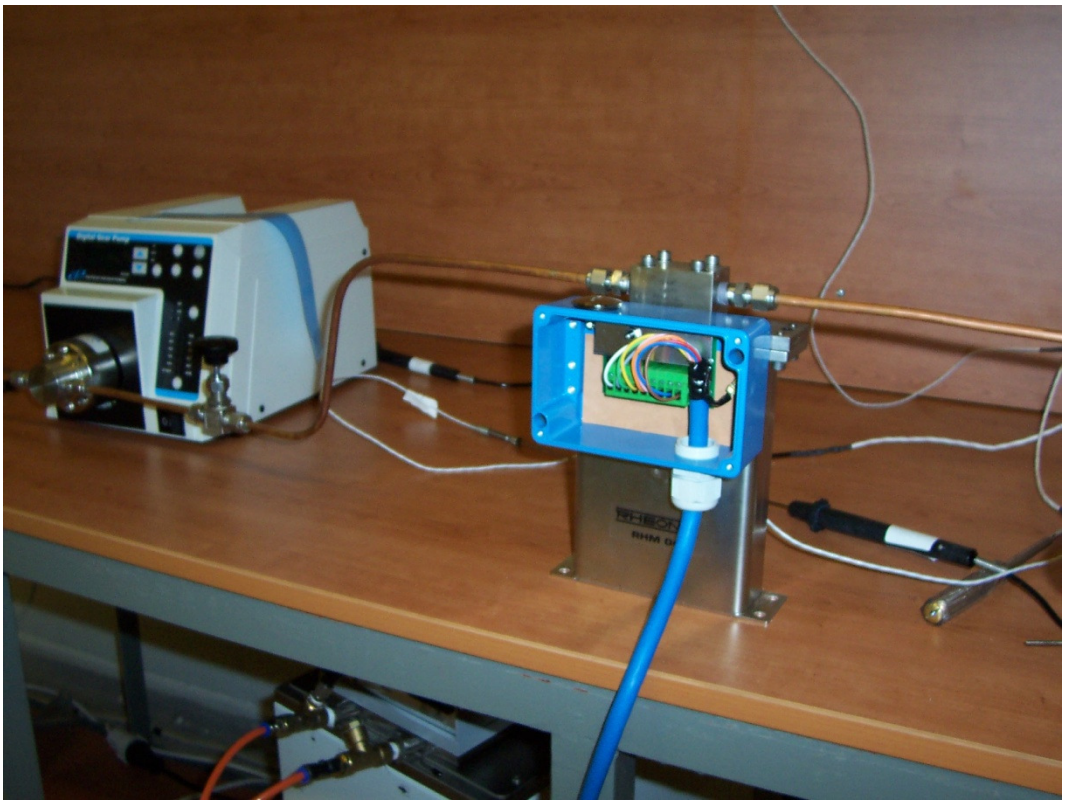

Figure 10: The refrigerant cycle (the pump and the flowmeter before by-pass line was added)

The micro-flowmeter was also connected to the cycle serially like the pump and after the pump. It was also fitted with threaded joints and pipes with countersink on to prevent leakage. On the other hand, valves were added to the inlet and exit of the flowmeter to make the “zeroing” at the first use and whenever needed. The use of the valves was strongly recommended by the manufacturer company in the operation manual and how to operate the zeroing procedure is explained in the “”Preliminary Tests” section. Moreover, straight pipes at the inlet and exit of the flowmeter were recommended with a length of 5 – 10 times the diameter of the pipe at the internal flow in order to minimize the variation of the flow speed. At the inlet and the exit each, 150 mm straight piping was prepared, which was much more than 10 times of the pipe outer diameter (6.35 x 10 = 63.5 mm). Besides, there must be single-phase (liquid) high velocity flow at the startup of the flowmeter, so a by-pass line was added parallel to the flowmeter to direct the flow there before opening the flowmeter valves in order to ensure the liquid flow. The by-pass line was prepared by placing pipe tees before the inlet valve of the flowmeter and after the exit valve of the flowmeter. These pipe tees were made of copper as well, and pipes were cut there and they were oxy-welded to the pipes. Copper pipes coming from both pipe tees were connected at the bottom of the flowmeter at the by-pass line with a valve to open and close that line when needed. This valve also had threaded joints. The pictures of pump and flowmeter (before by-pass line was added) are given in Figure 10 and the picture of flowmeter with the by-pass line is given in Figure 11.

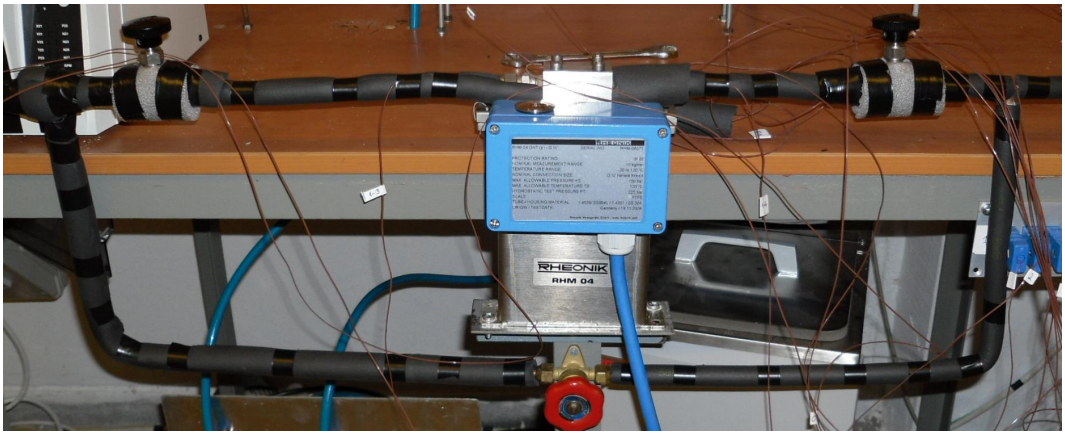

Figure 11: The photo of flowmeter and by-pass line

The refrigerant cycle continued with compact pressure transducer and RTD after the micro-flowmeter. The state at the exit of the flowmeter must be known in terms of temperature and pressure so there must be a single-phase (liquid) refrigerant flowing at that point since pressure and temperature are not independent properties for two-phase. The RTD connection was made the same as the other RTDs. The pressure transducer was also connected with a pipe tee which was oxy-welded to the cycle serially. Two ends of the pipe tee were for the refrigerant flow, the third one was for the transducer connection. The transducer had threaded joint as a fitting so a connector part, one end internally threaded and the other to be welded to the pipe tee, was used to place it to its location.

The refrigerant cycle was completed with the pre-heater after the measurements before the test section. To provide the ease of use and control, the pre-heater part was made from a resistance electrical heater which was placed in an electrically insulated cable and used by winding it around the copper tube. There were 4 alternatives with 4 different power values they could provide. These were 10 W, 25 W, 60 W and 150 W. The initial calculations showed that 60 W for pre-heater power would be sufficient, but when the possible future work, with larger flow rates or different fluids, it was decided to implement the 150 W cable to the system. The precision of the measurements would be worse with a larger scale but this problem was decided to be solved by calibrating the heat input to the refrigerant with the power input to the electrical resistance. The cable with electrical resistance heater inside that worked as the pre-heater is given in Figure 12 before and after winding.

Figure 12: The pre-heater before and after winding

The need for the pre-heater was, as mentioned before, to specify the quality value at the inlet of the test section. Therefore, it was desired to know the power input to the system and determine the state, so to control the heat input and know the value added to the refrigerant, a control unit was decided to acquire. The previously mentioned control box could control the power input both manually and automatically. To control the pre-heater from the computer, a multiplexer card was decided to be purchased, but it was delayed because of economical and technical problems and a power transducer was used instead. This power transducer read the power input values from the control box to the heater and it was transferred to the computer by the data acquisition unit. The output of the power transducer was in volts but the empty spot for current could be used by implementing a bridge to be able to read voltage. The control box and the power transducer photos are given in Figure 13.

Figure 13: The control box and the power transducer of the pre-heater

2.4.4 Water (Water + Ethylene Glycol Mixture) Cycle

The second cycle in the system was the one using water and ethylene glycol mixture as the working fluid. For the simplicity, it is mentioned as “water cycle” and “water side” within this thesis. In the experiments, the main area of interest was two-phase flow of the refrigerant; therefore it was needed to try to maintain constant wall temperature by adjusting the water flow rate. The temperature of the refrigerant would be almost (since constant temperature at phase change is a model, and it changes indeed even in small values) constant due to the phase change at the test section. If this condition can also be achieved for the water side, the heat transfer coefficient variation with respect to quality change can be studied for constant wall temperature approach. To minimize the temperature change of the water at the test section, the mass flow rate of water was designed to be much more than the flow rate of refrigerant. Also the heat capacity of the working fluid should be a large value and water satisfies this consideration. Moreover, the mixture has even larger specific heat value than water. The mixture composed of the same fluids like in the bath of the refrigerant because of the fact that the freezing point decreases at a considerable value. The lowest possible working pressure for the refrigerant was the atmospheric pressure, at which – as mentioned before – the saturation temperature was -26.3ºC. Considering that, the mixture was prepared as one-to-one, water and ethylene glycol, in volume basis [47] and the freezing point of the mixture was calculated to be approximately between -35ºC and -40ºC. Decreasing the freezing point was important in terms of making the temperature difference of the two cycles as small as possible at test section to provide the constant wall temperature boundary condition. The water cycle had been changed after the initial design in order to adjust the flow rate and temperature easily. This section is explained in terms of the new condition of the set-up which was given in Figure 5. As in the refrigerant cycle, the devices, fittings, and measurement tools are explained in this section from test section exit to test section inlet. Although it was thought to have minimum temperature difference between the fluids at the test section, counter flow was designed in order to increase the heat exchanger performance. These are presented in “Test Section”.

In the water cycle, a pneumatic hose was used to connect the devices and provide the flow because of the fact that it was easy to make connections, resistant to working pressure and temperature values, and it did not react with the working fluid. The geometry of the hose was 6 mm outer, 4 mm inner diameter. The fitting parts were selected to be compatible with the hose and the device connections. These fittings were elbows, pipe tees (for pneumatic hose), and one side threaded, one side hose entrance connectors. One of the most important aims to use pneumatic hose was that it did not need any welding process as in the refrigerant side and the length could be changed with respect to the positions of the devices easily and comfortably. The hose can operate at the temperatures in the range of -50 – +100ºC so any problem with the flow was not expected.

At the exit of the test section for water cycle; a pipe tee, which had threaded ends, was used to connect the RTD to measure the water temperature. This RTD was with a thicker probe and the threaded joints were 1/4". One of the threaded ends was connected with a fitting – one end threaded one end hose connection. After the temperature measurement with the RTD, the water cycle continued with the circulating bath. The inlet and exit connections of the bath were 1/4" threaded joints. For the inlet of the bath, a pipe tee was used because both the by-pass line and the test exit after temperature measurement came to that point. The pipe tee was with one end threaded, and two ends hose exit. The threaded end was connected to another pipe tee with three ends threaded. This was done to measure the temperature of the water mixture at the inlet of the bath. One end of the second pipe tee was connected to the circulating bath and the other was left empty for an RTD measurement. Since there was no RTD left for that location it remained in this stage of preparation. Water and ethylene glycol mixture is not evaporative like R134a at room conditions and it remains in liquid phase. Therefore, there was no other medium used to condition the mixture and it directly flowed into and out of the bath with the desired temperature.

At the exit of the bath the flow was not divided into two as in the inlet. The cycle continued with the pump after the bath. The temperature was measured at the exit of the bath with an RTD. It was also mounted by a pipe tee as in the exit of the test section. The importance of the temperature measurement at the exit of

the bath was the ability to know the conditions of the experiment and performance of the bath by providing the ability to compare the temperature with the bath temperature.

After the temperature measurement at the exit of the bath, the water cycle continued with the pump. The connections were threaded joints at both the inlet and exit of the pump. These joints were one side hose exit and one side threaded. The pressure of the water was measured after the pump by the compact pressure transducer of the water side. The pressure transducer was connected by a pipe tee which had two hose exits and one threaded end used for the transducer side. The flow was divided into two by a pipe tee after the pressure measurement. One branch was directed to the test section whereas the other returned to the bath inlet. For both branches, needle valves were placed in order to adjust the flow rate. These valves were both side hose connection. The one in the by-pass part was used to decrease the possible back pressure on the pump and the one at the test section side was used to adjust the flow rate during the experiments.

Rotameters were put along the flow serially for each branch after the valves. The rotameters had both sides threaded joints, so the fittings that had one side threaded and one side hose were used to connect them to the cycle. They were selected identical for possible parallel use to increase the flow rate at the test section. They were placed vertically because this orientation was needed for proper readings. To place them vertically stable in their position, an L-shaped aluminum sheet was bent in the department machine shop and the rotameters were stabilized to that sheet with plastic bracelets. The readings were done manually since the rotameters were mechanical and had no computer interface or electronic components.

Afterwards, the flow came to the test section through the hose from the rotameter and before entering the test section, the temperature was measured with a thick probe RTD like at the exit of the test section with proper pipe tee and threaded joints.

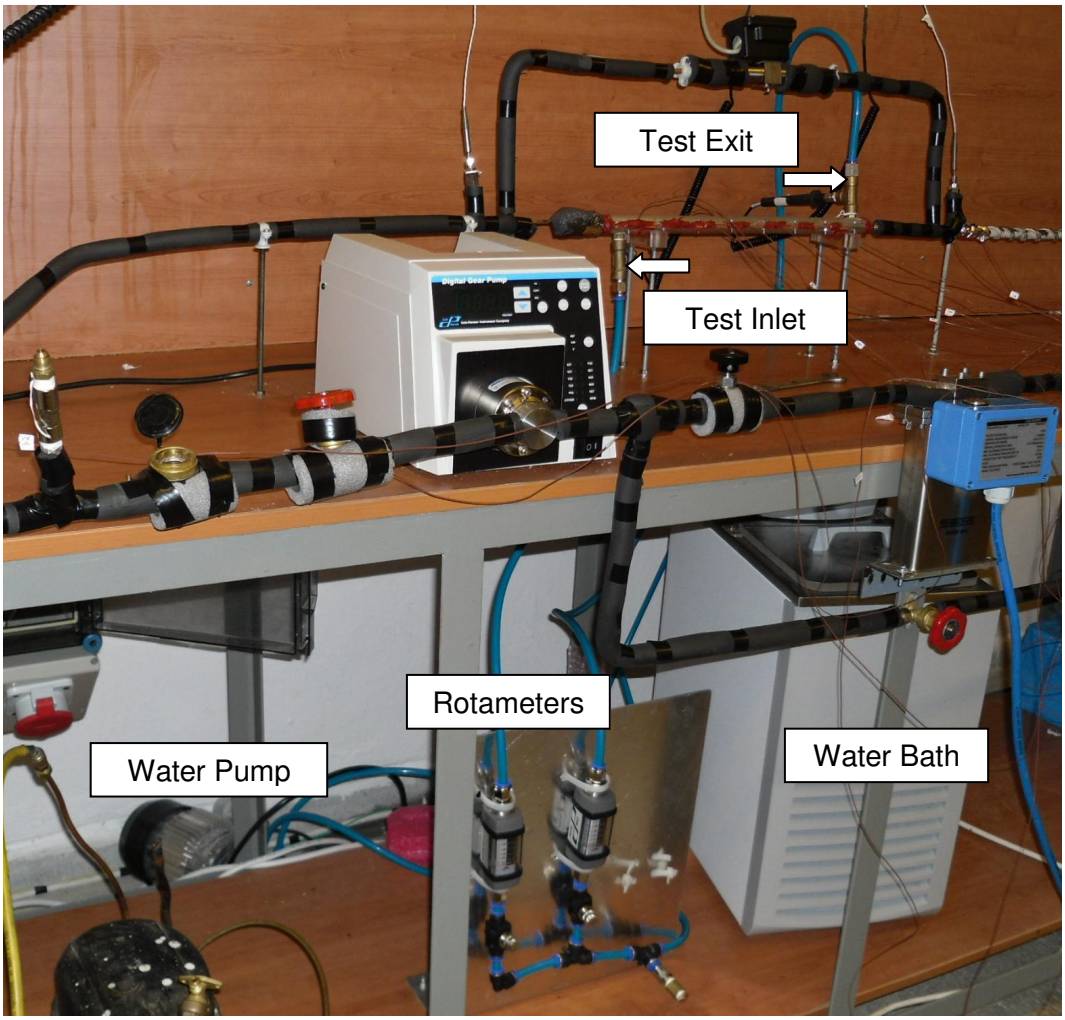

Figure 14: The water cycle

The hose was totally changed after the initial preparation of the system. The diameter, 4 mm, was not enough to compensate the flow rate that the rotameter could read, so the capacity was not used properly. Also the pump reached high temperatures, which was a risk for burn out or failure. Then, the hose was changed with another one of the same material having a larger diameter. The new one had 10 mm outer and 6 mm inner diameter. The picture of the water cycle with the changed hose and connections completed is given in Figure 14.

2.4.5 Test Section

For the test section in which the experiments would be made, many alternatives have been considered and a shell-and-tube type heat exchanger was decided to be built. The designs for the test section for the glass tube at the refrigerant side were made and until the manufacturing of these designs, a different version was mounted on the system to perform the leakage and preliminary tests. In this step, 5/8” outer diameter copper tube was used as the shell and 1/8” outer diameter copper tube was used as the tube side. The tube side was welded to the 1/4” copper tube that came from the pre-heater exit. After the heater and before welding the tubes and decreasing the diameter, there were 2 pipe tees placed for temperature and pressure measurements. The first pipe tee was for the RTD measurement. The 2 sides for inflow and outflow were welded to the cycle pipes and the last side was welded to a one end threaded short pipe to connect the RTD. The second pipe tee was connected to the differential pressure transducer. All three ends of the pipe tee were welded and third end went to the high pressure side of the pressure transducer. Since the transducer is differential, which means that it measures the difference of the pressure between two points, it was connected parallel to the test section along refrigerant flow. Therefore high pressure side was joined to the inlet side of the refrigerant at the test section. The low pressure side (exit) of the differential pressure transducer was welded to the exit of the test section by a pipe tee.

For both sides of the transducer, threaded joints were used with pipes having countersink at the ends. The exit of the test section was welded to 1/4” copper tube before it was welded to the pipe coming from pressure transducer by a pipe tee. The differential pressure transducer had been used because of the fact that it directly gave the value of the change in pressure at the test section for the refrigerant flow. After the pressure transducer low pressure side connection, the temperature at the exit of the test section was also measured by a thin probe RTD as in the inlet side. The outer pipe and the inner pipe were connected at the ends of the test section by welding with copper made covers. There were temperature measurements for the water side before and after the test section as well. These measurements were done with RTD probes. In the initial set-up,

water side connections were made with the initial hoses (4 mm inner diameter) and then they were modified as mentioned in the water cycle preparation. The test section at the first preparation is given in Figure 15.

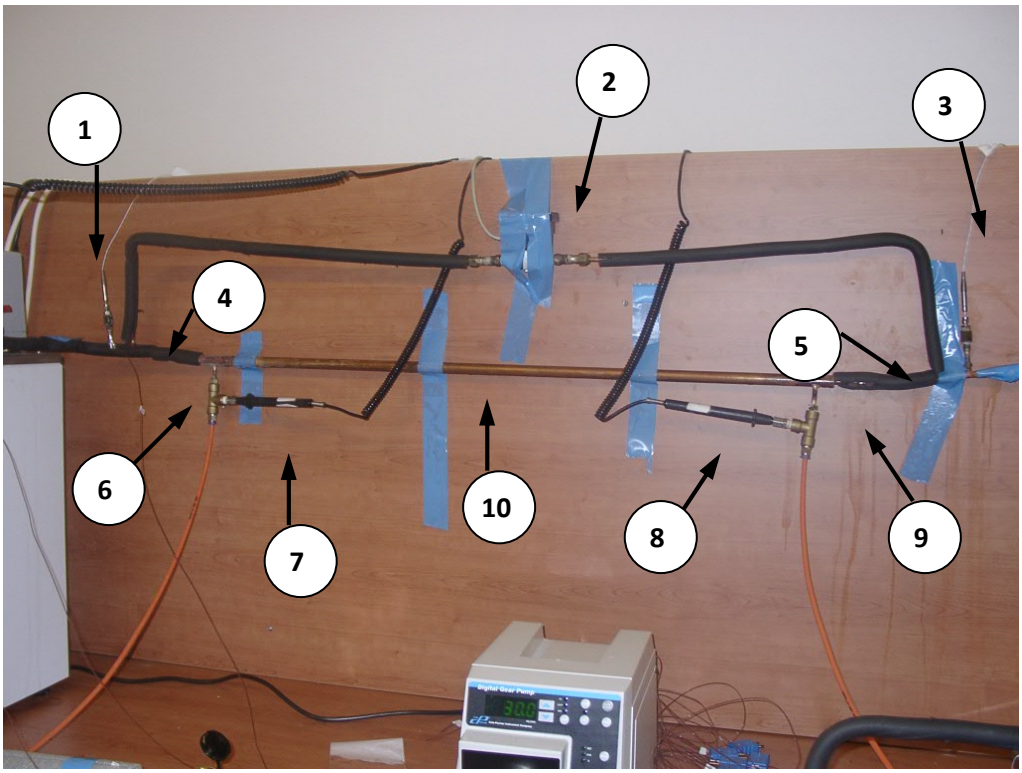

Figure 15: The photo of the test section at the initial preparation

1- Refrigerant test exit RTD
2- Differential pressure transducer
3- Refrigerant test inlet RTD
4- Refrigerant test exit
5- Refrigerant test inlet
6- Water test inlet
7- Water test inlet RTD
8- Water test exit RTD
9- Water test exit
10- Test section (shell and tube heat exhanger)

The design for the desired test section was composed of the test tube in which refrigerant will flow and the shell in which the water mixture will flow. The length of the test section was determined at the initial preparation and the design of the

shell was made according to it. The shell was made as a combination of identical parts. They were joined together by bolts and nuts to form the shell and the two flanges for the ends of the shell were designed in order to close the water side. The reason of two separate parts in the shell was to be able to get the temperature readings on the test tube wall. Thermocouples were placed on the wall at 7 different locations along the test tube and they were planned to cross the shell and leave it from small intervals left at the connection part of the shell sides. Measuring the wall temperature was very important for the experiments because themeasurements would be used to determine the availability of the constant wall temperature approach, therefore two-phase heat transfer coefficient for the constant wall temperature approach could be calculated and the variation of the heat transfer with quality could be revealed, which was one of the important motivations for the study. The technical drawings of the shell and flange to be used to form the shell are given in Appendices D.1 and D.2. The material was selected as aluminum since it was lightweight, easy to machine and available to be manufactured in short term.

After the leakage and the preliminary tests with this orientation, the test section was be changed with the glass tube and the shell designed for the experiments. These tests are explained in the next section.

2.4.6 The Leakage and Preliminary Tests for the Initial Design

2.4.6.1 The Leakage Tests

The most important part after the establishment and before the operation of the set-up was the leakage tests, which is a must for the proper operation of the closed-flow systems, and they were performed during the experiments after each modification or change in the system. These tests were done in the same way for each and every case.

The leakage tests were performed in two steps. These were tests for the water side and the refrigerant side, respectively. For the water side, the observation of any leakage was relatively easier because of the liquid phase of the mixture

(water + ethylene glycol). The bath was filled with the mixture and after the connections were checked, the bath and the pump were started to operate and the flow was observed. The bath had its own circulation pump; it was needed to operate the bath together, otherwise it could block the flow and cause the pump and the liquid to warm up. At some of the junctions, lakage was observed. The reason was the non-straight cutting of the hose. The flow was stopped and the hose was either changed or cut straight to prevent leakage. As a result, the leakage tests for water side were performed and no-leakage condition was provided with proper arrangements easily.

At the refrigerant side for the initial preparation, there was no need for the flow during the leakage tests; therefore the pump was not operated. On the other hand, the refrigerant available was in limited amount, so the leakage tests were performed by charging air into the cycle. The cycle would operate at clean conditions; therefore before pressurizing the refrigerant side, vacuum was applied in order to remove the humidity and possible residues from manufacturing or welding. After the vacuuming process, the cycle was filled with compressed air up to 10-12 bars. This value was not beyond the maximum operating pressure of the devices. The compressor and the charge valve were closed and the pressure was checked with a pressure gauge. Any pressure loss or larger leaks were determined easily and were closed by either fastening or welding in terms of their connection types. Then the system was again pressurized to a high pressure value. Smaller leaks occurred and the rate of air flowing out of system was considerably very low. At that point, bubbles made of detergent and water were used to find the locations of the leakages. It was a long and tiring process to prevent all leakages, but the no-leakage situation at the refrigerant side was then accomplished. Afterwards, the system was charged with the refrigerant and both cycles got ready for the preliminary tests.

2.4.6.2 Data Acquisition Process and the Preliminary Tests

When the leakage tests were completed, the data acquisition and preliminary tests were prepared. For the data acquisition process after the mounting of the RTDs, the thermocouples, and the transducers (power and pressure) to the

cycles; the connections to the data logger were done. The RTDs and the thermocouples were attached to the voltage slots and the power and pressure transducers were attached to the current slots. The calibrations of the measurement devices were done in Arçelik, and are presented in the "Calibrations" section. Also the computer interface used for gathering the data according to the data logger connections and connection types were installed by Arcelik to collect the experimental values. HP-VEE was used to create the interface and the flowchart to gather the data. The program was set in order to acquşre data every 15 seconds and that would be beneficial for steady-state determination and understanding the response time of the set-up to the different variables. For the analyses in the experiments, the steady-state conditions were determined in terms of successful consecutive measurements being in the range of sensitivity of the devices at least for 50 times (about 10 – 15 minutes).

Before the preliminary tests, the charging of the refrigerant and the filling of the baths with water and ethylene glycol procedures were done. For the water side, the mixture was used to decrease the freezing point as mentioned in the previous parts. During the leakages tests, 7200 gr of deionized water was used in the water side. Ethylene glycol was not added in that step because water was much more than ethylene glycol in amount and for the possible leakage losses, this was not desired. The water was discharged until about 3500 g was present in the bath. The minimum working temperature for the refrigerant was estimated to be -26.3ºC, the saturation temperature at atmospheric pressure, so, the volumetric mixture ratio of 1:1 was selected in order to decrease the freezing point to -37ºC [47]. The density of the ethylene glycol is 1.123 times the density of water at room conditions [47], so 3950 gr (± 30 gr) of it was added to the deionized water.

For the refrigerant side, the bath was filled with water and ethylene glycol mixture as well. The cooling of the refrigerant was provided by the heat exchanger placed inside the bath as mentioned before. The minimum working temperature of the bath was -40ºC and with a 2:3 of mixture of water and ethylene glycol (respectively) in volume, the freezing point of the mixture was decreased to -55ºC [40]. Then the refrigerant was charged from the charge valve. The valves at the inlet of the bath and after the sight glass were closed to cool the refrigerant in the

bath. The bath was operated and the refrigerant was to become a liquid and vapor mixture after the cooling. The pressure of the cooled refrigerant decreased and the charging could go on until the entire refrigerant inside condensed. The pump was compatible with single and two-phase flow but for the flowmeter, it was suggested to circulate liquid at high flow rate for at least 15 minutes at the first operation and also for the experiments, single phase flow was strongly recommended to get correct and accurate readings. To eliminate any risk of two-phase flow from the flowmeter, the by-pass line was left open and the inlet and exit valves of the flowmeter were closed. When the valves next to the bath were opened, the phase change could be seen from the sight glass that the liquid refrigerant vaporized because of the instantaneous increase in volume. After the verification of proper functioning of the data acquisition system and no leakage situation, the insulations of the pipes, connection points and the test section were made. The charge of the refrigerant increased the refrigerant side pressure to 5 – 6 bars. High pressure for the refrigerant was useful in terms of achieving liquid phase (high pressure = high boiling temperature). When there was two-phase refrigerant present inside the cycle as observed through the sight glass, the micro-flowmeter inlet and exit valves were closed. At this stage, the pump was started and the flow followed the by-pass line and the test section before coming back to the bath.

The water side was also started with the operation of the bath and the pump. The measurements were checked and when there was no leakage, the temperature of the bath was adjusted to cool the refrigerant side at the test section to have liquid refrigerant along the cycle. After the circulation of the water at low temperatures, the temperature of the refrigerant got low and the liquid amount in the sight glass increased. When the sight glass was totally filled with liquid, the flowmeter valves were opened and the system started to work in total. To prevent the instant changes inside the cycle, the by-pass line was not closed at the same time, but closed slowly in a while. After that procedure, the pump speed was increased to maximum to provide 15 minutes high flow rate in liquid phase. Then, the instructions in the manual of the flowmeter were applied and the zeroing was performed. The preliminary tests were finished with the analyses of the gathered data as a first study with the readings.

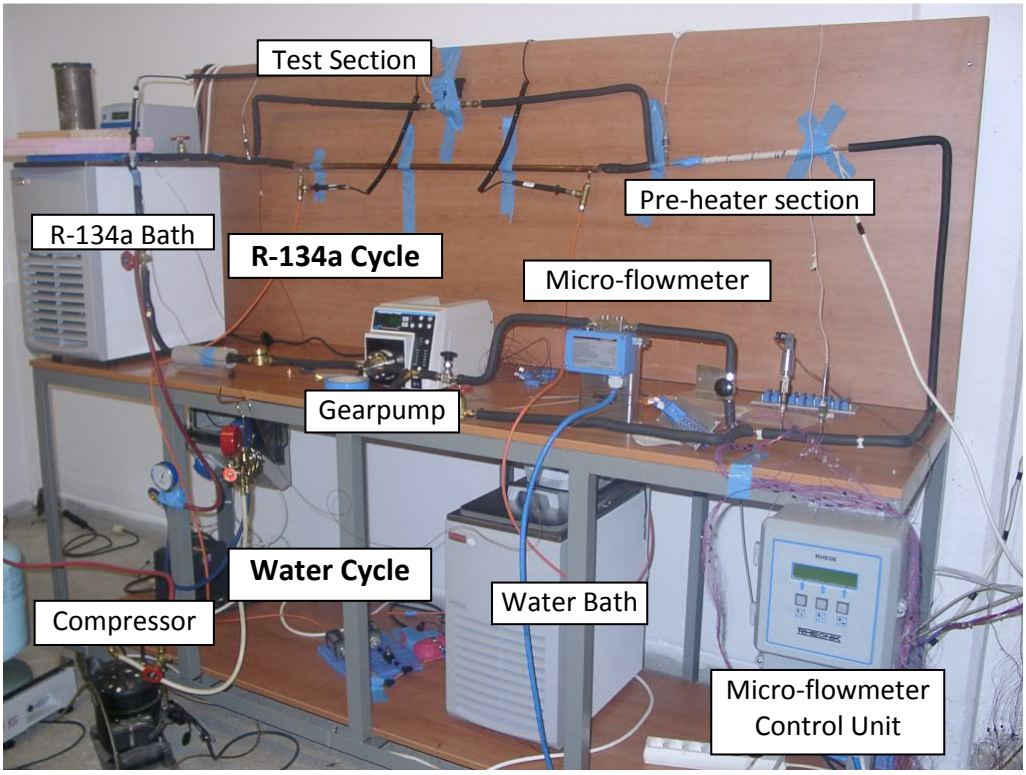

Figure 16: The photo of the set-up after the preliminary tests

The condition of the experimental set-up and the placements of the devices at this stage are given in Figure 16. Both of the cycles were closed and the flows for the cycles were performed successfully before the actual experiments.

2.5 MODIFICATIONS

When the preliminary tests were accomplished, the next stage was the change of test section with the glass tube and the shell made for it. During the preliminary tests, it was observed that the water pump did not operate properly and it heated up in the experiments. Therefore a second by-pass line for the water side was added to decrease the back pressure on the pump. There was a valve on that section as well, to adjust the flow rate and the pressure of the water side. The accumulation vessel on the refrigerant side was removed to decrease the volume

and also it was not useful in terms of liquid sustain to the pump because each time at the initial operation of the system, two-phase flow was observed. The final version of the schematic view of the set-up is given in Figure 17.

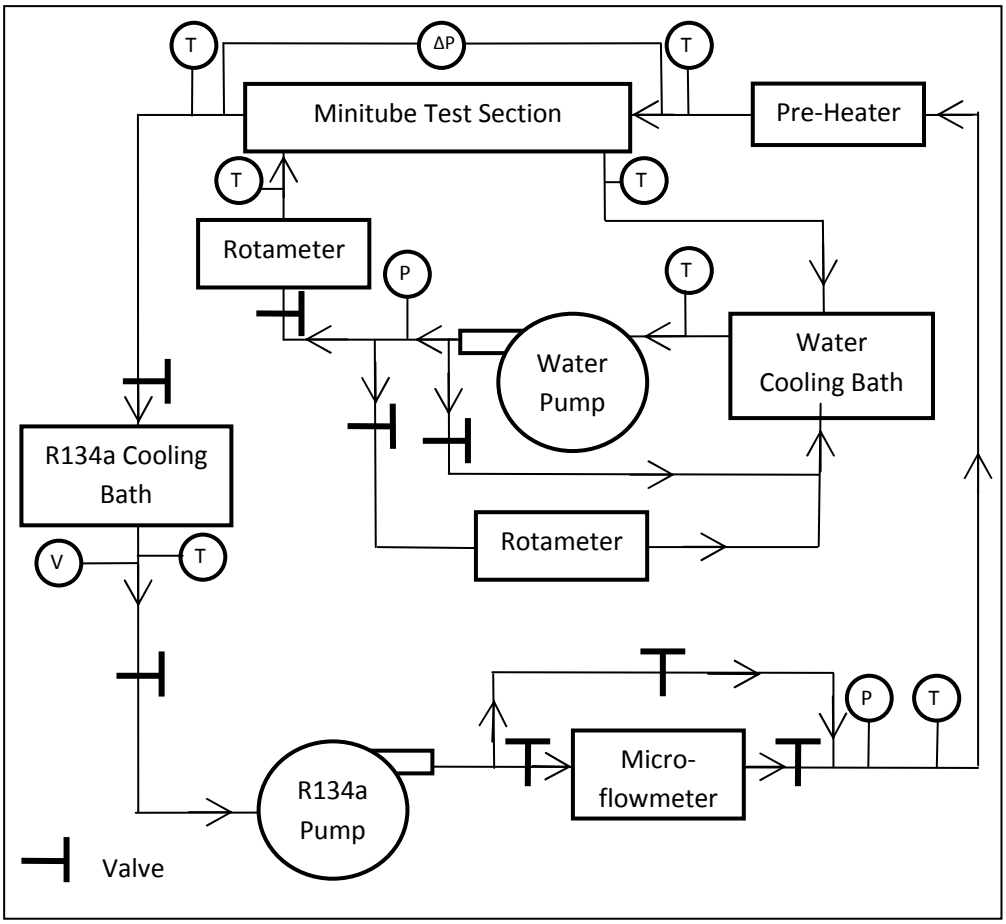

Figure 17: The schematic view of the set-up in the actual experiments

2.5.1 Ring and Bumper Design for the Glass Tube

When the glass tube and the aluminum shell were mounted on the system, the connections of the glass tube and the copper tube had been considered in terms of easy and effective fittings. The copper tubes at the inlet and exit before and after the test section had 1/8" outer diameter, which were welded to 1/4" outer diameter copper tubes that formed the cycle. The glass tube had 3 mm outer diameter which was close to 1/8" (= 3.175 mm), therefore threaded adapter parts

were decided to connect glass and copper tubes. These adapters were composed of 7 parts. One main part in the middle in which the ends of both tubes entered, two conical parts (one for each side) called “ring” prevented leakage, two bumper parts (one for each side) protected the ring from torsion and two head parts (one for each side) joined the main part by threads and fix the tubes inside the main part to maintain the connection. The ring and the bumper were the parts that touched the tubes. When the fitting was made, the glass tube broke because of the metal ring and bumper. The head applied force on these parts to maintain the connection and prevent leakage but metal parts broke the glass.

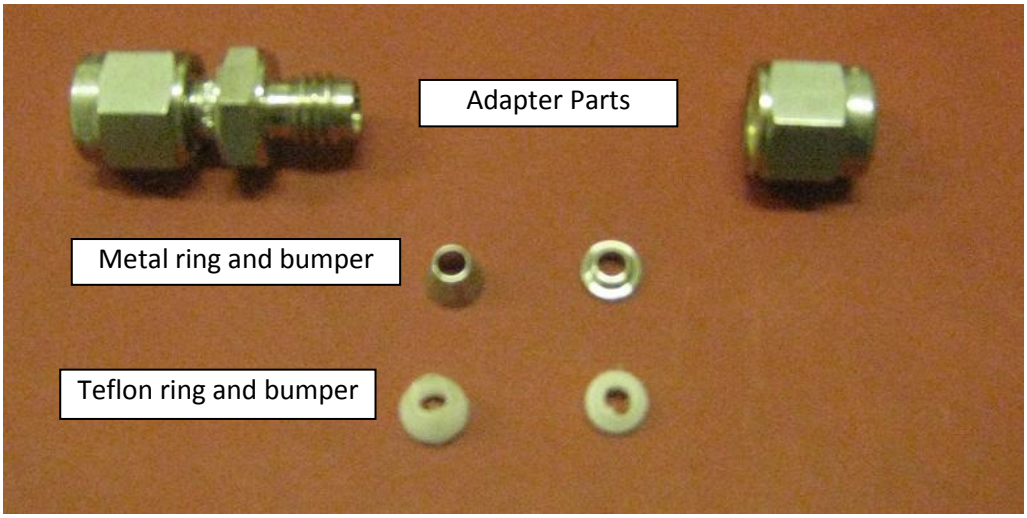

Figure 18: The adapter parts for glass - copper transition

The glass tube at the test section was changed with a new one and the problem occurred again. When the head was fastened the glass tube broke again and when it was not fastened tight there was leakage. Therefore, it was decided to manufacture the ring and the bumper parts from a softer material. The technical drawings for these parts were prepared, which can be seen in Appendix D.3. The material was selected as polytetrafluoroethylene (Teflon) due to its softness and machinability. The parts were manufactured according to the technical drawings in the machine shop of the department. The rings and the bumpers made of metal and Teflon are presented in Figure 18 and the glass copper transition with the adapter part is given in Figure 19. The two-part shell was not closed at that stage in order not to apply force on the glass tube before making copper

connections. The leakage tests were repeated after the connections and before closing the water side.

Figure 19: The adapter parts mounted on the cycle

Before closing the shell side, thermocouples were fixed on the glass tube by pasting with a glue that can operate at low temperatures. To provide no-leakage on the water side, O-rings were used in the flanges and gaskets in the shell. Thin openings along the shell at 7 points were made on the gaskets for thermocouples. After two separate parts of the shell were bolted to each other, silicone was applied by a silicone gun on the joints, openings and around the flanges to prevent any possible leakage. This silicone was selected in terms of pressure and low temperature resistance. The test section with the silicon applied is given in Figure 20. The photo was taken before insulation so the thermocouples coming out from the shell can be seen. Red parts on the shell are the silicone applied regions; blue hoses are water inlet and exit, while black cables are the RTD cables that go to the data logger. The red silicone is seen on the flanges too.

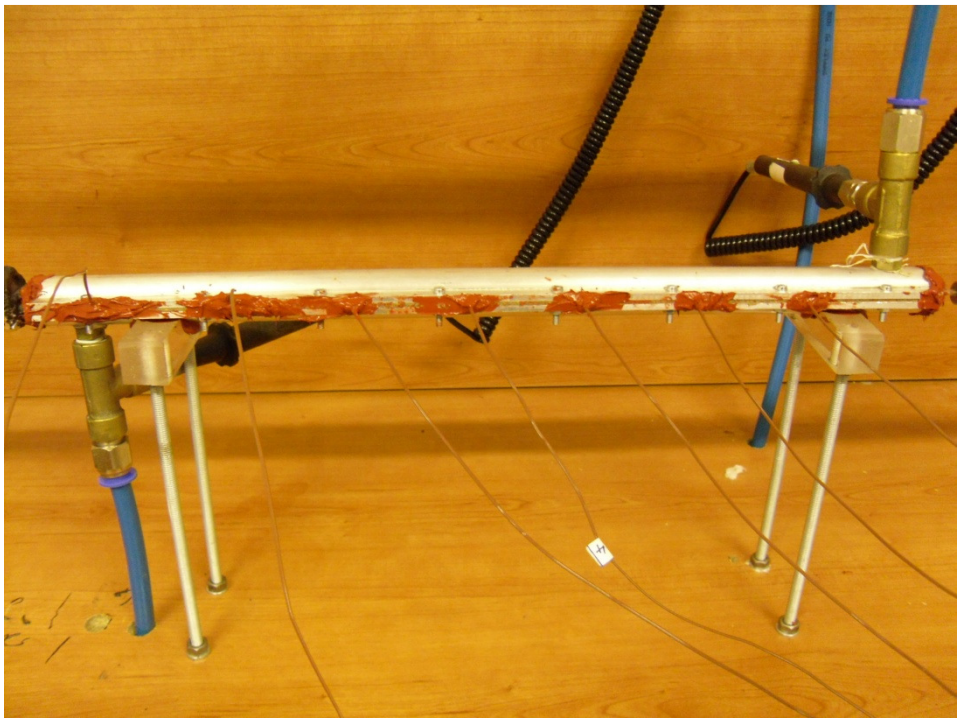

Figure 20: The test section after the shell was closed with bolts and silicone

2.5.2 Leakage Tests for the Glass Tube

The experiments were to be started after the construction of the test section with the glass tube and the aluminum shell. When the aluminum shell was closed and fixed to the set-up frame with silicone, the glass tube could not handle the stress and it broke as before the adapter parts were used. As the shell side was open and the flanges were not fixed to the glass tube, the longitudinal and lateral forces on the glass tube were compensated with the bending of the glass tube. Yet, after the procedure was followed and water side was closed as well, glass tube crashed down. For the sake of experiments, the glass tube was changed with a new one and the procedures were done from the beginning. The shell and the adapters were taken apart, the silicones were removed and the remaining was cleaned. The shell was placed on two Plexiglas housings as it is seen in Figure 20. The height could be adjusted but the lateral and longitudinal effects could not be handled since it was fixed to the ground with threaded parts and nuts. The connections were made again and the adapter parts were not fastened

so tight not to break the glass again. But when it was not tight, there was leakage because of the gas phase and high pressure of the refrigerant. The adapters were become tighter and there was a considerable effort in order not to break the glass tube again. When the no-leakage condition was satisfied, the insulation of the test section was needed. In any small touch while covering the test section with insulation material, the glass tube kept on breaking. For three more times the procedure was repeated but every time the glass was broken at least in the insulation process. At the last time, the glass was broken at the end of it, where it entered the adapter; then, it was decided to fill the adapter part with glue which was resistant to refrigerant, low temperatures and high pressures. A cylindrical mold to hold the glue was prepared and the adapter and the joints were filled with the glue. The leakage was decreased but it was observed that the rate of decrease in pressure increased in time. The pasting operation was also repeated again and again but the leakage problem could not be solved. The photo of the solidified glue can be seen in Figure 21.

Figure 21: The exit of the test section with solidified glue at the adapter

For the closed system of both sides, the experiments could not be conducted when there was leakage. Otherwise, the results would have deviated significantly because of the improper measurement of mass flow rate. The glass tube had been selected for the possibility of flow visualization; however, since the main aim of the set-up was to investigate multiport minichannels after the verification of the experimental set-up, the test section was decided to be change, as explained in the next section.

2.5.3 Copper Tube as a Replacement for the Glass Tube

The leakage problem with the glass tube could not be solved. Since the problems occurred due to the brittle structure of the glass material the most suitable replacement for the glass tube was considered as copper tube having 1/8” outer diameter. The threaded joints were one of the sources of leakage as well, so 1/4” diameter copper tube was decreased to 1/8” diameter copper tube before the test section.

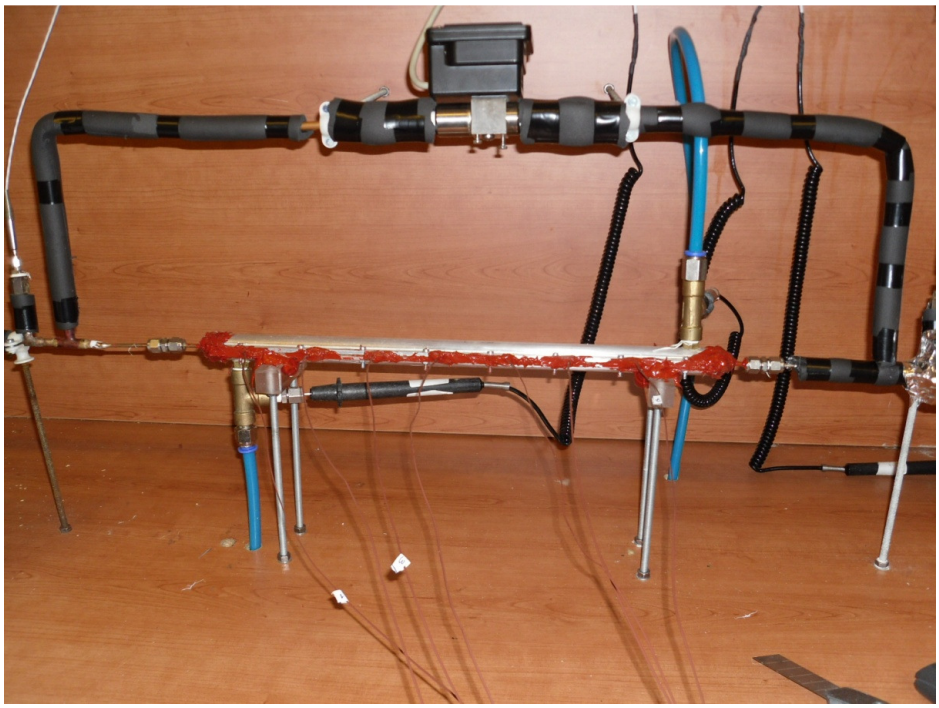

Figure 22: The test section with the copper tube

The internal diameter for the glass tube was 1.8 mm and the copper tube had 1.65 mm outer diameter. Therefore the change wwould not affect the heat and mass flux in a significant amount. The outer diameter change caused the change in the holes of the flanges. These holes were widened from 3 mm to 3.2 mm. Thus, the copper tube with 1.65 mm internal diameter and 3.065 mm outer diameter – about 1/8" (=3.175 mm) – were put to the test section. The test section after the replacement is presented in Figure 22.

The connections of the cooper tube were accomplished with welding it to the same diameter copper tube at the inlet and exit of the test section. The water side was the same – two-part shell and two flanges – and the no leakage condition was achieved easily with welding. The insulation of the test section and the tubes were made and the system became ready for the experiments. The insulated test section is given in Figure 23.

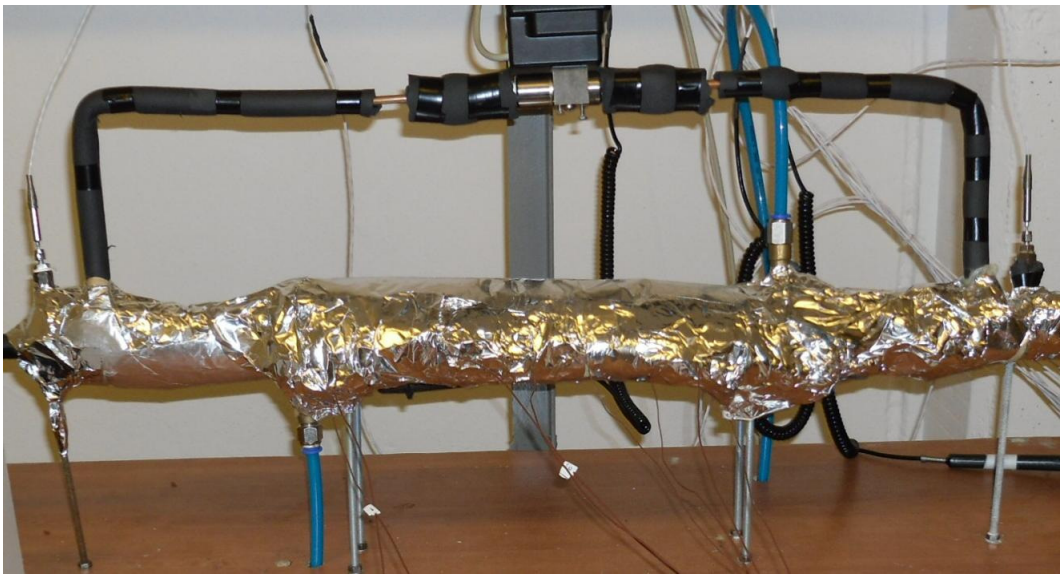

Figure 23: Test section with copper tube after insulation

2.6 CALIBRATIONS

The calibration of the components in the set-up can be investigated in two main parts: Calibrations of the measurement devices and calibrations of the losses from the parts that affected the experimental results.

The calibration of the micro-flowmeter had been done before the purchase by the company and the mass flow rate of the refrigerant was read from the transmitter unit. The transfer of this data to the computer could not be done because it needed a special card on the data acquisition unit, and the card was not acquired due to the economical reasons. The value was collected manually from the transmitter in unit of g/s. The rotameters were mechanical and they were calibrated default for liquid flow. The volumetric flow rate was read manually from the rotameters in l/min. The other measurement devices were the pressure measurement devices and the temperature measurement devices.

The losses from the system to the surroundings were important in terms of having proper readings and measurements to calculate the desired quantities correctly. There would be losses from all the components and pipes along the cycles. On the other hand, only the losses that affect the test section were taken into consideration since they designate the experimental results. These losses were the losses from the pre-heater and the losses from the test section. The pre-heater gave heat power input to the refrigerant but the given power could not be transferred to the refrigerant with 100% efficiency. The input power was very important in terms of finding the quality of the refrigerant at the inlet of the test section, thus the calibration of the pre-heater in terms of losses were done. The losses from the test section were calculated in terms of two different components. In total it was the loss from the water to the surroundings, since the refrigerant flowed inside the tube, the loss was from water side. It was composed of the loss and the viscous heating. In the subsections, these calibrations are explained in more detail.

2.6.1 RTD and Thermocouple Calibrations

The calibrations of the temperature measurement devices were done in Arçelik laboratories [48]. This subsection was prepared based on their study. For the calibration of thermocouples and RTDs, a cooling bath and a reference temperature measurement device (a reference RTD) were needed. The thermocouples and RTDs, which were to be calibrated, were put in the bath with the reference RTD. The temperature measurement data from all the devices were taken with varying bath temperatures. Based on the results of the reference RTD, the calibration constants for thermocouples and RTDs were found with curve fitting methods. The temperature intervals in the calibration should be determined according to the operation temperature range and the type of the temperature measurement device. The calibration values should be scanned in small temperature intervals at the operation temperature range and it can have larger temperature difference out of the range. The temperature curves for all RTDs and thermocouples were acquired. The curve fitting for all was linear and the constants of these calibrations were installed to the computer program. A sample calibration curve for an RTD is given in Appendix E.1.

2.6.2 Transducer Calibrations

The transducers used in the experiments were one differential pressure transducer, two compact pressure transducers and one power transducer.

The power transducer gave 0 – 10 V voltage output and measured 0 – 1000 W power values. This transducer was connected to the control box that adjusts the power input to the pre-heater. The output of the power transducer was connected to the empty current slot in the data logger cards and a bridge resistance was used to convert the voltage output to current so it could be read by the data logger and transferred to the computer program. The connections and the modifications in the reader card were done by Arçelik. The voltage to watt constant for the power transducer was 100 and it was written to the program as an input to read the correct values. The accuracy of this value was not important, because fırther calibrations were made for the pre-heater.

The calibrations of the pressure transducers were also performed by Arçelik in their laboratories in Istanbul. The calibrations for compact pressure transducers (CPT) were done together since they were identical and had the same range. A reference measurement device, reference pressure transducer (PT) was used and the CPTs were connected to a system in parallel with the reference PT. The pressure in the system (pressured nitrogen gas in a closed pipe with valves to control the pressure of the system) was varied from 0 to 200 psi which was the range of the CPTs. The variation of the pressure was first increasing from 0 to 200 psi and then decreasing from 200 to 0 psi. The outputs of the CPTs in the unit of mA were recorded for both of them, separately – although they were identical CPTs, each had to be calibrated. In the calibration process, 1 psi increments were used for the range of 0 – 15 psi and 5 psi increments were used for 15 – 200 psi values. The output of the CPTs were 4 – 20 mA and the pressure values corresponding to the output milliamperes were drawn and curve fitting was applied to designate the constants. For the two transducers, which would be used in refrigerant and water sides to measure the pressure, the following equations, for CPT 1 and CPT 2 were acquired, respectively.

$$P\ [psi] = 12682\ I\ [mA] - 50.417 \tag{14}$$

$$P\ [psi] = 12705\ I\ [mA] - 50.520 \tag{15}$$

In addition to the CPTs, the calibration of the differential pressure transducer (DPT) was accomplished, which would be used to determine the pressure drop at the test section. The range for the DPT was 0 – 5 psi (= 0 – 0.34 bar) so the calibrations were performed for this range. The reference PT that calibrated the CPTs had one exit, whereas the DPT had two sides, high pressure and low pressure sides. So while performing the calibrations, the high pressure end of the DPT was connected parallel to the reference PT and the other end was released open to the atmosphere. For the first value of the DPT, which was “0” bar, the high pressure side was not pressurized and the current output corresponding to this “0” pressure difference condition was recorded. Then for the increasing temperature of the high pressure side, the output current values were recorded

corresponding to the pressure values read. The effect of the atmospheric pressure was subtracted from the pressure value read at the reference PT so the calibration of the DPT was successfully completed. Curve fitting to the calibration results was also applied as in the CPTs and the following equation was obtained.

$$DP\ [bar] = 21.452\ I\ [mA] - 0.0878 \quad (16)$$

The calibration results and the calibration curves for the pressure transducers are given in Appendices E.2 – E.6.

2.6.3 Heater Loss Calibrations

The heater (pre-heater), was placed before the test section for two-phase experiments. Before explaining the calibration of the pre-heater, its purpose should be mentioned again. The temperature and the pressure of the refrigerant are measured at the exit of micro-flowmeter and for the state determination, these properties should be independent; therefore, at that location the refrigerant should be in liquid phase. For the two-phase flow, pre-heating was decided to be applied. To a known state, heater power is induced and the enthalpy of the refrigerant was increased until the desired quality was achieved. The quality designation was a significant process and there should be as much accuracy as possible. The pre-heater power, which was electrical resistance and wounded around the copper pipe before the test section, was selected as 150 W and a control unit was prepared to adjust the input power manually and automatically. In the experiments, the automatic control was not activated due to the technical problems of the related data logger card. The manually adjusted power input was transferred to the data logger by a power transducer and it could be read from the computer program. After the pre-heater was mounted on the system, it was covered with insulation material (Armaflex flexible thermal insulation made from Elastomeric foam based on synthetic rubber [49]). The thickness of the insulation material was 6 mm with a thermal conductivity of 0.040 W/mK. For the verification of possible heat losses, three thermocouples were placed along the pre-heater. One thermocouple was put on the copper pipe under pre-heater, one between the pre-heater cable and insulation – on the pre-heater, and one on the insulation. When the preliminary tests were being conducted, it was observed

that there was temperature difference between the two faces of the insulation, and the outer face of the insulation was at a higher temperature than the surroundings temperature, which meant there was loss from the heater section.

The calibration of the pre-heater was done with single phase flow of the refrigerant. The temperature and the pressure of the refrigerant was measured at the inlet of the pre-heater and to calculate the power transferred to the refrigerant from the pre-heater, the state of the refrigerant should be determined at the exit of the pre-heater. The temperature was measured at that position and for the state determination at the exit of the pre-heater, single-phase flow was needed.

When the control volume analysis was performed at the pre-heater section for the refrigerant, there was one inlet and one exit, no work, and positive heat transfer along the control volume as it is seen in Figure 24.

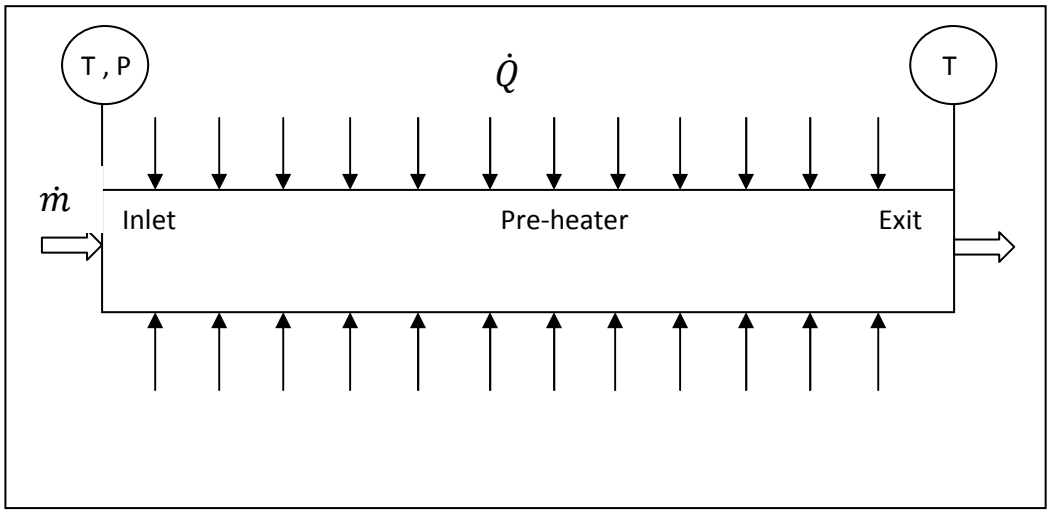

Figure 24: The pre-heater section of refrigerant cycle as control volume

The continuity equation for the refrigerant cycle at the pre-heater section is Eq. (8), since there was one inlet and one exit, with constant mass flow rate. The first law of thermodynamics for the control volume is given below.

$$\dot{Q}_{RI} = \dot{m}_R(h_{he} - h_{hi}) \tag{17}$$

In this equation; $\dot{Q}_{RI}$ is the heat transfer rate as input to the refrigerant at the pre-heater section, $\dot{m}_R$ is the mass flow rate of the refrigerant, h_{he} is the enthalpy of the refrigerant at the pre-heater exit, and h_{hi} is the enthalpy of the refrigerant at the pre-heater inlet. The enthalpies of the refrigerant at the mentioned locations were determined with the pressure and temperature values. The phase of the fluid was adjusted by the pump and the bath to be liquid. The pressure at the exit of the pre-heater was assumed the same as the inlet because the pressure loss from the inlet to exit was calculated as negligible.

Table 1: The states for the calibrations of the pre-heater

Name	**Unit**	**Experiment 1**	**Experiment 2**	**Experiment 3**
Mass flow rate	g/s	1.50	2.30	1.96
R134a pressure	bar	4.61	3.39	3.61
Pre-heater inlet	ºC	4.70	-2.55	-2.07
Inlet enthalpy	kJ/kg	205.92	196.45	197.29
Pre-heater exit	ºC	12.58	-1.20	2.57
Exit enthalpy	kJ/kg	217.15	198.64	203.90
Pre-heater input	W	19.11	9.59	15.71
Pre-heater transferred	W	16.83	5.03	12.94

Name	**Unit**	**Experiment 4**	**Experiment 5**	**Experiment 6**
Mass flow rate	g/s	1.86	1.67	1.94
R134a pressure	bar	4.72	4.42	3.79
Pre-heater inlet	ºC	-0.27	-0.51	-4.97
Inlet enthalpy	kJ/kg	199.70	199.34	193.47
Pre-heater exit	ºC	13.66	10.91	5.70
Exit enthalpy	kJ/kg	218.96	215.14	207.72
Pre-heater input	W	39.13	32.75	32.81
Pre-heater transferred	W	35.78	26.34	27.65

The mass flow rate was read from the monitor of the micro-flowmeter. When the oscillations were in a small range, 50 consecutive values were recorded and the average was taken like in the other measurements gathered by the data logger. When the enthalpies and the mass flow rate for the pre-heater section were determined, the power input (heat transfer rate) to the refrigerant could be found. The pre-heater power input could be adjusted manually from the control box and the value was transferred to the computer program by the power transducer. For different power input values; the mass flow rate, and the enthalpies were

designated and the graph of the heat transfer rate transferred to the refrigerant at the pre-heater section versus power input from the pre-heater was drawn to find a relation to be used in the experiments for two-phase flow. The states for six pre-heater calibration experiments are given in Table 1.

In the given table, the previously mentioned properties, power input value and mass flow rate were measured for each experiment and the necessary properties were found from the thermodynamic properties of R-134a. The “Pre-heater input” value stands for the power transducer reading value from the computer program, while the “Pre-heater transferred” value was the calculated heat transfer rate (Eq. (17)). These values, which were used to calculate the pre-heater calibration curve, are given in Table 2.

Table 2: The pre-heater calibration curve values

Pre-heater Input	**Pre-heater Transferred**
W	**W**
9.59	5.03
15.71	12.94
19.11	16.83
32.75	26.34
32.81	27.65
39.13	35.78

The calibration curve is presented in Fig. 25. This curve was used for the two-phase experiments for the determination of pre-heater power input values. The pre-heater calibration experiments were conducted at 3 – 5 bar refrigerant pressure values and the two-phase experiments were made at 4 – 7 bar pressure values. The saturation pressure dependence in two-phase experiments were concluded to be insignificant, so the difference had no important effects. On the other hand, the two-phase flow experiments were made at saturation temperatures, whereas the pre-heater calibration experiments were conducted for single-phase flow. The calibration experiments were at temperatures close to saturation at the pre-heater exit and the room temperature was between 20 – 22 ºC during the experiments (the difference was due to seasonal change and it did

not cause any considerable effect on the results). The correlation in the calibration curve came out as:

$$\dot{Q}_{RI} = 0.9534\,\dot{Q}_H - 2.9294 \tag{18}$$

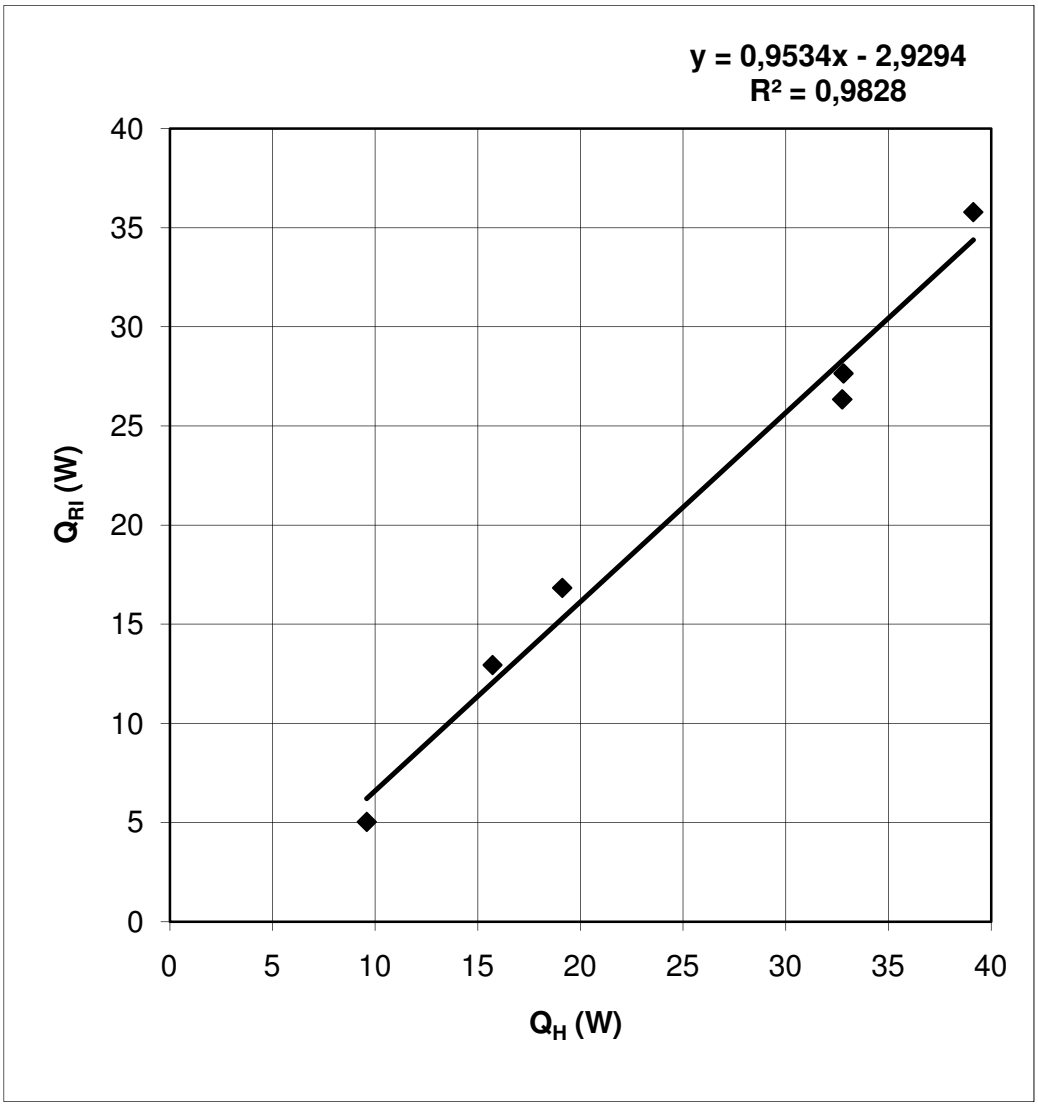

Figure 25: The calibration curve of the pre-heater

2.6.4 Test Section Loss Calibrations

In the test section, there was counter-flow shell-and-tube heat exchanger with one shell and one tube pass constructed as mentioned before. In the tube side,

refrigerant flowed and in the shell side there was water and ethylene glycol mixture. The calculation of the heat transfer rate from the water side to the refrigerant side could not be done using the refrigerant temperature and pressure values, since two-phase flow was aimed in the refrigerant side and the temperature was not an independent property from pressure. Therefore, it was to be calculated from the water side measurements and calculations. The water side was covered with insulation to minimize the losses but if the losses had been assumed to be negligible, the results would have deviated in a significant magnitude. The losses from the test section – in other words, from the water side – was to be found. These losses were categorized in two ways: viscous heating and the loss to the surroundings. The heat transfer rate from the water side to the refrigerant side, $\dot{Q}_W$, was:

$$\dot{Q}_W = \dot{V}_w \cdot \rho_w (h_{wi} - h_{we}) + \dot{Q}_V - \dot{Q}_{W,loss} \tag{19}$$

In this formula, $\dot{V}_w$ is the volumetric flow rate of the water, ρ_w is the density of the water, h_{wi} and h_{we} are the water side inlet and exit enthalpies, $\dot{Q}_V$ is the viscous heating, and $\dot{Q}_{W,loss}$ is the water side heat loss to the surroundings.

For the calculation of the difference of the enthalpies at the inlet and exit of the water side in the test section, the equation below was used due to the fact that the water mixture was liquid.

$$h_{wi} - h_{we} = c_p \, (T_{wi} - T_{we}) \tag{20}$$

Here T_{wi} and T_{we} are the temperatures of the water at the inlet and exit of the test section, respectively.

The viscous heating is an important consideration in low velocity and low Reynolds number flows of very viscous fluids [50]. Before calculating the viscous heating value, the geometry of the shell side is presented in Table 3. The technical drawing is also provided in Appendix D.2. Inner diameter is the outer diameter of the copper tube and the outer diameter is the inner diameter of the

shell. The cross sectional area is the water flow area and the hydraulic diameter is the ratio of 4 times the cross sectional area over the wetted perimeter (the sum of inner and outer perimeter).

Table 3: Water side geometrical constraints

Inner diameter (mm)	3.18
Outer diameter (mm)	10.00
Inner perimeter (mm)	9.97
Outer perimeter (mm)	31.42
Cross sectional area (mm^2)	70.62
Hydraulic diameter (mm)	6.83

For the different temperatures of water and ethylene glycol mixture, the properties were also needed for the calculations of the calibrations and the experiments. The properties of the mixture for different mixture ratios are presented for different temperature values [40]. The behaviors are not given and the temperature intervals are relatively large for accurate property readings. Therefore, with the use of these data points as reference, property curves for water and ethylene glycol 1:1 ratio volume basis were prepared. These properties are specific gravity (the ratio of the density of the mixture over the density of the pure water), specific heat, dynamic viscosity, and thermal conductivity.

The properties were taken as functions of temperature only, because the mixture was assumed to be incompressible. The data points of the properties and the corresponding temperature values are presented in Appendices F.1 – F.4 [47]. Among these four properties given in the tables, specific gravity, specific heat, and thermal conductivity showed a linear dependence on the temperature, while dynamic viscosity had a second order function with temperature. The graphs and the curve fittings with the equations are also presented in Appendices F.1 – F.4. In the curve fittings, “y” is the property in that graph and “x” is the temperature. The relations were also found for the temperature in degrees Celcius (℃).

These properties for the water mixture were used in all calculations of the water side. They were not given in the two-phase flow experiments or the results section since the same tables and graphs were used to determine the properties. For the designation of the viscous heating on the water side, the temperatures of the water side and the refrigerant side were equalized with the temperature of the surroundings. The temperature of the water and refrigerant sides were controlled from the inlet and exit RTDs, and the surrounding temperature was followed from the thermocouples that were open to the surroundings. For these conditions, the water side was operated with different flow rates to see the effect of Reynolds number (Re) on the viscous heating. Several experiments were conducted and 4 successful readings were taken to make the calculations. Although the number of successful readings was seemed to be not enough, the same readings were recorded for the same Re values on water side in 5 – 10 % range. On the other hand, the dependence of viscous heating on Re was observed to be linear showing that the results were sufficient. The viscous heating value was found in terms of watts (W) and the table, the graph, and the correlation are presented in Table 4, Figure 26, and Eq. (21), respectively.

Table 4: Viscous heating experimental values

	Unit	Exp. 1	Exp. 2	Exp. 3	Exp. 4
P_{water}	bar	13.20	12.77	13.06	12.63
V_{water}	l/min	1.15	1.85	1.50	1.60
$T_{water, mean}$	°C	20.01	19.86	20.36	19.83
ρ_{water}	kg/m^3	1080.59	1080.67	1080.42	1080.68
m_{water}	kg/s	0.0207	0.0333	0.0270	0.0288
C_p	J/kgK	3387.21	3386.70	3388.35	3386.61
μ	kg/ms	0.00268	0.00269	0.00266	0.00269
k	W/mK	0.403	0.403	0.403	0.403
V	m/s	0.271	0.437	0.354	0.378
Re	-	747.81	1198.93	981.97	1036.34
Q_V	W	9.69	14.50	12.55	11.91
$T_{water} - T_{R-134a}$	°C	-0.19	-0.52	-0.20	-0.18

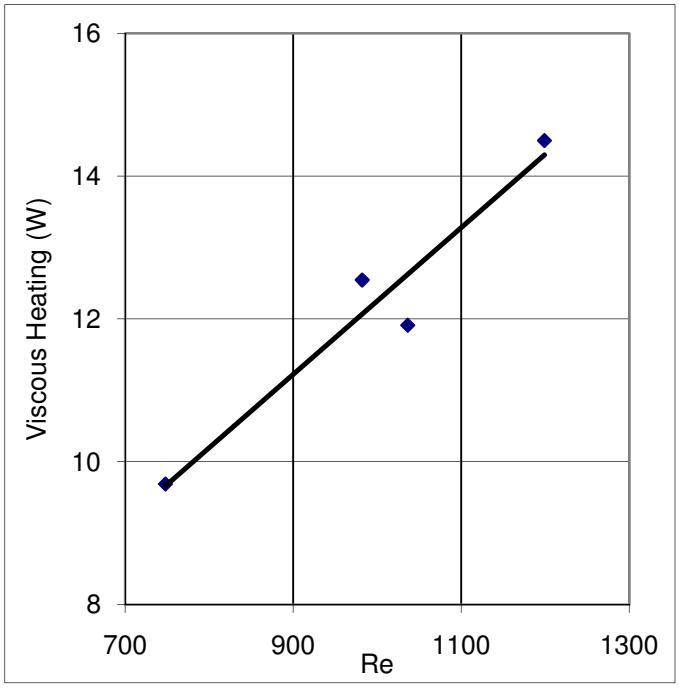

Figure 26: Viscous heating versus Reynolds number

$$\dot{Q}_V[W] = 0.0103 \cdot Re_{water} + 1.9879 \tag{21}$$

Besides the viscous heating, there is heat loss to the surroundings through the insulation and the edges of the heat exchanger. The dependence of the heat loss on the temperature difference between the water side and the surroundings was to be determined. The water side temperature was 35℃ maximum and the ambient temperature in the experiment room was 20℃ minimum. The loss was calculated from the equation (22) for these extreme temperature values.

$$\dot{Q}_{W,loss}[W] = \frac{\Delta T}{\frac{1}{\pi d_{si} L h_W} + \frac{ln(d_{so}/d_{si})}{2\pi k_{Al} L} + \frac{ln(d_{ins}/d_{so})}{2\pi k_{ins} L} + \frac{1}{\pi d_{ins} L h_{air}}} \tag{22}$$

In this equation, the first term in the denominator is the convection resistance for the water side, and h_W is the heat transfer coefficient of the water. The second and the third terms are the conduction resistances along the aluminum shell and

the insulation. The last term is the convection resistance on the air side (ambient), since the temperature of the room is recorded.

The water side heat transfer coefficient was calculated using four different equations. The correlations that were used to determine the heat transfer coefficient of the water are given in equations (23-26) below. The thermally developing flow correlations were taken for all experiments.

Correlation of Gnielinski [52]:

$$Nu = \left[3.66^3 + 1.61^3 \left(\frac{Pe_b d}{L}\right)\right]^{1/3} \tag{23}$$

valid for $0.1 < \frac{Pe_b d}{L} < 10000.$

Correlation of Hausen [52]:

$$Nu = 3.66 + \frac{0.19(Pe_b d/L)^{0.8}}{1+0.117(Pe_b d/L)^{0.467}} \tag{24}$$

also valid for $0.1 < \frac{Pe_b d}{L} < 10000.$

“Asymptotic mean Nusselt number in circular ducts” [52]:

$$Nu = 1.953 \left(\frac{Pe_b d}{L}\right)^{1/3} \tag{25}$$

valid for $\frac{Pe_b d}{L} > 100.$

Correlation of Pohlhausen [52]:

$$Nu = 0.664 \left(\frac{Pe_b d}{L}\right)^{1/2} {Pr_b}^{-1/6} \tag{26}$$

valid for $0.5 < Pr_b < 500$ & $\frac{Pe_b d}{L} > 1000.$

In these equations, Nu is the Nusselt number, Pe is the Peclet number, d is the hydraulic diameter and L is the length of the shell. Pe is the multiplication of Re (Reynolds number) and Pr (Prandtl number).

The water side geometry given in Table 5 was used in the viscous heating calibrations. For the heat loss to the surroundings, some of the other necessary geometrical parameters are also presented in Table 5.

Table 5: The water side geometry for heat loss calculations

Inner diameter (mm)	3.175
Outer diameter (mm)	10
Inner perimeter (mm)	9.97
Outer perimeter (mm)	31.42
Cross sectional area (mm^2)	70.62
Hydraulic diameter (mm)	6.83
Equivalent diameter (mm)	28.32
Test length (mm)	400

The temperature dependence of the loss to the surroundings was to be found, but after the calculations for the maximum temperature difference and the maximum heat transfer coefficient for the water side, it was decided to neglect this term. The geometrical parameters, thermal conductivity, and results for the heat loss are given in Table 6.

The heat loss came out to be 1.22 W for the maximum case. The heat transfer coefficient for the water side was selected as the maximum of the results of equations (23-26). The heat transfer to the refrigerant for the maximum case was about 50 W, so the maximum loss was about 2.5%. Also the situation was investigated for the minimum heat transfer and maximum losses, and the result was 0.25 W heat loss for 9.5 W heat transfer rate. So the loss was again about 2.5%. In order to ease the calculations, the term was neglected in the experimental calculations.

Table 6: The results for the maximum heat loss to the surroundings

d_{si}	mm	10
d_{so}	mm	20
t_{ins}	mm	20
d_{ins}	mm	60
k_{al}	W/mK	230
k_{ins}	W/mK	0.04
h_W	W/m²K	1000
h_{air}	W/m²K	10
L	mm	400
ΔT	K	15
Q	W	1.22

CHAPTER 3

TWO-PHASE FLOW EXPERIMENTS

After the construction of the set-up, connecting the devices, making preliminary experiments and calculating the losses to the surroundings; the next step was the two-phase flow experiments. This Chapter is divided into 5 sections: Approach, Conditions, Flow Chart, Data Analysis, and Calculations.

3.1 APPROACH

Two-phase flow of refrigerant inside the test section was desired. The studies in the literature were focused on the constant heat flux approach. Moreover, the mass flux values were relatively large for the refrigeration processes. The main goals in the two-phase flow were to achieve these conditions; constant wall temperature and low mass fow rates. The quality and the heat flux were mentioned to be the most dominant parameters on the two-phase heat transfer coefficient. Therefore, the quality variation was an important consideration in the investigation. On the other hand, mass flux, saturation temperature and pressure, and the pressure drop were the other parameters to be examined.

The quality of the refrigerant could not be measured like pressure and temperature. Moreover, the temperature and pressure are not independent properties for phase-change. Therefore another independent property is needed to determine the state for a two-phase location. The pressure was selected as one of the properties to designate the state, since the measured temperature fluctuates for a two-phase flow; the constant temperature approach during phase-change is an approximation [51]. In fact, the temperature tends to show an

oscillatory behavior and the average value is taken to find the saturation temperature. The refrigerant was pre-heated and the single-phase refrigerant became two-phase before the test section. The quality right after the pre-heater was taken as the inlet quality, and along the test section, the constant wall temperature approach was applied and the heat transfer was given from water side to the refrigerant side. This heat transfer rate was calculated from the heat loss and viscous heating correlations (Eq. (19)) and the energy of the refrigerant was increased.

The quality and enthalpy were known at the inlet. Adding the heat transfer rate to the inlet conditions and applying the first law gave the exit enthalpy. The pressure drop was measured at the test section, so the exit pressure was known for the refrigerant side. Combining the exit enthalpy and pressure, the state at the exit was determined. The adjustments of the test section, flow rate, temperature and pressure values to get successful readings and the data analysis are presented in the “Flow Chart” and “Data Analysis” sections.

3.2 CONDITIONS

The two-phase flow experiments were conducted for varying conditions. These parameters can be divided into three parts: Refrigerant side, water side and the pre-heater power input.

The refrigerant side conditions are given in Table 7. The properties of the refrigerant were read from the program [54] and the graphs were prepared according to the saturation pressure [54], given in Appendix G. The conditions for the two-phase flow that changed in the test section were the mass flow rate, the inlet and exit pressure and temperature, the inlet and exit quality, and the pressure drop.

Table 7 shows that the mass flow rate of the refrigerant was between 0.34 and 0.94 g/s. These values were selected according to the operation flow rates of the refrigerants in actual refrigerators. The range for the refrigerator operations is 0.2 – 1.0 g/s. The maximum value could be satisfied but the flowmeter problems did

not let successful readings for the minimum flow rate experiments. Yet, the experiments could be considered sufficient in terms of the mass flow rate range since the majority of the range was investigated.

Table 7: The refrigerant conditions for the test section in two-phase flow

Parameter	**unit**	**minimum**	**maximum**
Refrigerant mass flow rate	g/s	0.34	0.94
Refrigerant inlet pressure	bar	4.59	7.76
Refrigerant inlet temperature	ºC	13.08	30.26
Refrigerant inlet quality	-	1.20%	70.16%
Refrigerant pressure drop	bar	0.02	0.21
Refrigerant exit pressure	bar	4.38	7.71
Refrigerant exit temperature	ºC	11.65	30.03
Refrigerant exit quality	-	16.57%	95.68%

The inlet pressure values to the test section were relatively large for the refrigerator applications. The reason was that the condensation of the refrigerant at low pressures was a problem in terms of the cooling bath performance for the refrigerant side. The bath temperature could decrease to -35 – -40ºC but the refrigerant temperature could not be decreased to these values since there was a coil heat exchanger used instead of circulating the refrigerant inside the bath. On the other hand, the studies in the literature showed that for the two phase experiments, the saturation pressure effects were almost negligible. Therefore, the experiments were made with inlet pressure values of 4.5 – 8 bars. The pressure drop was between 0.02 – 0.21 bar (0.29 – 4.58 %, the minimum/maximum pressure drops were not for the minimum/maximum inlet pressures), so there was no significant difference between the inlet and exit pressure values. Therefore, the saturation pressure was taken as the average of the inlet and exit pressures.

The quality values of the refrigerant at the test section inlet was changed from 1.20% to 70.16% and the exit was from 16.57% - 95.68%. When calculating the heat transfer coefficient, the average of the inlet and exit was taken as the quality value for the test section, similar to analyses in literature. The average quality

increase in the test section was 20%, so taking the average quality value as the experimental parameter while presenting the results was acceptable.

Considering the average pressure of the refrigerant as the saturation pressure and the average quality as the quality of the experiment, Table 8 shows the two-phase experimental conditions for the refrigerant in terms of mentioned parameters.

Table 8: The average refrigerant side parameters for the two-phase experiments

Parameter	**unit**	**minimum**	**maximum**
Refrigerant saturation pressure	bar	4.49	7.73
Refrigerant saturation temperature	ºC	12.41	30.13
Refrigerant average quality	-	8.29%	82.92%

Based on the change in the refrigerant properties, water side was adjusted in terms of flow rate and bath temperature. The pressure on the water side was about 10-12 bars because of the pump power and the small diameter pneumatic hose. However, the pressure change did not affect the properties of the water since the mixture was in liquid phase and almost incompressible. Water side parameter ranges during the two-phase flow experiments are given in Table 9.

Table 9: The water side parameter ranges for the two-phase flow experiments

Parameter	**unit**	**minimum**	**maximum**
Water volumetric flow rate	l/min	0.3	2.1
Water mass flow rate	g/s	5.37	37.62
Water Reynolds number	-	136.94	1333.54
Water inlet temperature	ºC	14.6	34.37
Water exit temperature	ºC	14.45	34.32

The flow rate on the water side was adjusted from the valves and the flow rate was manually read from the rotameter. The range of the rotameter was 0 – 2.1 l/min, and the highest value was used in the high flow of the refrigerant. The temperature of the water was adapted to the refrigerant temperature to get constant wall temperature at the test section. When the water side losses were

calculated, the correlations for developing laminar flow were selected. From the table, it can be seen that even for the highest flow rate value, the Re value did not exceed 1335. Moreover, the lowest value of water mass flow rate was about 6 times the highest flow rate of the refrigerant, and the average mass flow rate of the water was 33 times the average mass flow rate of refrigerant. The reason was that the higher the water mass flow rate, the closer was the constant wall temperature approach.

Besides the parameters of the two cycles, the heat transfer rates were varied due to the pre-heater power input and Re of the water. The ranges for the pre-heater section and the losses from the test section, in addition to the heat transfer rate from the water side to the refrigerant side are given in Table 10.

Table 10: The pre-heater and the test section heat transfer rates for two-phase experiments

Parameter	**unit**	**minimum**	**maximum**
Pre-heater power input	W	3.6	57.18
Pre-heater net power transferred	W	0.50	51.59
Viscous heating	W	3.40	15.72
Heat transfer rate to the refrigerant	W	9.70	49.91

The pre-heater power was varied to get different inlet quality values for the refrigerant. It was seen that the refrigerant was pre-heated as much as it was evaporated at the test section. The importance of the calibrations can also be verified from the comparison of the pre-heater input and net power transferred values, and the test section gains and losses.

In experimental work, repeatability of the experiments is one of the main approaches for the accuracy and reliability of the results. In the experiments of this thesis, repeatability could not be followed for all of the experiments due to the fact that the thesis was based on a research project and the schedule was to be followed strictly in order to finalize the project.

3.3 FLOW ORDER

In this section, the two-phase flow experiments are explained in a detailed way by using a flow order. The sequence of the operation of the devices, the changes with respect to the measurements are given in Tables 11 and 12.

The first part of the flow order is presented in Table 11 as the sequence from the computer start-up to refrigerant pump start-up.

Table 11: Flow order part 1: from computer start-up to refrigerant pump start-up

1		Turn on the computer, DC power supply, and the data logger
2		Start the data acquisition program on the computer
3		Check the refrigerant pressure
4		Is it zero?
	YES	Charge the cycle with R-134a Go back to step 3
	NO	Continue with step 5
5		Is the refrigerant in liquid phase* **?
	YES	Go to step 7
	NO	Close the valves of the refrigerant bath Turn on the bath to decrease the temperature Continue with step 6
6		Is the liquid refrigerant seen in the sight glass?
	YES	Go to step 7
	NO	Charge the cycle more with R-134a Decrease the bath temperature Go back to step 5
7		Close the flowmeter valves and start the refrigerant pump
	*	Check from the computer
	**	Check the sight glass

After the pump was started to operate, the flowmeter and the pre-heater were turned on and so was the water side. Then, by following the flow order presented in Table 12, the experiments were conducted.

Table 12: Flow order part 2: from refrigerant pump start-up until the end

8		Set the refrigerant pump speed to a desired value
9		Is the refrigerant in liquid phase for the whole cycle* **?
	YES	Continue with step 10
	NO	Go back to step 6
10		Turn on the flowmeter and open the flowmeter valves
11		Turn on the water bath and pump
12		Turn on the pre-heater and adjust a small power input value
13		Increase the power input of the pre-heater
14		Adjust water temperature w.r.t. R-134a saturation temperature
15		Check the steady-state conditions***
16		Is the water temperature close to and higher than the refrigerant temperature?
	YES	Continue with step 17
	NO	Go back to step 14
17		Does the water temperature decrease in the test section?
	YES	Continue with step 18
	NO	Go back to step 14
18		Is the constant wall-temperature acquired at the test section?
	YES	Continue with step 19
	NO	Adjust water flow rate Go back to step 14
19		Record the flow rate of the refrigerant (50 readings minimum)
20		Is the refrigerant in two-phase at the inlet* ****?
	YES	Continue with step 21
	NO	Go back to step 13
21		Note down the time and record the flow rate of water
22		Is the experiment finished for the specified saturation pressure?
	YES	Continue with step 23
	NO	Go back to step 8 (to change the flow rate)
23		Are the experiments finished for all saturation temperatures?
	YES	**END**
	NO	Change the saturation pressure by charging or discharging the refrigerant Go back to step 8
	*	Check from the computer
	**	Check the sight glass
	***	50 successful consecutive readings in the range of device accuracy
	****	Apply the calculations

3.4 DATA ANALYSIS

When the 23 step flow order of two-phase flow experiments were finished, the analyses of the data gathered came into consideration. These analyses can be classified in two main groups: the analysis of the manual measurements and the analysis of the recorded measurements by the computer.

The manual measurements were the refrigerant mass flow rate and the water volumetric flow rate. These measurements were performed at the time of the experiments since the values were not recorded automatically. For the accuracy and consistency, they were noted down after the steady-state conditions achieved and continued at least for 15 minutes. The refrigerant mass flow rate was recorded from the flowmeter transmitter digital screen in the units of g/s. Even for the steady-state conditions, oscillations were observed. Therefore, at least 50 measurements were recorded and the average was taken. The volumetric flow rate of water was read on the mechanical rotameter manually and recorded in the experiment data sheet. Since the value did not appear on a digital screen as in the flowmeter, the value was noted down several times after the steady-state conditions were reached. The average value of the readings was accepted as the volumetric flow rate of the water.

The power, temperature, and pressure measurements were the ones that were recorded in the computer through the data acquisition unit. These measurements were performed by the power and pressure transducers, RTDs, and thermocouples. The computer program scanned the data logger to gather the data for 15 second time intervals during the whole procedure. The read values were plotted on graphs just after the readings were done. Therefore, the steady-state was easily followed from the graphs. After the steady-state conditions were reached, the average value of the power input and the final values of the pressure of the refrigerant, and the temperatures of the refrigerant at the inlet and exit of the pre-heater (at the flowmeter exit and the inlet of the test section) were recorded. These values and the mass flow rate of the refrigerant were used to calculate the state at the inlet of the test section. When there was a quality value calculated (two-phase flow was reached), and the other procedure in the test

section was followed for the two-phase experiments, the time of the experiment was noted down and the experiments were continued for different mass flow rates, saturation pressures, and quality values. The data analysis was left to be performed when the experiments during that session were completed. The computer program collected the data in a single file for a session, so it was more efficient and easier to analyze the data when the session was ended. The analysis of the data was made in terms of steady-state approach. The measurements versus the time were drawn as a graph and it was combined with the times of the mass flow rate record. The averages of 50 readings (minimum) of the power, temperature, and pressure measurements were taken and they formed the experiments data. The “Calculations” section continued the procedure after the experimental data was present.

3.5 CALCULATIONS

The heat transfer coefficient calculation for the two-phase flow of R-134a was the main aim in the calculations. Through the procedure, many other parameters, properties, and variables were measured and calculated. The calculations were performed in two main ways. These are the experimental calculations and the calculations of correlations in the literature based on the experimental data. The refrigerant side geometry given in Table 13, was needed to perform the calculations.

Table 13: The refrigerant side geometry in the test section

Inner diameter (mm)	1.65
Outer diameter (mm)	3.175
Inner perimeter (mm)	5.18
Cross sectional area (mm^2)	2.14
Hydraulic diameter (mm)	1.65
Equivalent diameter (mm)	1.65
Test length (mm)	400
Heat transfer area (mm^2)	2073.5

3.5.1 Experimental Calculations

The calculations of the experiments based on the experimental data were performed to calculate the average heat transfer coefficient of the refrigerant side for the varying quality (average quality) values of the refrigerant. As mentioned in the “Calibrations” section, the refrigerant at the test inlet was desired to be in two-phase conditions, so the refrigerant was pre-heated before the test section. The enthalpy of the refrigerant was increased with the pre-heater power input in Eq. (17) and the determination of the quality of the refrigerant was done by finding the actual power transfer to the refrigerant by the pre-heater calibration Eq. (18). The refrigerant pre-heater exit condition was the test section inlet condition, therefore:

$$h_{he} = h_{ri} \tag{27}$$

h_{ri} is the test section inlet enthalpy of the refrigerant. Along the test section, the heat transfer took place from the water side to the refrigerant side. This heat transfer rate was calculated with Eq. (19). The viscous heating for the water side was calculated from Eq. (21). When the enthalpy change in the water along the test section was also added from Eq. (20), the net heat transfer rate could be found. The exit enthalpy of the test section for the refrigerant could be found with all other parameters known including the mass flow rate.

$$h_{re} = \frac{\dot{Q}_W}{\dot{m}_R} + h_{ri} \tag{28}$$

$\dot{m}_R$ is the mass flow rate of the refrigerant, h_{re} is the test section exit enthalpy of the refrigerant. Knowing the exit enthalpy and the pressure drop along the test section, the refrigerant state at the exit could be determined. As mentioned in the previous sections, the pressure at the exit (inlet pressure - pressure drop) of the test section was taken into consideration instead of the temperature value. The temperature of the exit state was found from the pressure and enthalpy values. The difference of the temperatures at the inlet and exit of the test section between the calculated and measured values was between -0.69 – 0.17ºC for the

inlet and -0.23 – 0.32ºC for the exit. Moreover the quality value at the exit state was calculated. The temperature at the inlet state was read from the tables with the same procedure, by combining the pressure (inlet pressure) and the enthalpy.

The wall temperature was needed in the calculations of the average heat transfer coefficient. The temperature of the wall of the copper tube was measured at 7 locations with 50 mm intervals. The constant-wall temperature approach was accepted when the maximum temperature difference for these 7 locations was lower than 0.5℃. Then the average value was taken in the heat transfer coefficient calculations. The logarithmic mean temperature difference (LMTD) method was applied to calculate the overall heat transfer coefficient and the average heat transfer coefficient. The mean temperature difference was not applied because the temperature of the refrigerant changed along the test section unlike the wall temperature. The logarithmic mean temperature difference for the test section is given in Eq. (29).

$$\Delta T_{LM} = \frac{(T_w - T_{ri}) - (T_w - T_{re})}{ln\left(\frac{T_w - T_{ri}}{T_w - T_{re}}\right)} \tag{29}$$

T_w is the wall temperature, T_{ri} is the test inlet temperature of the refrigerant, and T_{re} is the test exit temperature of the refrigerant. The heat transfer area was calculated easily from the geometry of the test section. Therefore, the overall heat transfer coefficient was calculated with Eq. (30).

$$U_i = \frac{\dot{Q}_W}{A_i \cdot \Delta T_{LM}} \tag{30}$$

The overall heat transfer coefficient, U_i, was based on the inner heat transfer area, A_i, which is:

$$A_i = 2 \cdot \pi \cdot r_i \cdot L \tag{31}$$

r_i is the inner radius of the copper tube and L is the length of the test section. The overall heat transfer coefficient had the refrigerant convection coefficient and the

conduction coefficient across the copper tube. Thus, the average heat transfer coefficient for the two-phase refrigerant flow is:

$$\bar{h}_{TP} = \left(\frac{1}{U} - \frac{r_i \ln (r_o/r_i)}{k_c}\right)^{-1} \quad (32)$$

In Eq. (32), r_o is the outer radius of the copper tube and k_c is the thermal conductivity of copper. Apart from the heat transfer coefficient calculations, the pressure drop was recorded along the test section for the two-phase refrigerant flow. These values are presented in the results section.

3.5.2 Calculations with Correlations in Literature

The heat transfer coefficient calculations were also performed using the correlations available in the literature. In the flow boiling for internal flow, there are mainly two types of boiling in terms of the bulk fluid temperature [52]. The fluid, which is in liquid-phase, is heated along the pipe or channel in which it flows. The temperature of the fluid increases at the walls of the pipe/channel and bubble formation occurs. These bubbles collapse when they flow into the bulk liquid because the temperature of the liquid is lower than the boiling temperature. This type flow boiling is called sub-cooled boiling. On the other hand, when the temperature of the liquid also becomes equal to the saturation temperature, two-phase boiling emerges and the heat transfer coefficient increases by a significant amount. The two-phase boiling has two forms, which are convective boiling and nucleate boiling. For low quality values, nucleate boiling dominates heat transfer, while convective boiling plays the active role for higher quality values. For moderate values, they both have important effects. The correlations that were used to calculate the two-phase heat transfer coefficient were based on the theory mentioned and the outcomes are presented in the Results section to compare with the experimental results.

3.5.2.1 Güngör and Winterton Correlation

Two scientists, Güngör and Winterton [52], studied flow-boiling heat transfer of halocarbon refrigerants and proposed the correlation given in Eq. (33):

$$\bar{h}_{TP} = E\bar{h}_l + S\bar{h}_p \tag{33}$$

$\bar{h}_{TP}$ is the average heat transfer coefficient for two-phase flow, E is an enhancement factor, $\bar{h}_l$ is the heat transfer coefficient for the liquid phase at the specified condition, S is the suppression factor, and $\bar{h}_p$ is the pool boiling term. $\bar{h}_l$ can be calculated from any single-phase heat transfer coefficient formula available in the literature with respect to the flow type and Re limitations. The calculation of E, the enhancement factor, is given in below.

$$E = 1 + 2.4 \times 10^{-4} Bo^{1.16} + 1.37(1/X_{tt})^{0.86} \tag{34}$$

In Eq. (34), Bo is the boiling number and $1/X_{tt}$ is the Lochart-Martinelli parameter. Bo is given in Eq. (35) and $1/X_{tt}$ is defined in Eq. (36).

$$Bo = \frac{q''}{G \cdot i_{lv}} \tag{35}$$

$$\frac{1}{X_{tt}} = \frac{x}{(1-x)^{0.9}} \left(\frac{\rho_l}{\rho_v}\right)^{0.5} \left(\frac{\mu_v}{\mu_l}\right)^{0.1} \tag{36}$$

In Eqs. (35) and (36), q" is the heat flux, G is the mass flux, i_{lv} is the vaporization enthalpy of the refrigerant, ρ is the density and μ is the viscosity, and l and v are the subscripts for the liquid and vapor phases.

In Eq. (33), S and $\bar{h}_p$ are the remaining unknowns. S is defined as:

$$S = \left(1 + 1.15 \times 10^{-6} E^2 {Re_l}^{1.17}\right)^{-1} \tag{37}$$

In this equation, Re_l is the Reynolds number for the liquid and it is defined as:

$$Re_l = \frac{2G(1-x)r_i}{\mu_l} \tag{38}$$

The remaining term, $\bar{h}_p$, is the pool boiling term:

$$\bar{h}_p = 55{p_r}^{0.12}(-log p_r)^{-0.55}M^{-0.5}{q"}^{0.67} \tag{39}$$

In the final equation of Güngör and Winterton correlation, p_r is the reduced pressure, and M is the molecular weight of the fluid.

3.5.2.2 Chen Correlation

This correlation [52] combines the nucleate boiling, $\bar{h}_{nb}$, and convective boiling, $\bar{h}_{cb}$, terms by calculating them separately. The two-phase boiling heat transfer coefficient is given in Eq. (40).

$$\bar{h}_{TP} = \bar{h}_{cb} + \bar{h}_{nb} = \bar{h}_l F_o + \bar{h}_p S \tag{40}$$

$\bar{h}_l$ and S are the same as in Eq. (33). The boiling enhancement factor, F_o is calculated from:

$$F_o = F(1-x) \tag{41}$$

$$F = \begin{cases} 1, for\ 1/X_{tt} \leq 0.1 \\ 2.35(0.213 + 1/X_{tt})^{0.736}, for\ 1/X_{tt} > 0.1 \end{cases} \tag{42}$$

$\bar{h}_p$ is the pool boiling term and it is calculated by:

$$\bar{h}_p = 0.00122\frac{{k_l}^{0.079}{c_{p,l}}^{0.45}{\rho_l}^{0.49}{\theta_b}^{0.24}{\Delta p_v}^{0.75}}{\sigma^{0.5}{\mu_l}^{0.29}(i_{lv}\rho_v)^{0.24}} \tag{43}$$

k_l is the liquid thermal conductivity, $c_{p,l}$ is the liquid specific heat, θ_b is the wall superheat, σ is the surface tension, and Δp_v is the pressure for vaporization the liquid at the specified conditions. Δp_v is calculated from the Clapeyron Equation.

$$\Delta p_v = \frac{\theta_b i_{lv} \rho_v}{T_{sat}} \tag{44}$$

3.5.2.3 Bertsch Correlation

Bertsch correlation [53] is similar to the Chen correlation in terms of the separate calculation of the nucleate boiling and the convective boiling. This correlation is relatively new and the formulation is given as below.

$$\bar{h}_{TP} = \bar{h}_{nb}(1-x) + \bar{h}_{cb}[1 + 80(x^2 - x^6)e^{-0.6\,Co}] \tag{45}$$

$\bar{h}_{nb}$ is the nucleate boiling heat transfer coefficient and it is calculated from the same equations of Chen correlation. The confinement number, Co, is:

$$Co = \left[\frac{\sigma}{g(\rho_l - \rho_v){D_h}^2}\right]^{1/2} \tag{46}$$

The convective boiling term, $\bar{h}_{cb}$, is calculated using the following equation.

$$\bar{h}_{cb} = \bar{h}_{conv,l}(1-x) + \bar{h}_{conv,v}x \tag{47}$$

$\bar{h}_{conv,l}$ is the liquid phase convective heat transfer coefficient and $\bar{h}_{conv,v}$ is the vapor phase convective heat transfer coefficient. They are given in the following equations.

$$\bar{h}_{conv,l} = \left(3.66 + \frac{0.0668\cdot(D_h/L)\cdot Re_l Pr_l}{1+0.04\cdot[(D_h/L)\cdot Re_l Pr_l]^{2/3}}\right)\cdot\frac{k_l}{D_h} \tag{48}$$

$$\bar{h}_{conv,v} = \left(3.66 + \frac{0.0668\cdot(D_h/L)\cdot Re_v Pr_v}{1+0.04\cdot[(D_h/L)\cdot Re_v Pr_v]^{2/3}}\right)\cdot\frac{k_v}{D_h} \tag{49}$$

For the calculations with the correlations, the properties of the refrigerant were needed. Therefore, for data points of the properties, curve fitting was applied similar to the water side. The property tables and graphs with curve fittings are given in Appendix G.

CHAPTER 4

EXPERIMENTAL RESULTS AND DISCUSSION

The calculations based on the experimental data were performed in order to find the two-phase (boiling) heat transfer coefficient of R-134a. Moreover, the pressure drop of R-134a along the test section was recorded as mentioned before; therefore, the pressure drop in two-phase flow is presented in addition to the heat transfer coefficient. In total, 35 experiments were conducted. Due to the experimental conditions and errors, 7 of them were eliminated. On the other hand, while presenting the results, one parameter was tried to be fixed and the other one was investigated in terms of the effect on the heat transfer coefficient and pressure drop. In such a situation, the successful experimental results were also selected in terms of the other parameters' effects, because there were many variables in the tests. For instance, when the considering effect of saturation pressure on the heat transfer coefficient for constant quality, the results with closer mass flux values were selected, because the mass flux had an important effect the heat transfer coefficient.

The experimental results are presented in two sections: Heat Transfer Coefficient and Pressure Drop. All data related to the calculations are given for one experiment as an example in Appendix H. The refrigerant and water side geometries at the test section, the test conditions, the states of the refrigerant at the experiment related locations, the properties of both fluids, and the results of the theoretical and experimental calculations are presented therein.

4.1 HEAT TRANSFER COEFFICIENT

The heat transfer coefficient has been calculated in two ways: experimentally and through the correlations presented above, referred to as theoretically. Since the constant wall temperature approach was applied in the experiments, the results were prepared in terms of constant quality and constant mass flux values. Constant heat flux curves, which are very common in the literature to see the effect of other variables on the heat transfer coefficient, were not drawn since the local heat flux along the flow was not uniform.

4.1.1 Constant Quality Results of the Experiments

During the experiments, it was difficult to adjust the quality of the fluid, because there were many variables that affected the results. When the analyses of the experimental data were performed and the results were calculated, the experiments with closer average quality values were selected in order to draw the graphs. These values were considered as constant quality values. Two graphs and two tables with the data of these graphs were prepared. In Table 14 and Figure 27, the saturation pressure effect on the heat transfer coefficient for constant quality values was examined. The quality values for the constant assumption are also given in the table. The difficulty of the quality adjustment caused this assumption, but the results gave an understanding of the effect in a range of $\pm$ 5% for 18% and 25% quality values and $\pm$ 10% for 50% quality value.

From Figure 27, it is seen that the heat transfer coefficient does not depend on the saturation pressure significantly except for 18% quality. Although there are some oscillations for each and every constant quality value, from this graph, it can be concluded that the experimental results match most of studies in the literature claiming the independency of the heat transfer coefficient from saturation pressure. On the other hand, the heat transfer coefficient value is larger for lower quality values than higher quality values for the same saturation pressure value.

Table 14: Heat transfer coefficient dependence on saturation pressure for constant refrigerant quality

18%			25%			50%		
P_{sat}	h_{exp}	x (%)	P_{sat}	h_{exp}	x (%)	P_{sat}	h_{exp}	x (%)
bar	W/m²K	-	bar	W/m²K	-	bar	W/m²K	-
4.96	6324.71	20.42	5.42	4550.70	26.28	6.24	4364.40	45.76
5.25	5890.32	14.94	5.57	5458.17	32.44	6.45	3708.17	47.61
5.25	7024.43	18.63	6.07	4462.30	28.89	6.68	3963.87	60.02
5.55	5750.29	18.20	6.56	4383.87	24.24	6.74	3661.30	61.56
5.66	5404.12	23.32	6.75	3525.54	21.61	7.73	3374.88	52.01
6.89	4764.25	21.36	6.89	4764.25	21.36			
			7.30	4318.26	30.75			

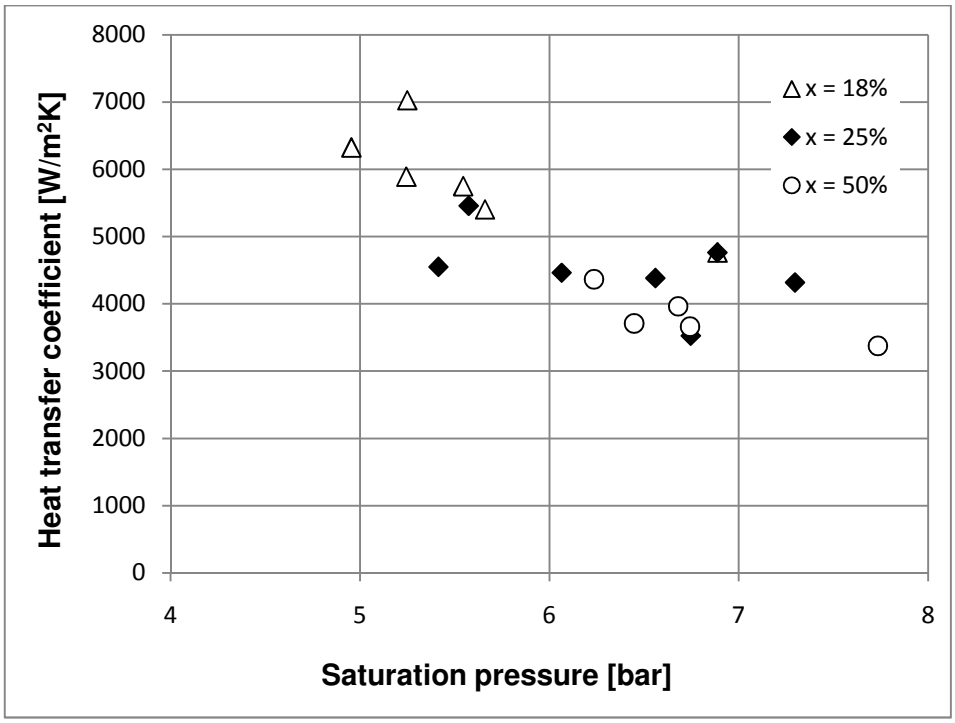

Figure 27: Heat transfer coefficient versus saturation pressure for constant refrigerant quality

Another analysis about the constant quality results was performed to examine the effect of mass flux on the heat transfer coefficient. The mass flux range for the experiments (150 - 450 kg/m^{2}s) was not wide since the experiments were conducted for low mass flow rates. However, to analyze the effects in the range, Table 15 and Figure 28 were studied. As in the previous table, the assumed constant quality values are presented here.

Table 15: Heat transfer coefficient dependence on mass flux for constant refrigerant quality

18%			**25%**			**50%**		
Mass flux	**h_{exp}**	**x (%)**	**Mass flux**	**h_{exp}**	**x (%)**	**Mass flux**	**h_{exp}**	**x (%)**
kg/m²s	**W/m²K**	**-**	**kg/m²s**	**W/m²K**	**-**	**kg/m²s**	**W/m²K**	**-**
158.73	2962.64	23.90	158.73	2962.64	23.90	180.80	3661.30	61.56
219.13	3654.03	14.00	235.33	4462.30	28.89	192.38	3708.17	47.61
246.73	3525.54	21.61	236.40	4318.26	30.75	194.87	4364.40	45.76
255.81	5404.12	23.32	255.81	5404.12	23.32	195.01	3963.87	60.02
325.59	5890.32	14.94	272.38	4764.25	21.36	207.83	5971.38	47.58
339.34	6324.71	20.42	339.34	6324.70	20.42	219.48	5543.35	56.56
343.27	7024.43	18.63						

The number of data points for each quality value is not the same because of the previously mentioned difficulties in the experiment procedure and property, states and test points.

Figure 28 shows that the heat transfer coefficient increases with the increasing mass flux values. The trend can be considered as valid for different constant quality values. Therefore, it is easy to comment that the mass flux and the two-phase heat transfer coefficient scale with each other in the range of the mass fluxes studied.

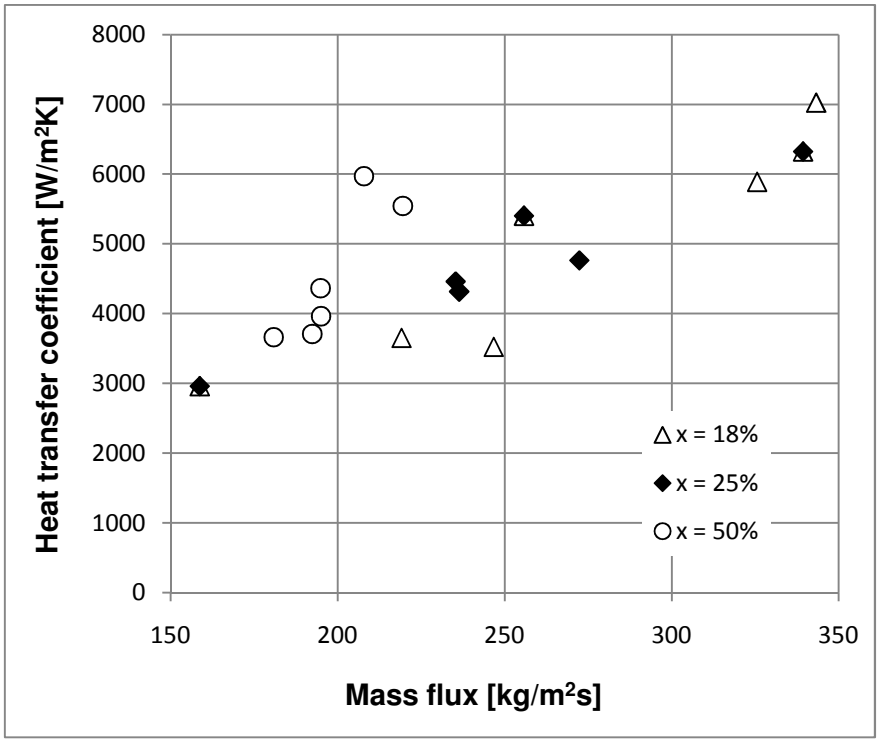

Figure 28: Heat transfer coefficient versus mass flux for constant refrigerant quality

4.1.2 Constant Mass Flux Results of the Experiments

Besides the constant quality results, the constant mass flux results were selected and analyzed from all of the experimental results. As in the constant quality analyses, the mass flux constancy could not be adjusted definitely. A change of the volumetric flow rate provided by the pump was observed due to the material deterioration (PPS) of the gears of the pump. Achieving two-phase flow, gathering data successfully, and performing experiments for different test conditions were focused on during the experiments. For this reason, the ranges in ∓ 5-10% of the nominal values were accepted as the constant mass flux value.

Table 16: Heat transfer coefficient dependence on saturation pressure for constant refrigerant mass flux

200			250		
P_{sat}	h_{exp}	Mass flux	P_{sat}	h_{exp}	Mass flux
bar	W/m²K	kg/m²s	bar	W/m²K	kg/m²s
6.24	4364.40	194.87	5.42	4550.70	250.05
6.45	3708.17	192.38	5.66	5404.12	255.81
6.65	3654.03	219.13	6.07	4462.30	235.33
6.68	3963.87	195.01	6.56	4383.87	249.64
6.74	3661.30	180.80	7.30	4318.26	236.40
7.18	3118.05	205.27			
7.73	3074.88	193.07			

Table 16 and Figure 29 reveal the effect of saturation pressure on heat transfer coefficient for the constant mass flux of the refrigerant in the test section.

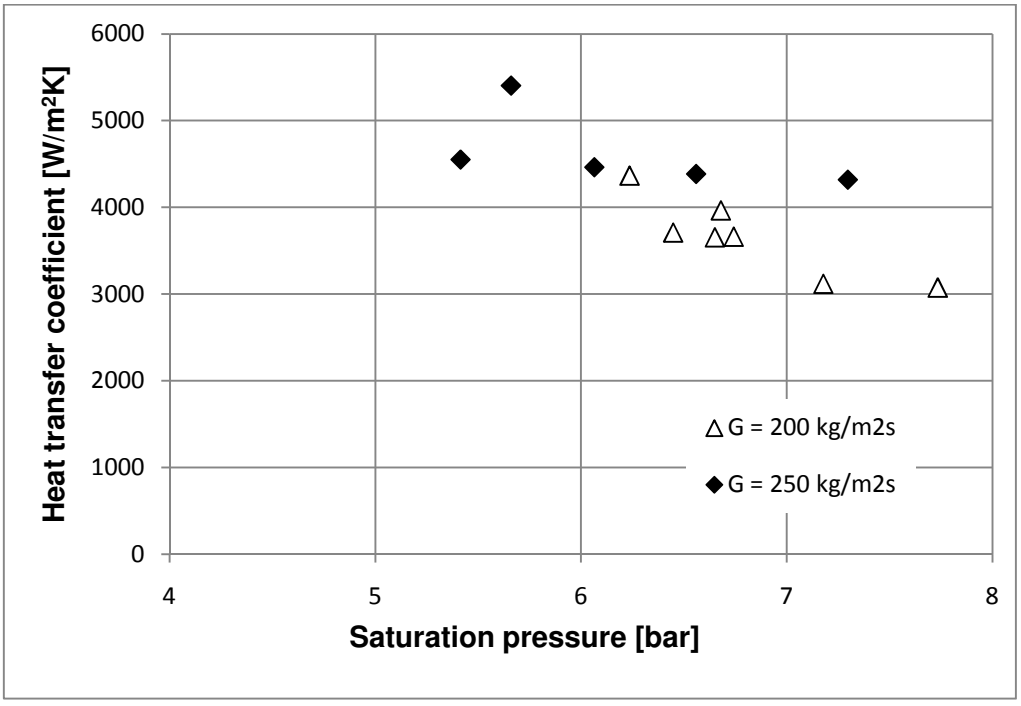

Figure 29: Heat transfer coefficient versus saturation pressure for constant refrigerant mass flux

It can be observed in Table 16 that the mass flux values were between 180 and 220 kg/m^{2}s for the 200 kg/m^{2}s mass flux value and 235 and 260 kg/m^{2}s for the 250 kg/m^{2}s. The saturation pressure effect on the heat transfer coefficient for the constant mass flux is negligible as in the constant quality analysis. Therefore, the study of the comparison of the experimental results, the correlations and the studies in the literature in terms of the saturation pressure effect on the heat transfer coefficient were not included to this thesis.

The most common type of the analysis of the heat transfer in two-phase flow is the effect of quality on the heat transfer coefficient for the constant mass flux. The table and the figure were prepared for two different mass flux values as in the saturation pressure effect analysis. The quality values calculated were from 11.70% to 67.05% for the mass flux value of 200 kg/m^{2}s and from 12.75% to 29.27% for 250 kg/m^{2}s. The ranges were not for the whole quality values but the majority of the studies in the literature showed that the heat transfer coefficient tended to increase with the increasing quality up to 30 – 40 % quality and it decreased for the higher quality values.

Table 17 and Figure 30 show the experimental results of the effect of quality variation on the heat transfer coefficient.

The heat transfer coefficient increases with the increasing quality up to 30% for both mass flux values. The higher quality values are not present for mass flux of 250 kg/m^{2}s, therefore further discussion cannot be performed for that value. For 200 kg/m^{2}s mass flux, the heat transfer coefficient decreases for higher quality values, so the experimental results are consistent with the studies in the literature.

Table 17: Heat transfer coefficient dependence on quality for constant refrigerant mass flux

200			250		
x (%)	h_{exp}	Mass flux	x (%)	h_{exp}	Mass flux
-	W/m²K	kg/m²s	-	W/m²K	kg/m²s
14.00	3654.03	219.13	15.15	3335.30	266.20
32.44	5458.17	195.56	21.61	3525.54	246.73
30.95	5426.60	211.85	24.24	4383.87	249.64
42.58	5971.38	207.83	26.28	4550.70	250.05
46.33	5294.66	185.37	28.89	4462.30	235.33
60.02	3963.87	195.01	30.75	4618.26	236.40
61.56	3661.30	180.80			
68.50	3118.05	205.27			

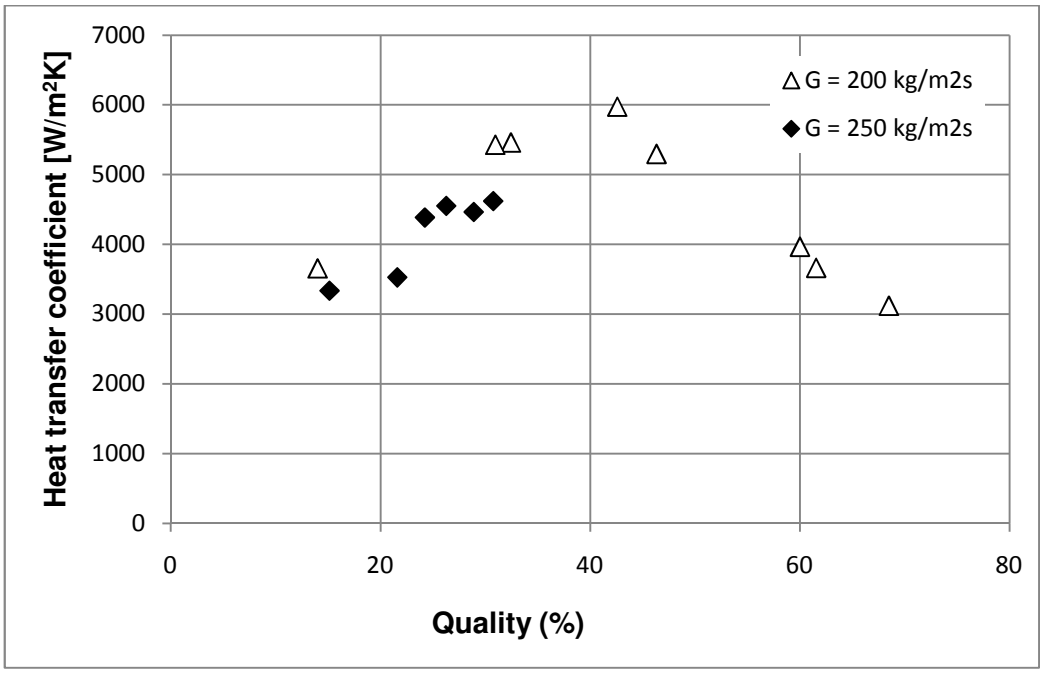

Figure 30: Heat transfer coefficient versus quality for constant refrigerant mass flux

4.1.3 Comparison with Literature

The experimental results are compared with the correlations mentioned in Chapter 3 and two sets of experimental results presented in Chapter 1; references [23] (Shiferaw) and [28] (Tibiriçá). The calculations with the correlations were made with the steps described in the "Calculations with Correlations in Literature" section. The first comparison was performed for constant quality. The mass flux was varied from 150 to 350 kg/m^{2}s and the results are presented in Table 18 and Figure 31 for the experiments and three correlations.

Table 18: Comparison of experimental results for the heat transfer coefficient for constant quality and varying mass flux

18%	**Heat Transfer Coefficient**				
Mass flux	Experimental	Güngör	Bertsch	Chen	x (%)
kg/m²s	W/m²K	W/m²K	W/m²K	W/m²K	-
158.73	2962.64	3581.25	3094.91	3061.59	23.90
219.13	3654.03	2877.85	2637.25	1843.13	14.00
255.81	5404.12	5157.85	4702.44	3314.23	23.32
325.59	5890.32	7979.57	4662.81	4575.11	14.94
339.34	6324.71	8652.69	4791.09	4928.33	20.42
343.27	7024.43	8432.82	4760.44	4566.63	18.63

		$h_{exp} / h_{calculated}$ x 100		
Mass flux	h_{exp}	Güngör	Bertsch	Chen
kg/m²s	W/m²K	-	-	-
158.73	2962.64	82.73	95.73	96.77
219.13	3654.03	126.97	138.55	198.25
255.81	5404.12	104.77	114.92	163.06
325.59	5890.32	73.82	126.33	128.75
339.34	6324.71	73.10	132.01	128.33
343.27	7024.43	83.30	147.56	153.82

The constant quality is 18% and the quality values are also presented in Table 18. In order to have a better understanding of the comparison of the experimental

results and the results of the previous studies, the ratio of the experimental heat transfer coefficient over the heat transfer coefficient calculated from the correlations are also presented in Table 18, as a percentage. It can be seen from the table that when the extreme results of the Chen correlation are neglected; the experimental results are in the range of 75% – 150% of the results calculated from the correlations.

All the results in Figure 31 are similar in terms the mass flux effect on the heat transfer coefficient, that increasing mass flux leads to an increase in the heat transfer coefficient. The experimental results are also in a good match with the correlations. All results are close for low and moderate mass fluxes. The experimental results are also close to Bertsch and Chen correlation results for higher values of mass flux values, while Güngör and Winterton correlation gives higher heat transfer coefficient values.

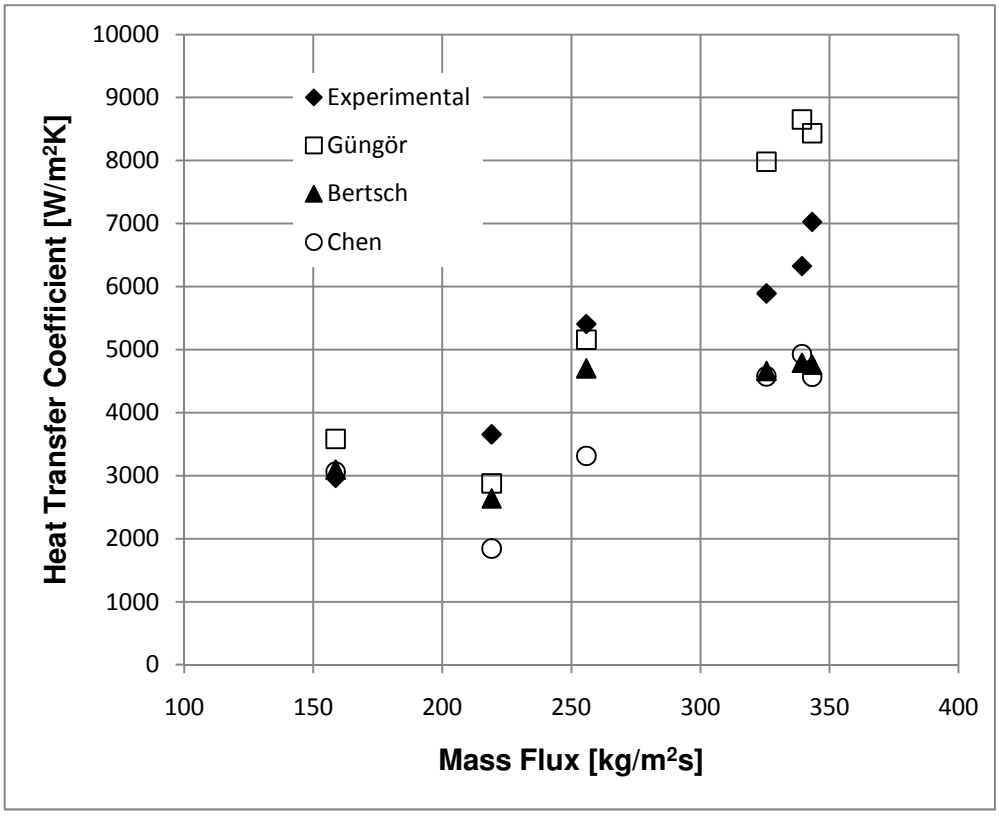

Figure 31: Experimental results and results of correlations in the literature for heat transfer coefficient versus mass flux, x = 18%

The results in terms of the ratios in Table 18 are given in Figure 32. The experimental results are in a better match with Bertsch correlation results. Güngör and Winterton correlation gave higher results than the experimental results, whereas it was the opposite for the Chen correlation.

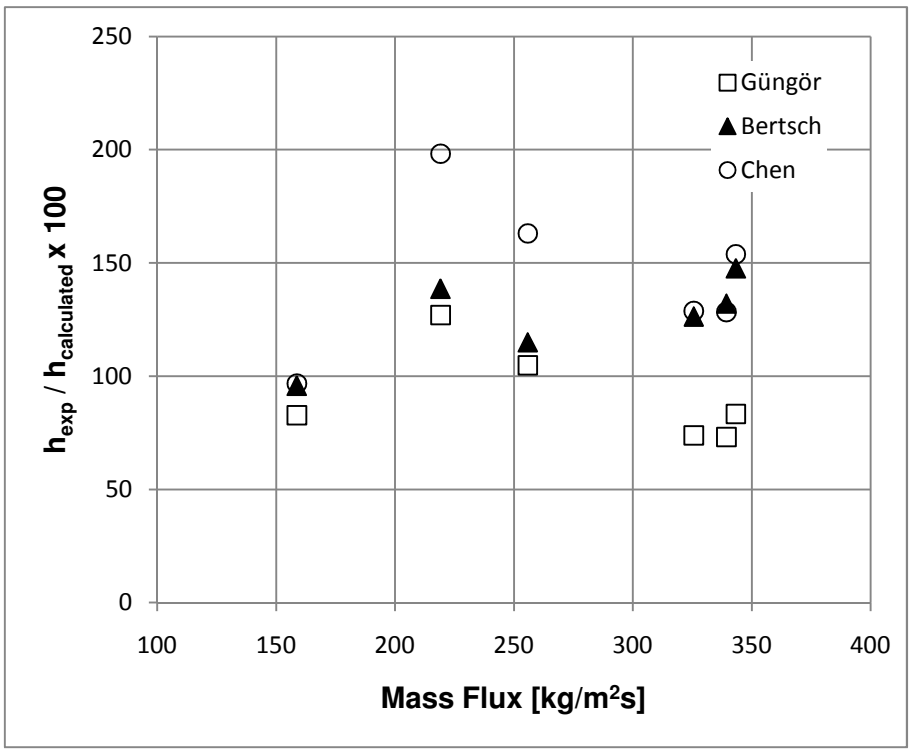

Figure 32: Heat transfer coefficient ratio versus mass flux, x = 18%

For the rest of all comparisons, the heat transfer coefficient change with quality is analyzed for a constant mass flux value of 200 kg/m^{2}s. The experimental heat transfer coefficient was compared with the correlations above and the results of the experimental studies mentioned in Chapter 1. The comparisons were made separately in order to comment on the accuracy of the experimental results more effectively.

The comparison of the heat transfer coefficient with the correlations is presented in Table 19 and Figure 33.

Table 19: Comparison of experimental results for the heat transfer coefficient for varying quality

x (%)	Mass flux	Experimental	Güngör	Bertsch	Chen
-	kg/m²s	W/m²K	W/m²K	W/m²K	W/m²K
14.00	219.13	3654.03	2877.85	2637.25	1843.13
30.95	211.85	5426.60	4756.95	4261.66	2711.90
42.58	207.83	5971.38	4578.98	4200.61	2358.72
46.33	185.37	5294.66	5005.38	4364.83	2828.96
60.02	195.01	3963.87	3924.13	3780.37	2165.83
61.56	180.80	3661.30	4040.46	3705.83	2319.03
68.50	205.27	3118.05	4045.40	3662.16	2299.16

It can be observed in Fig. 33 that the experimental results, Güngör and Winterton correlation, and Bertsch correlation show a maximum deviation at about 40% quality and tend to decrease for higher quality values. Bertsch correlation gives lower heat transfer coefficient values.

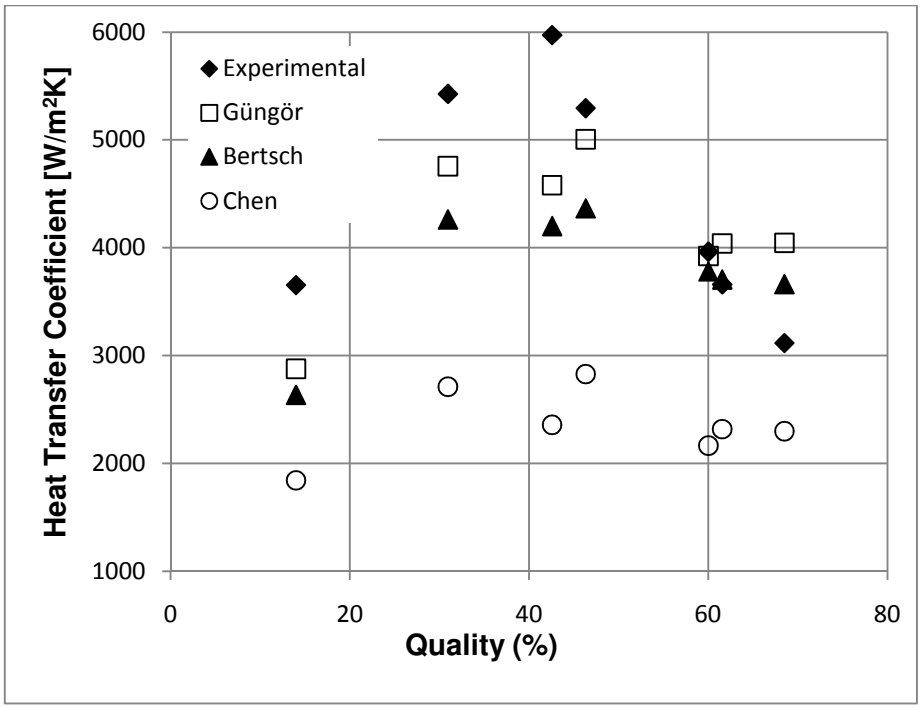

Figure 33: Experimental results and results of correlations in the literature for the heat transfer coefficient versus quality

Table 20 and Figure 34 are the comparison of the experimental results with the experimental results of Tibiriçá [28]. This study was performed with constant heat flux approach and different heat fluxes were applied. The authors gave the results of the study of Yan [28] and it is also adapted.

Table 20: Comparison of experimental results with Tibiriçá [28] in terms of quality dependence

G = 200 kg/m^{2}s			Yan [28]
x (%)	Experimental	x (%)	(q" = 5 kW/m^2)
-	W/m²K	-	W/m²K
14.00	3654.03	10	2950
32.44	5458.17	16.5	2700
30.95	5426.60	20	2700
42.58	5971.38	29.5	3100
46.33	5294.66	40	3050
60.02	3963.87	50	3450
61.56	3661.30	54	3500
68.50	3118.05	70	3600
		83	3800

	Yan [28]		h_{exp} [28]
x (%)	(q" = 15 kW/m^2)	x (%)	(q" = 5 kW/m^2)
-	W/m²K	-	W/m²K
43	3650	15	2900
54	3950	25	2950
64	4200	35	2650
75	4700	45	3000
84	5500	55	3450
94	6600	65	3800
		75	4300
		85	4800
		95	5800

For the increasing quality values, the heat transfer coefficient increases for the compared results. There is no peak point for the quality value, which is contrary to the majority of the studies, but also matches some of the studies in the

literature. When the results are compared with the experimental results, it is observed that the experimental heat transfer coefficient is close to the results in literature. The tendency difference is noted down in this figure.

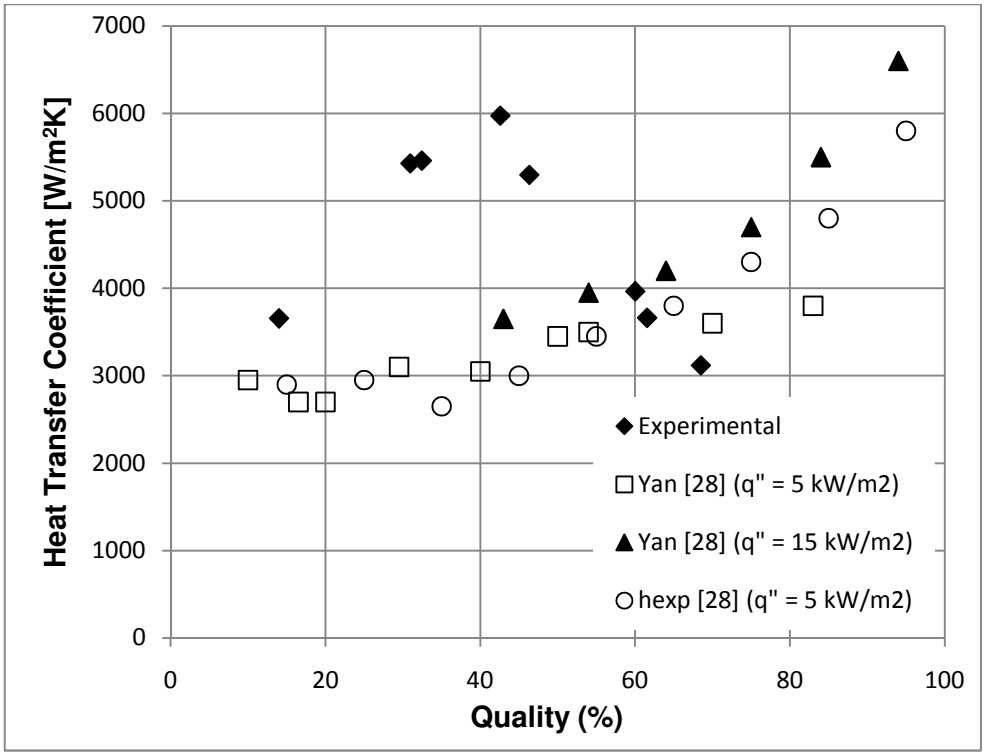

Figure 34: Heat transfer coefficient versus quality for current experiments and results of Tibiriçá [28]

The comparison for the constant mass flux and varying quality was also performed for another experimental study by Shiferaw [23]. Similar to the previous compared study, the author applied different values of constant heat flux for separate sets of experiments and collected the data to find the two-phase heat transfer coefficient.

The results of the study and the experimental results are presented in Table 21 and Figure 35. The heat flux was varied from 17 to 69 kW/m^{2}K. These values are relatively higher than the experimental conditions. The heat flux values of the experiments were not presented, but the average heat flux along the test section

for the refrigerant side was in the range of 4 – 20 kW/m^{2}K. Therefore the experimental results were expected to deviate from the results of the study but the chance for the investigation of the tendency would be a good opportunity to evaluate the experimental set-up.

Table 21: Comparison of experimental results with Shiferaw [23] in terms of quality dependence

G = 200 kg/m^{2}s			h_{exp} [23]		h_{exp} [23]
x (%)	Experimental	x (%)	(q" = 17 kW/m^2)	x (%)	(q" = 27 kW/m^2)
-	W/m²K	-	W/m²K	-	W/m²K
14.00	3654.03	1	6050	6	9600
32.44	5458.17	2	6000	13	9600
30.95	5426.60	4	5950	20	10000
42.58	5971.38	6	5900	27	11000
46.33	5294.66	7	5800	31	11700
60.02	3963.87	9	5850	34	11400
61.56	3661.30	12	5900		
68.50	3118.05	14	6200		
		16	6800		
		18	6100		
	h_{exp} [23]		h_{exp} [23]		h_{exp} [23]
x (%)	(q" = 34 kW/m^2)	x (%)	(q" = 53 kW/m^2)	x (%)	(q" = 69 kW/m^2)
-	W/m²K	-	W/m²K	-	W/m²K
2	9000	2	14000	7	14200
5	9250	7	15300	15	15300
9	9000	13	15300	23	15500
13	8900	19	15300	31	15700
16	8850	25	15100	38	15500
20	8750	31	14900	47	15300
25	8800	37	14800	54	14100
28	9000	43	15000	62	11000
31	9050	49	14100	69	8000
36	9950	56	14100	77	6000
39	10100	62	11200	85	4200
42	9050	67	8000	93	3200

Figure 35 shows that the heat transfer coefficient increases for the moderate heat flux experiments, but the same comment cannot be made for the high quality results. For the high heat flux experiments, heat transfer coefficient does not change significantly up to about 50% quality and then there was a dramatic decrease for the high quality values, which could be caused by dry-out as it was explained in many studies in the literature.

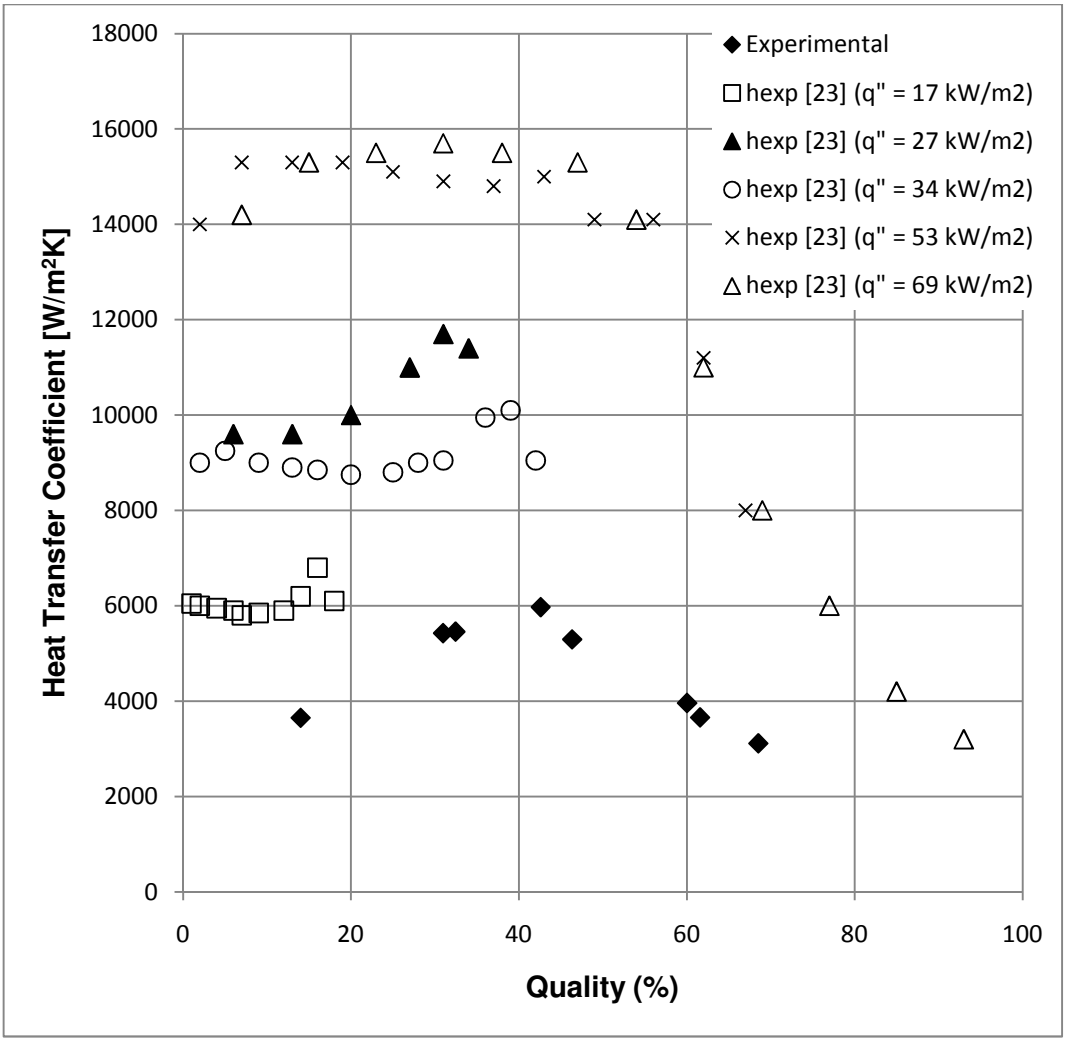

Figure 35: Heat transfer coefficient versus quality for the current experiments and those of Shiferaw [23], G = 200 kg/m^{2}s

4.2 PRESSURE DROP

The pressure drop along the test section was measure using the DPT. The results are presented in this section. No calculations were performed but the effects of different parameters on the pressure drop were observed by preparing tables and figures. As for the heat transfer coefficient, the constant quality and the constant mass flux effects on the pressure drop were examined.

The pressure drop was measured in the units of [bar], and it was not changed in the tables and figure. Table 22 and Figure 36 present the effect of mass flux on pressure drop. The constant assumed quality values are also presented.

Table 22: Dependence of pressure drop on mass flux for constant quality

18%			**25%**			**50%**		
Mass flux	**ΔP**	**x (%)**	**Mass flux**	**ΔP**	**x (%)**	**Mass flux**	**ΔP**	**x (%)**
kg/m²s	**bar**	**-**	**kg/m²s**	**bar**	**-**	**kg/m²s**	**bar**	**-**
219.13	0.02	14.00	195.56	0.03	32.44	171.51	0.05	58.61
246.73	0.03	21.61	211.85	0.03	30.95	180.80	0.06	61.56
266.20	0.05	15.15	236.40	0.05	30.75	185.37	0.05	46.33
272.38	0.05	21.36	241.41	0.05	30.63	193.07	0.05	52.01
325.59	0.09	14.94	249.64	0.04	24.24	194.87	0.05	45.76
339.34	0.15	20.42	252.83	0.06	27.11	195.01	0.06	60.02
343.27	0.16	18.63	255.81	0.06	23.32	199.03	0.07	56.33
						207.83	0.06	47.58
						219.48	0.07	56.56

The pressure drop increases with the increasing mass flux values for all three qualities. The increase for the 18% quality is much more dramatic for the available data points than it is for the other values.

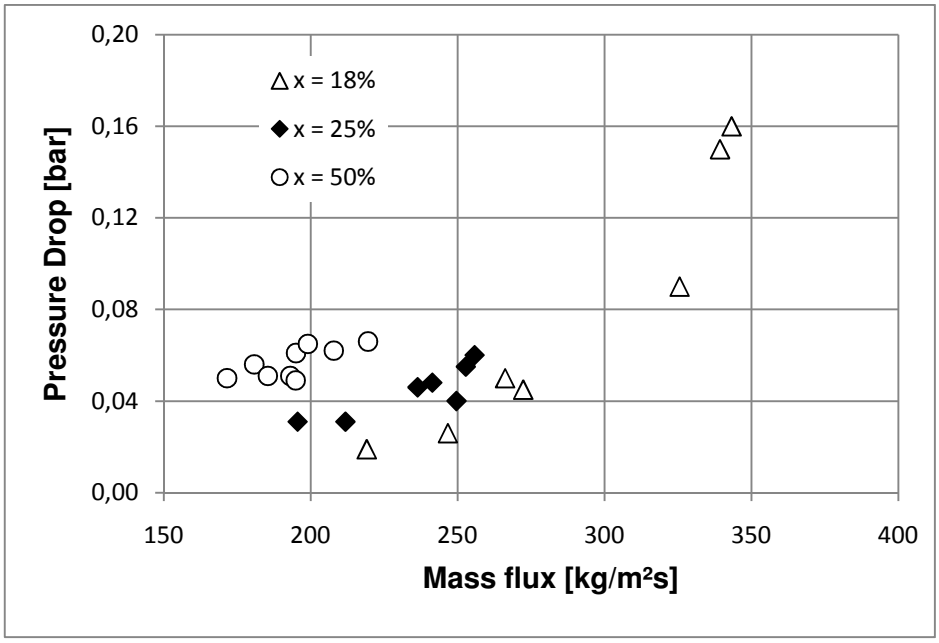

Figure 36: Pressure drop versus mass flux for constant refrigerant quality

The pressure drop change with quality change for constant mass flux was the second investigation subject about the pressure drop considerations. The pressure drop was considered as an important factor in two-phase flow due to the fact that it is larger than the single-phase (liquid) pressure drop. Table 23 and Figure 37 give the values of pressure drop with changing quality. The constant assumed mass flux values are presented in the table for the possible experimental errors. The graph shows the increase of the pressure drop with the increasing quality values. It is an expected result when it is compared with the studies in the literature.

Table 23: Dependence of pressure drop on quality for constant refrigerant mass flux

200		
x (%)	ΔP	Mass flux
-	bar	kg/m²s
14.00	0.02	219.13
32.44	0.03	195.56
30.95	0.03	211.85
45.76	0.05	194.87
46.33	0.05	185.37
47.61	0.05	192.38
52.01	0.05	193.07
60.02	0.06	195.01
61.56	0.06	180.80
68.50	0.06	205.27

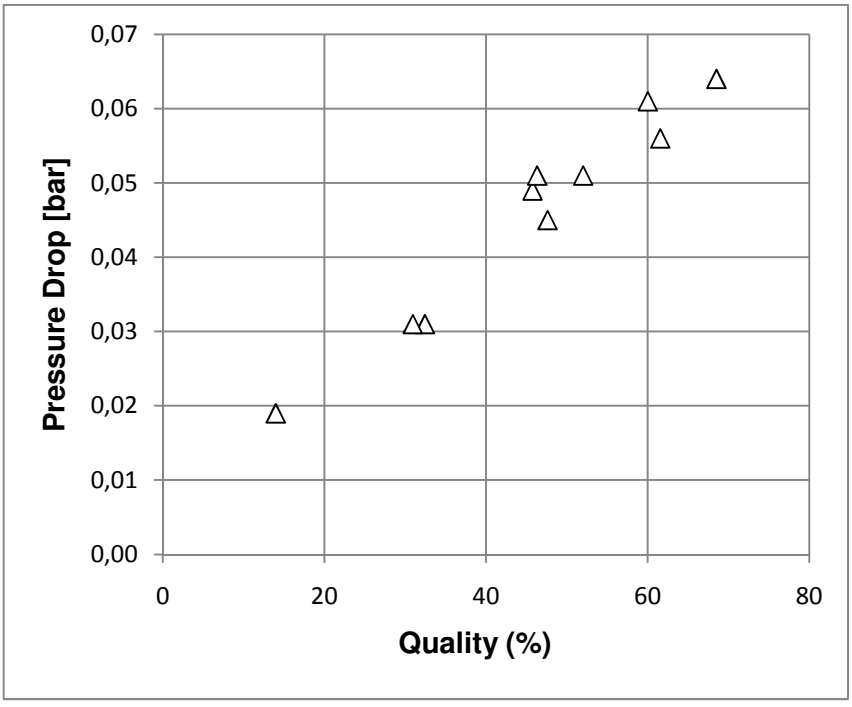

Figure 37: Pressure drop versus quality for the constant refrigerant mass flux, G = 200 kg/m^{2}s

CHAPTER 5

CONCLUSIONS

5.1 SUMMARY & CONCLUSIONS

In this thesis, the process and the progress of the experimental set-up construction to perform experiments of two-phase R-134a flow in a 1.65 mm tube were presented. The advantages of heat transfer in small scale media were explained and the need for the low flow rate and constant wall temperature approach studies in the literature were pointed out. Many studies in the literature were given with their relations to the current study. Based on these studies and the needs in the establishment of the infrastructure about the subject, the motivation and the aims of the experiments were shaped.

From the design to the experiments, the set-up was described in detail in terms of the devices used, the placement and operation of the devices, the experimental conditions, the experimental procedures, and the experimental results. These results were compared with some of the available theoretical and experimental studies in the literature and the comments and discussions were made.

This study was focused on the set-up construction, and the approaches and data analyses for the two-phase flow experiments. The results were not enough due to the mentioned difficulties in terms of sufficient data points to propose any correlations. On the other hand, the available results were observed to match with the results of the compared correlations and experimental studies. The results of both heat transfer coefficient calculations and pressure drop did not

deviate much; in addition, the tendencies were compatible with the majority of the studies in the literature.

To sum up, the study aimed to support the widening of the two-phase flow database in small scale media experimentally. The more the studies about this subject with constant wall temperature approach; the higher chance is the use in domestic refrigerators.

5.2 SUGGESTIONS FOR FUTURE WORK

The experimental set-up is ready to operate for other experiments and to test many other tubes and channels. By only changing the test section, the set-up can be used with different tubes and channels. For the future studies with the experimental set-up, proper vacuuming after each opening of the cycles is strongly recommended. Moreover, an extra pump parallel to the existing pump can be mounted on the system to prevent damage in the gears of the pump since they tend to wear out with the flow of the refrigerant in vapor phase. The calibrations for the pre-heater and the test section are to be performed for any modifications of the test section in terms of major changes in flow geometry.

In the existing study, the focus was on the two-phase flow. Single-phase flow of the refrigerant can be also studied for not only laminar, but also turbulent flow. On the other hand, the constant wall temperature approach with single-phase flow would be more difficult to apply.

Besides from the different geometry tests and single-phase flow, the working fluids can be changed and the experiments for other refrigerants and other fluids can be made. Since there are two independent cycles in the set-up, with the consideration of the compatibility of the devices, both sides single-phase, both sides two-phase, and one-side liquid one-side gas flow experiments can be performed. Moreover, numerical studies could be performed in addition to the experimental studies and the results could be compared to verify the numerical model. With these possible future work subjects, many researches can be made and valuable contributions to the literature about the internal flow can be added.

REFERENCES

[1] Energy Information Administration, Electricity Consumption by End Use in U.S. Households, 2001, www.eia.doe.gov, last visited on 31.01.2011.

[2] Advanced Technology Program, Mechanical Refrigeration, www.atp.nist.gov, last visited on 31.01.2011.

[3] Kandlikar, *S.G., Heat Transfer Mechanisms During Flow Boiling in Microchannels*, ASME, 2004, 126, pp. 8-16.

[4] Tuckerman, D.B. and Pease, R.F., *Optimized Convective Cooling using Micromachined Structure*, Journal of the Electrochemical Society, 1982, 129(3), pp. C98.

[5] Choi, S.B., Barron R.F., and Warrington R.O., *Fluid Flow and Heat Transfer in Microtubes, Micromechanical Sensors, Actuators, and Systems*, ASME DSC, 1991, 32, pp. 123-134.

[6] Harms, T.M., Kazmierczak, M.J., and Gerner, F.M., *Developing Convective Heat Transfer in Deep Rectangular Microchannels*, International Journal of Heat Fluid Flow, 1999, 20, pp. 149-157.

[7] Jung, J.Y., Kwak, H.Y., *Fluid flow and heat transfer in microchannels with rectangular cross section*, Heat Mass Transfer, 2007, 44, pp. 1041-1049.

[8] Park, H.S., Punch, J., *Friction factor and heat transfer in multiple microchannels with uniform flow distribution*, Int. J. Heat and Mass Transfer, 2008, 51, pp. 4535-4543.

[9] Kandlikar, S.G., *Fundamental issues related to flow boiling in minichannels and microchannels, Experimental Thermal and Fluid Science*, 2002, 26, pp. 389-407.

[10] Qu, W., Mudawar, I., *Flow boiling heat transfer in two-phase micro-channel heat sinks – I. Experimental investigation and assessment of correlation methods,* Int. J. Heat and Mass Transfer, 2003, 46, pp. 2755-2771.

[11] Saitoh, S., Daiguji, H., Hihara, E., *Effect of tube diameter on boiling heat transfer of R-134a in horizontal small-diameter tubes, Int. J. Heat and Mass Transfer*, 2005, 48, pp. 4973-4984.

[12] Bertsch, S.S., Groll, E.A., Garimella, S.V., *Effects of heat flux, mass flux, vapor quality, and saturation temperature on flow boiling heat transfer in microchannels*, Int. J. Multiphase Flow, November 2008, 35, pp. 142-154.

[13] Revellin, R., and Thome, J.R., *Experimental Investigation of R-134a and R-245fa Two-Phase Flow in Microchannels for Different Flow Conditions*, International Journal of Heat and Fluid Flow, 2007, 28, pp. 63-71.

[14] Bertsch, S.S., Groll, E.A., Garimella, S.V., *Refrigerant flow boiling heat transfer in parallel microchannels as a function of local vapor quality*, Int. J. Heat and Mass Transfer, 2008, 51, pp. 4775-4787.

[15] Yan, Y.Y., Lin, T.F., *Evaporation heat transfer and pressure drop of refrigerant R-134a in a small-pipe, Int. J. Heat and Mass Transfer*, 1998, 41, pp. 4183-4194.

[16] Liu, J.T., Peng, X.F., Yan, W.M., *Numerical study of fluid flow and heat transfer in microchannel cooling passages*, Int. J. Heat and Mass Transfer, 2006, 50, pp. 1855-1864.

[17] Liu, D., Garimella, S.V., *Flow Boiling Heat Transfer in Microchannels, ASME Journal of Heat Transfer*, 2008, 129, pp. 1321-1332.

[18] Agostini, B., Bontemps, A., *Vertical flow boiling of refrigerant R134a in small channels*, Int. J. Heat and Fluid Flow, 2005, 26, pp. 296-306.

[19] Djordjevic, E., Kabelac, S., *Flow boiling of R134a and ammonia in a plate heat exchanger*, Int. J. Heat and Mass Transfer, 2006, 31, pp. 1-19.

[20] De Rossi, F., Mauro, A.W., Rosato, A., *Local heat transfer coefficients and pressure gradients for R-134a during flow boiling at temperatures between -9ºC and +20ºC,* Energy Conversion and Management, 2009, 50, pp. 1714-1721.

[21] Ong, C.L., Thome, J.R., *Flow boiling heat transfer of R134a, R236fa and R245fa in a horizontal 1.030 mm circular channel*, Experimental Thermal and Fluid Science, 2009, 33, pp. 651-663.

[22] Choi, K.I., Pamitran, A.S., Oh, C.Y., Oh, J.T*., Boiling heat transfer of R-22, R-134a, and CO_2 in horizontal smooth minichannels*, Int. J. Refrigeration, 2007, 30, pp. 1336-1346.

[23] Shiferaw, D., Karayiannis, T.G., Kenning, D.B.R., *Flow boiling in a 1.1 mm tube with R134a: Experimental results and comparison with model*, Int. J. Thermal Sciences, 2009, 48, pp. 331-341.

[24] Matkovic, M., Cavallini, A., Col, D.D., Rossetto, L., *Experimental study on condensation heat transfer inside a single circular minichannel*, Int. J. Heat and Mass Transfer, 2009, 52, pp. 2311-2323.

[25] Revellin, R., Mishima, K., Thome, J.R., *Status of prediction methods for critical heat fluxes in mini and microchannels*, Int. J. Heat and Fluid Flow, 2009, 30, pp. 983-992.

[26] In, S., Jeong, S., *Flow boiling heat transfer characteristics of R123 and R134a in a micro-channel, Int. J. Multiphase Flow*, 2009, 35, pp. 987-1000.

[27] Park, J.E., Thome J.R., *Critical heat flux in multi-microchannel copper elements with low pressure refrigerants*, Int. J. Heat and Mass Transfer, 2010, 53, pp. 110-122.

[28] Tibiriçá, C. B., Ribatski, G., *Flow boiling heat transfer of R134a and R245fa in a 2.3 mm tube*, Int. J. Heat and Mass Transfer, 2010, doi:10.1016/j.ijheatmasstransfer.2010.01.038

[29] Raja, B., Mohan Lal, D., Saravanan, R., *Flow boiling heat transfer study of R-134a/R-290/R-600a mixture in 9.52 and 12.7 mm smooth horizontal tubes: Experimental Investigation*, Experimental Thermal and Fluid Science, 2009, 33, pp. 542-550.

[30] Ding, G., Hu Haitao, D., Huang, X., Deng, B., Gao, Y., *Experimental investigation and correlation of two-phase frictional pressure drop of R410A–oil mixture flow boiling in a 5mm microfin tube*, International Journal of Refrigeration, 2009, 32, pp. 150-161.

[31] Chen, C. A., Lee, C. Y., Lin, T. F., *Experimental study of R-134a evaporation heat transfer in a narrow annular duct*, Int. J. Heat and Mass Transfer, 2010, 53, pp. 2218-2228.

[32] Saisorn, S., Kaew-on, J., Wongwises, S., *Flow pattern and heat transfer characteristics of R-134a refrigerant during flow boiling in a horizontal circular mini-channel*, Int. J. Heat and Mass Transfer, 2010, 53, pp. 4023-4038.

[33] Consolini, L., Thome, J. R., *Micro-channel flow boiling heat transfer of R-134a, R-236fa, and R-245fa*, Microfluid Nanofluid, 2009, 6, pp. 731-746.

[34] Kakaç, S., Yener, Y., *Convective Heat Transfer*, Middle East Technical University, Ankara, 1980.

[35] Cole Parmer, Thermo Scientific NESLAB RTE-series Refrigerated Circulating Baths, http://www.coleparmer.com/catalog/product_view.asp?sku=1350030&pfx=KH, last visited on 31.01.2011.

[36] Cole Parmer, Benchtop Digital Drive, http://www.coleparmer.com/catalog/Product_view.asp?sku=7401455&pfx=KH&referred_id=2269, last visited on 31.01.2011.

[37] Rhenoik, RHM Coriolis Flow Sensors & RHE Coriolis Flow Transmitters, http://www.ge-mcs.com/, last visited on 31.01.2011.

[38] Cole Parmer, Glass-tubing, http://www.coleparmer.com/catalog/Product_view.asp?sku=3474200&pfx=KH&referred_id=2269, last visited on 31.01.2011.

[39] Cole Parmer, Compact Pressure Transducer, http://www.coleparmer.com/catalog/product_view.asp?sku=6834740, last visited on 31.01.2011.

[40] Cole Parmer, Oakton Integral handle RTD probes, http://www.coleparmer.com/catalog/Product_view.asp?sku=0811780&pfx=KH&referred_id=2269, last visited on 31.01.2011.

[41] Cole Parmer, 30-gauge wire, http://www.coleparmer.co.uk/catalog/product_view.asp?sku=0854204&pfx=KH, last visited on 31.01.2011.

[42] Cole Parmer, 303 SS Flowmeters for Water, http://www.coleparmer.com/catalog/product_view.asp?sku=3220502, last visited on 31.01.2011.

[43] Cole Parmer, Cole Parmer® Wet/Wet Differential Pressure Transmitters, http://www.coleparmer.com/catalog/Product_view.asp?sku=6807156&pfx=KH&referred_id=2269, last visited on 31.01.2011.

[44] Egerate, MCH TECHNIC 305D-2 DC Power Supply, http://www.egerate-store.com/Default.aspx?_Args=ProductInfo,43&LNG=EN last visited on 31.01.2011.

[45] Agilent, 34970A Data Acquisition / Data Logger Switch Unit, http://www.home.agilent.com/agilent/product.jspx?cc=TR&lc=eng&ckey=1000001313:epsg:pro&nid=-33640.536881544.00&id=1000001313:epsg:pro, last visited on 31.01.2011.

[46] Thermo Electric, CNN-11300-TX Standard Connector Plug, www.thermo-electric.nl, last visited on 31.01.2011.

[47] Engineering Toolbox, Ethylene Glycol Heat-Transfer Fluid, http://www.engineeringtoolbox.com/ethylene-glycol-d_146.html, last visited on 31.01.2011.

[48] Kerpiççi, H., Personal communication.

[49] Industrial Insulation, Armaflex® Pipe Insulation, www.industrialinsulation.com, last visited on 31.01.2011.

[50] Morini, G., L., *Viscous heating in liquid flows in micro-channels*, Int. J. Heat and Mass Transfer, 2005, 48, pp. 3637-3647.

[51] Bejan, A., *Advanced Engineering Thermodynamics*, Wiley, New York, p. 239-263, 1988.

[52] Kakaç, S. and Liu, H., *Heat Exchangers: Selection, Rating, and Thermal Design*, CRC, Florida, 2002.

[53] Bertsch, S.S., Groll, E.A., Garimella, S.V., *A composite heat transfer correlation for saturated flow boiling in small channels*, International Journal of Heat and Mass Transfer, 2009, 52, pp. 2110-2118.

[54] Sonntag, R., E., Borgnakke, C., Van Wylen, G., J., Fundamentals of Thermodynamics, Wiley, 6th edition, Phoenix, 2003.

APPENDIX A

SPECIFICATIONS OF DEVICES IN THE EXPERIMENTAL SET-UP

A.1 REFRIGERATED CIRCULATING BATH

This bath is used for both cycles to condition the fluids inside [35].

Brand Name: Cole Parmer
Catalog Number: KH-13500-30

Bath Capacity	7 Liters
Temperature Range	-40 to 200℃
Temperature stability	±0.01℃
Temperature control	PID
Temperature setting	Digital
Temperature display	LED
Temperature sensor	100 Ω Pt RTD
Cooling capacity	800 W @ 20℃, 650 W @ 0℃, 500 W @ -10℃
Wattage: 2550 W total, 2000 W heater	
Pressure pump:	Max flow 15 L/min, Max head 5 psi
Compressor	1/2 hp
Refrigerant	R-404A
Bath opening	6 5/8" x 7 1/4”
Working depth	6"
Overall dimensions	26 5/8"W x 11 3/8"H x 18 7/8"D
Power Input	230 VAC, 50 Hz
Amperes	12 A

A.2 DIGITAL GEAR PUMP SYSTEM

This pump is used to circulate the refrigerant and to adjust the flow rate of the refrigerant [36].

Brand Name: Cole Parmer
Catalog Number: KH-74014-55

Wetted parts	Body: 316 SS
	Gears: PPS
	Seals: PTFE
Flow rate:	0.316 mL/rev
	18.96 mL/min at 60 rpm
	1137.6 mL/min at 3600 rpm
Differential pressure	75 psi (max)
Max system pressure	300 psi
Max temperature	40℃ (system)
Temperature range	-46 to 54℃
Port size	1/8" NPT(F)
Viscosity	0.2 to 1500 cp
Dimensions	7 3/4"L x 11 1/2"W x 7 1/4"H
Power VAC	220 VAC

A.3 MICRO-FLOWMETER

This micro-flowmeter is used to measure the mass flow rate. It is Coriolis type mass flowmeter [37].

Brand Name: Rheonik
Flowmeter Model: RHM 04 Universal Coriolis Mass Flowmeter with particular Fast Response

Pressure	up to 250 bar
Range	from 0.1 kg/min to 10 kg/min
Minimal flow	0.05 kg/min
Response time	30 ms and better
Flow Accuracy	0.10%
Repeatability	0.05%

Transmitter Model: RHE 08 Rheonik advanced transmitters

Version	Wall mounting
Analog Outputs	Two (0/4 - 20/22 mA)
Pulse/frequency	1 output - 2 inputs
Supply voltages	Available in all common
Multifunctions	density, brix, concentration
Power consumption	< 15 W
Temperature range	-40℃ to 60℃

A.4 GLASS TUBE

The glass tube was selected to be used in the test section in the first design [38], but was changed due to the reasons and complications mentioned in the “Preparation” and “Modifications” parts.

Brand Name: Cole Parmer
Catalog Number: KH-34742-00

Outside Diamter:	3.0 mm
Thickness:	0.6 mm
Material:	Borosilicate Glass
Softening point:	821ºC
Working point:	1252 ºC
Length:	48” (each piece)

A.5 COMPACT PRESSURE TRANSDUCER

Compact pressure transducers are used for both cycles to determine the pressure of the system [39].

Brand Name: Cole Parmer
Catalog Number: KH-68347-40

Output	4-20 mA
Process connection	1/4" NPT (M)
Range	200 psia
Accuracy	0.5% full scale
Power	8 to 30 VDC

A.6 RTD PROBE

RTDs are used in both cycles to determine the temperature at the specified locations from the fluids flowing inside the tubes [40].

Brand Name: Cole Parmer
Catalog Number: KH-08117-80

Temp range	-50 to 500℃
Probe length	2"
Diameter	0.093"
Time constant	10 seconds
Sheath material	316 SS

A.7 THERMOCOUPLE WIRE

Thermocouples are used to measure the temperature at the walls of the materials in which fluids flow [41].

Brand Name: Cole Parmer
Catalog Number: KH-08542-04

Length	1000 ft
Temp range	-200 TO 204℃
Error limit	±1.5% reading from -200 to -65℃;
	±1℃ from -65 to 130℃
	±0.75% reading from 130 to 350℃
Type	T
Advantages	Chemical, moisture and abrasion resistance
Gauge	30
ID	0.0100" (0.25 mm) dia
OD	0.030" x 0.048"
Model	T30-2-506

A.8 ROTAMETER

Rotameters are used to measure volumetric flow rate of water at two locations along the water cycle [42].

Brand Name: Cole Parmer
Catalog Number: EW-32205-02 (KH-32205-02)

Media	water
Max operating temperature	240℉ (115℃)
Max pressure	6000 psi
Flow rate	water 0.2 to 1.8 LPM;
Accuracy	±2% full-scale
Connections	1/4" NPT(F)
Repeatability	±1.0%
Housing Material	304 Stainless Steel
Dimensions	1 3/4” W x 4 13/16” H x 1 15/16” D

A.9 DIFFERENTIAL PRESSURE TRANSDUCER

Differential pressure transducer reads the pressure drop at the test section for the refrigerant flow [43].

Brand Name: Cole Parmer
Catalog Number: KH-68071-56

Dimensions	3"L x 2 1/8"W x 3"H
Output	4 to 20 mA
Operating temperature	0 to 175℉ (-17 to 80℃)
Process connection	1/4" NPT(F)
Range	0 to 5.0 psid
Accuracy	±0.25% full scale
Power	11 to 30 VDC (unregulated)

A.10 DC POWER SUPPLY

DC power supply is used to power the pressure transducers [44].

Brand Name: MCH Technic
Catalog Number: MCH 305D-2 DC Power Supply

Voltage:	0-30V Adjustable	
Current:	0-5A Adjustable	
Dual-Output DC Power Source	Two Independent:	30V-5A
	With Serial Button:	60V-5A
	With Parallel Button:	30V-10A

Voltage	0 to Descripted Continuously Variable	
	Stability	Voltage: ≤0.01%+2mV
	Load:	≤0.0%+2mV
	Recover Time	≤100μS
	Ripple & Noise	≤1MVRMS（efficent）
	Temperature Factor	≤300PPM/ºC

Current	0 to Descripted Continuously Variable	
	Current, Load Stability	≤0.2%+3mA
	Ripple & Noise	≤3mArms

Working Condition

Line Power Supply	220V±10% 50/60Hz
Operating Temperature:	-10ºC to 40ºC Moisture≤90%
Storage Temperature:	-20ºC to 80ºC Moisture≤80%

A.11 DATA ACQUISITION SYSTEM

Data acquisition system is used to gather the pressure and temperature readings from pressure transducers, RTDs, and thermocouples and transfer them to the computer interface [45].

Brand Name: Agilent
Catalog Number: 34970A Data Acquisition / Switch Unit

Slot	3
Interface	GPIB and RS232
Multimeter	Digital and internal with 6 1/2-digit (22-bit)
Scanning	up to 250 channels per second
Modules	8 switch and control plug-in
Memory	50k readings
Alarm	Hi/Lo on each channel
Measurement	Thermocouples, RTDs and thermistors, ac/dc volts and current; resistance; frequency and period
Software	Free Bench Link data logger software enables tests without programming

Brand Name: Agilent
Catalog Number: 34901A 20-Channel Multiplexer + 2 Current Channels Module
(Built-in thermocouple reference junction)

Model description	34901A 20 ch Multiplexer+ 2 current channels
Type	2-wire armature (4-wire selectable)
Speed(ch/sec)	60
Max volts	300 V
Max amps	1 A

APPENDIX B

SKETCH OF EXPERIMENTAL SET-UP IN THE PRELIMINARY DESIGN

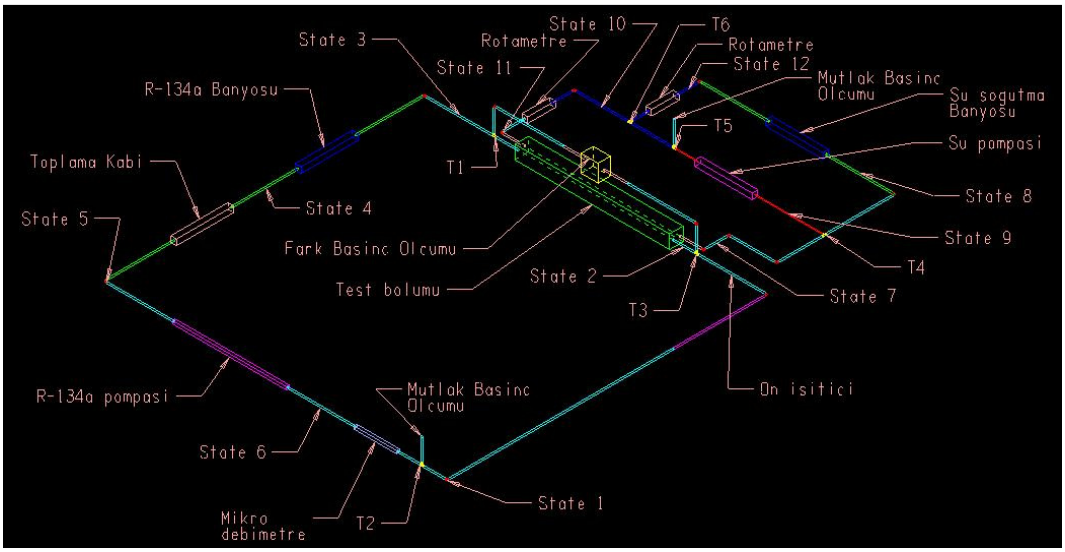

Figure B.1: Sketch of the experimental set-up in the preliminary design

APPENDIX C

CONNECTIONS OF THE EXPERIMENTAL SET-UP IN THE PRELIMINARY DESIGN

Table C.1: The necessary pipes for the set-up connections

Pipe (diameter)	**Length (mm)**
1/8" pipe	350
1/4" pipe	5800
1/4" tube	2000

Table C.2: Elbows and T-connections

Elbow and T-Connections	**#**
1/4" NPT (M) pipe (1000 mm)	1
1/4" NPT (F) * 1/4" tube elbow	4
1/4" NPT (F) * 1/4" NPT (F) elbow	7
(2) 1/4" NPT (F) * (1) 1/4" NPT (M) T-connection	1
(3) 1/4" NPT (F) T-connection	3
(2) 1/4" NPT (F) * (1) 1/8" NPT (F) T-connection	1
(1) 1/4" NPT (F) * (1) 1/4" NPT (M) * (1) 1/8" NPT (F) T-connection	1

Table C.3: Refrigerant (R-134a) cycle connectors and pipes

Location	**Material**
T1_3	1/4" NPT (M) pipe (300 mm)
3	1/4" NPT (F) * 1/4" tube elbow
3_bath	1/4" tube (300 mm)
4	1/4" tube (300 mm)
4_5	1/4" tube (300 mm)
5	1/4" NPT (F) * 1/4" tube elbow
5_6	1/4" NPT (M) pipe (300 mm)
6	1/4" NPT (M) pipe (300 mm)
6_T2	1/4" NPT (M) pipe (100 mm)
T2	(2) 1/4" NPT (F) * (1) 1/4" NPT (M) T-connection
T2-P	1/4" NPT (F) pipe (100 mm)
T2_1	1/4" NPT (M) pipe (100 mm)
1	1/4" NPT (F) * 1/4" NPT (F) elbow
pipe (1_2)	1/4" NPT (M) pipe (1000 mm)
elbow (1_2)	1/4" NPT (F) * 1/4" NPT (F) elbow
elbow_2	1/4" NPT (M) pipe (300 mm)
T3	(3) 1/4" NPT (F) T-connection
T3_elbow (DPT inlet)	1/4" NPT (M) pipe (100 mm)
elbow (DPT inlet)	1/4" NPT (F) * 1/4" NPT (F) elbow
DPT inlet_DPT	1/4" NPT (M) pipe (300 mm)
DPT_DPT exit	1/4" NPT (M) pipe (300 mm)
elbow (DPT exit)	1/4" NPT (F) * 1/4" NPT (F) elbow
elbow_T1	1/4" NPT (M) pipe (300 mm)
T1	(3) 1/4" NPT (F) T-bağlantısı
test_T1	1/4" NPT (M) pipe (100 mm)
T2_test	1/4" NPT (M) pipe (100 mm)

Table C.4: Water cycle connectors and pipes

Location	**Material**
test_7	1/4" NPT (M) pipe (100 mm)
7	1/4" NPT (F) * 1/4" NPT (F) elbow
7_9 pipe	1/4" NPT (M) pipe (200 mm)
7_9 elbow	1/4" NPT (F) * 1/4" NPT (F) elbow
7_9 pipe2	1/4" NPT (M) pipe (200 mm)
9 (T4)	(2) 1/4" NPT (F) * (1) 1/8" NPT (F) T-connection
9_8	1/4" NPT (M) pipe (300 mm)
8	1/4" NPT (F) * 1/4" tube elbow
8_bath	1/4" tube (300 mm)
bath_12	1/4" tube (300 mm)
12	1/4" NPT (F) * 1/4" tube elbow
12_rotameter	1/4" NPT (M) pipe (300 mm)
rotameter_10	1/4" NPT (M) pipe (300 mm)
9_pump	1/8" NPT (M) pipe (300 mm)
pump_T5	1/8" NPT (M) pipe (100 mm)
T5	(2) 1/4" NPT (F) * (1) 1/8" NPT (F) T-connection
T5_P	1/4" NPT (M) pipe (100 mm)
T5_10 (T6)	1/4" NPT (M) pipe (100 mm)
10	(3) 1/4" NPT (F) T-connection
10_elbow	1/4" NPT (M) pipe (300 mm)
Elbow	1/4" NPT (F) * 1/4" NPT (F) elbow
elbow_rotameter	1/4" NPT (M) pipe (100 mm)
rotameter_11	1/4" NPT (M) pipe (100 mm)
11_test	1/4" NPT (M) pipe (100 mm)

APPENDIX D

TECHNICAL DRAWINGS OF THE PARTS IN THE TEST SECTION

D.1 TECHNICAL DRAWING OF THE FLANGE

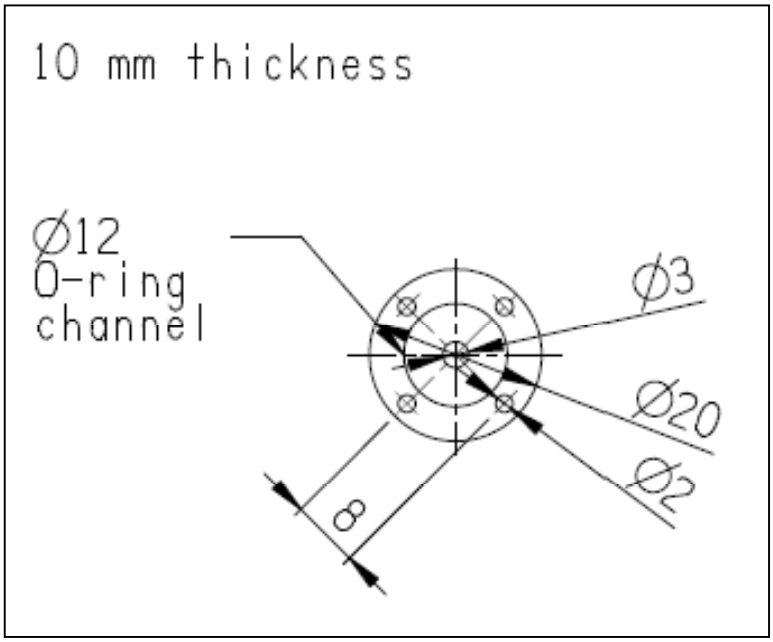

Figure D.1: Technical drawing of the flange

D.2 TECHNICAL DRAWING OF THE SHELL

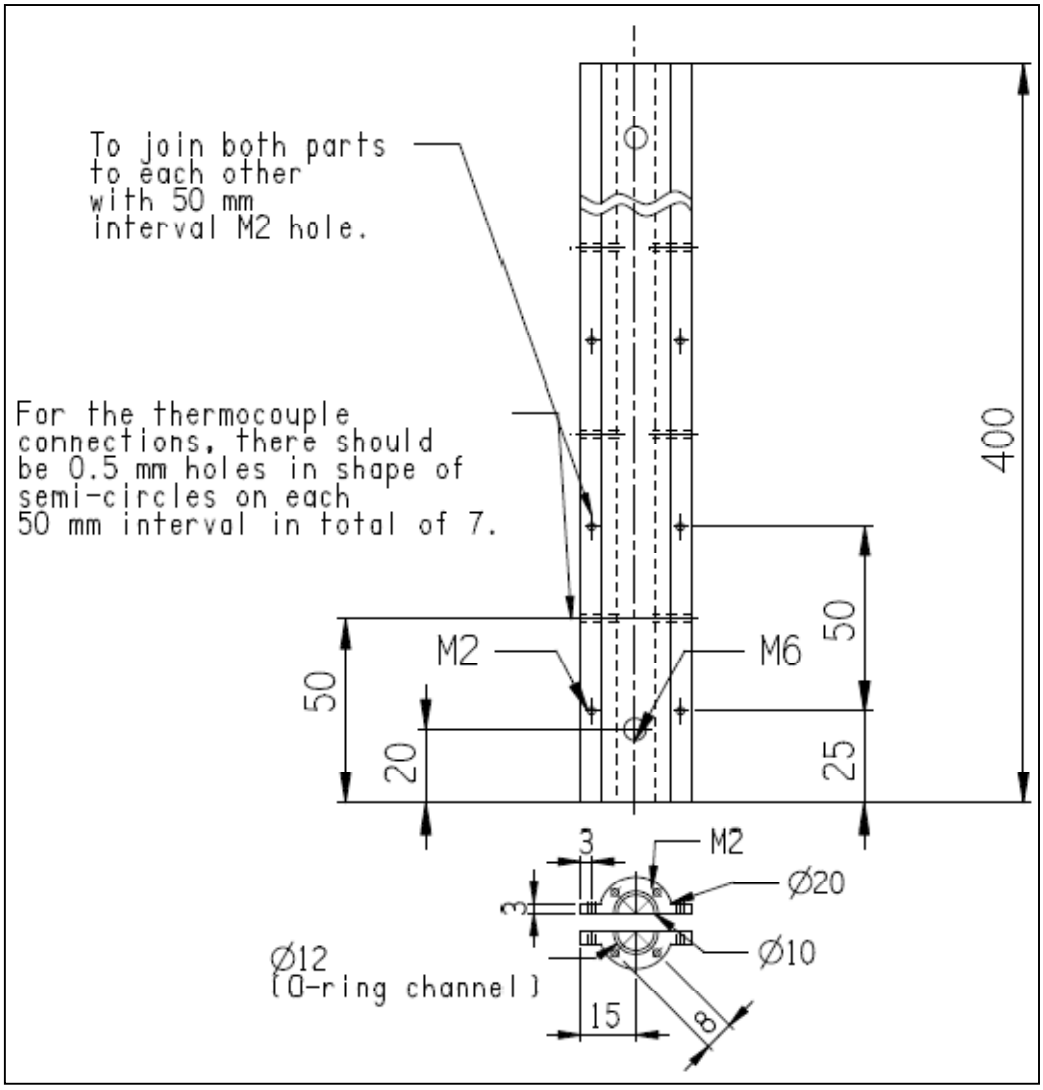

Figure D.2: Technical drawing of the shell

D.3 TECHNICAL DRAWINGS OF THE RING AND THE BUMPER

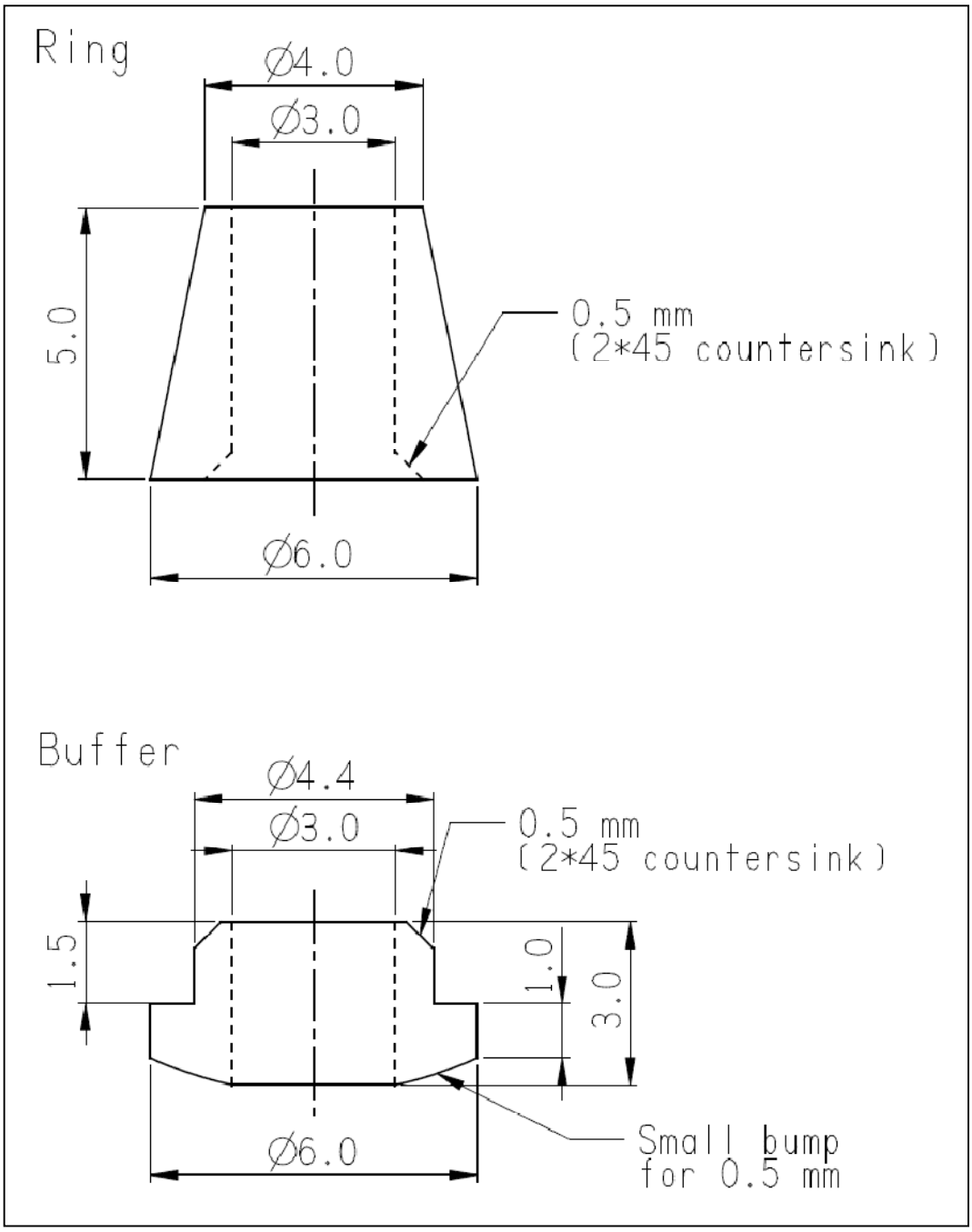

Figure D.3: Technical drawings of the ring and the bumper

APPENDIX E

THE CALIBRATION TABLES AND GRAPHS FOR MEASUREMENT DEVICES

E.1 A SAMPLE CALIBRATION CURVE FOR A CALIBRATED RTD

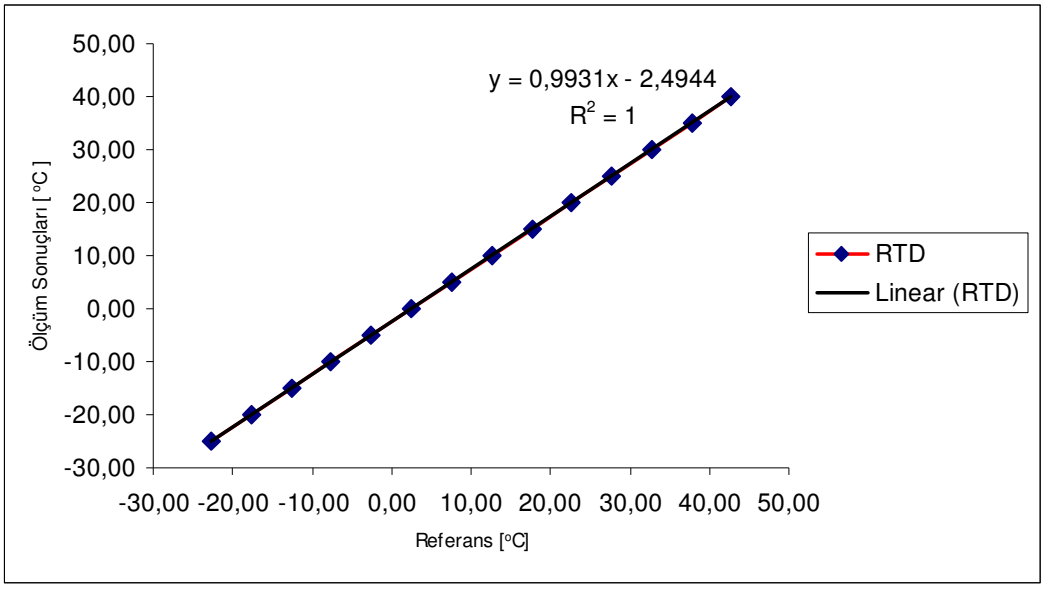

Figure E.1: A sample calibration curve for an RTD

E.2 THE CALIBRATION RESULTS FOR THE CPTS

Table E.1: The calibration results for the compact pressure transducers

PSI	221	222	PSI	221	222	PSI	221 (A)	222 (A)
0-200 psi çıkış			0-200 psi iniş			0-200 psi ortalama		
0	0,003983	0,003985	0	0,003982	0,003989	0	0,003983	0,003987
1	0,004064	0,004063	1	0,004061	0,004065	1	0,004063	0,004064
2	0,004137	0,004136	2	0,00414	0,004143	2	0,004138	0,00414
3	0,004212	0,004214	3	0,004216	0,004217	3	0,004214	0,004215
4	0,004291	0,004295	4	0,004298	0,004299	4	0,004295	0,004297
5	0,004366	0,00437	5	0,004376	0,004377	5	0,004371	0,004373
6	0,004445	0,004448	6	0,004453	0,004454	6	0,004449	0,004451
7	0,004524	0,004526	7	0,00453	0,00453	7	0,004527	0,004528
8	0,004601	0,004602	8	0,004606	0,004607	8	0,004603	0,004604
9	0,00468	0,00468	9	0,004683	0,004684	9	0,004681	0,004682
10	0,004759	0,004758	10	0,004764	0,004761	10	0,004761	0,00476
11	0,004838	0,004837	11	0,004841	0,004842	11	0,004839	0,00484
12	0,004917	0,004915	12	0,004918	0,004917	12	0,004917	0,004916
13	0,004997	0,004994	13	0,004996	0,004995	13	0,004997	0,004994
14	0,005078	0,005073	14	0,005078	0,005076	14	0,005078	0,005074
15	0,005152	0,005147	15	0,005156	0,005152	15	0,005154	0,00515
20	0,005543	0,005536	20	0,005551	0,005545	20	0,005547	0,00554
40	0,007121	0,007114	40	0,007133	0,007124	40	0,007127	0,007119
60	0,008742	0,008733	60	0,008706	0,008695	60	0,008724	0,008714
80	0,010273	0,01026	80	0,010282	0,010268	80	0,010277	0,010264
100	0,011859	0,011846	100	0,011862	0,011847	100	0,011861	0,011846
120	0,013432	0,013416	120	0,013435	0,013417	120	0,013433	0,013417
140	0,01502	0,015001	140	0,015017	0,014993	140	0,015018	0,014997
160	0,016588	0,016564	160	0,016597	0,016574	160	0,016592	0,016569
180	0,018162	0,018146	180	0,018169	0,018148	180	0,018165	0,018147
200	0,019752	0,019717	200	0,019747	0,019723	200	0,019749	0,01972

E.3 THE CALIBRATION CURVE FOR THE CPT 1

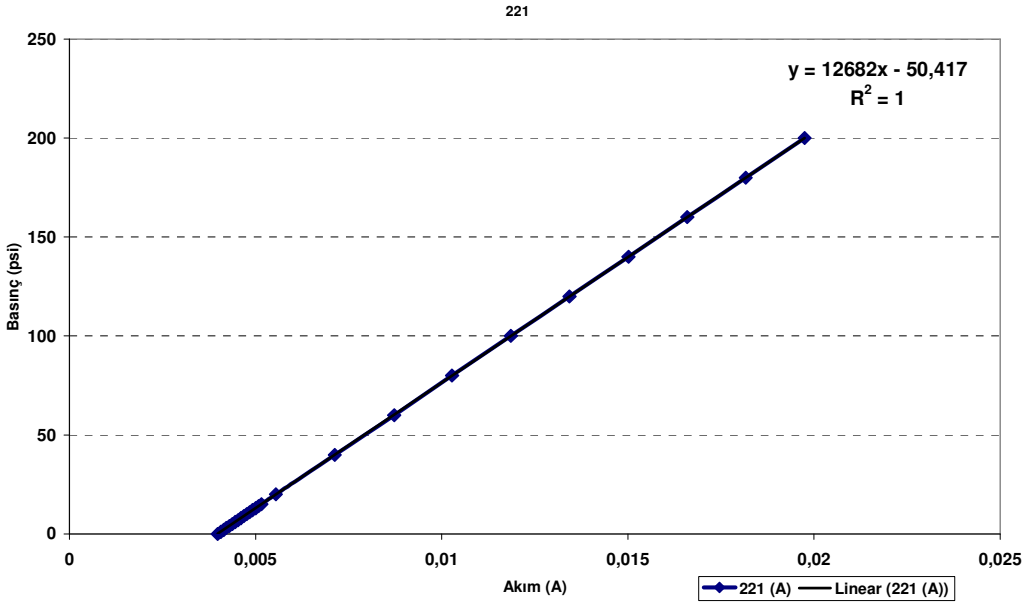

Figure E.2: The calibration curve for the compact pressure transducer 1

E.4: THE CALIBRATION CURVE FOR THE CPT 2

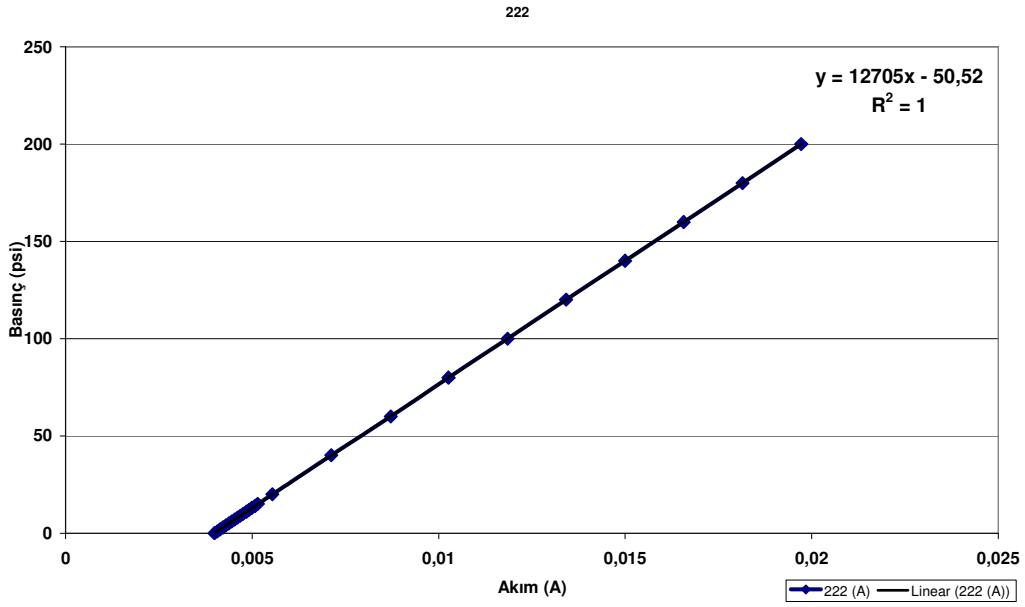

Figure E.3: The calibration curve for the compact pressure transducer 2

E.5 THE CALIBRATION RESULTS FOR THE DPT

Table E.2: The calibration results for the differential pressure transducer

bar	A
0	0,004069
0,02	0,00503
0,04	0,005966
0,06	0,006871
0,08	0,007818
0,1	0,008794
0,12	0,009678
0,14	0,01061
0,16	0,011569
0,18	0,012514
0,2	0,013423
0,22	0,014318
0,24	0,015271
0,26	0,016219
0,28	0,017132
0,3	0,018052
0,32	0,019025
0,34	0,019949

E.6 THE CALIBRATION CURVE FOR THE DPT

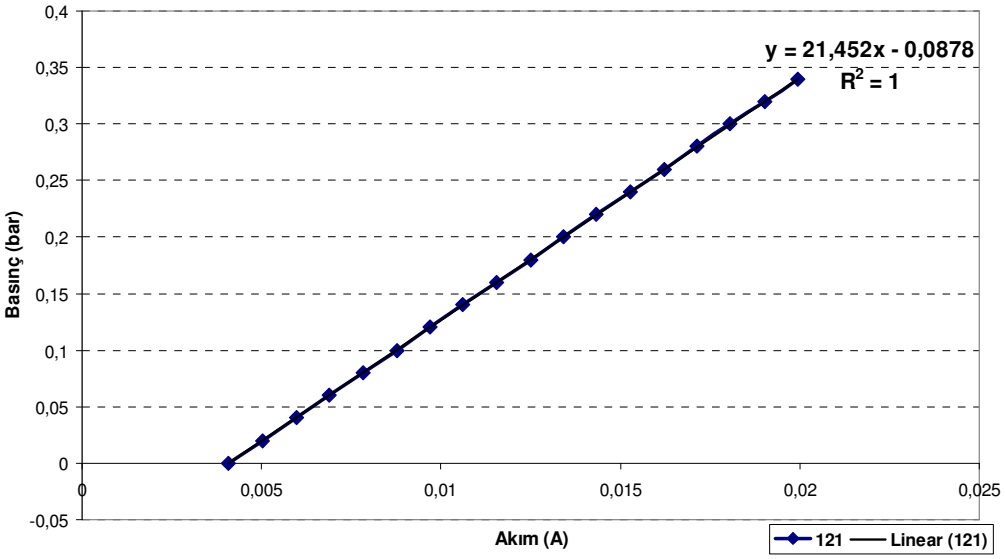

Figure E.4: The calibration curve for the differential pressure transducer

APPENDIX F

WATER-ETHYLENE GLYCOL 1:1 VOLUMETRIC MIXTURE PROPERTIES

F.1: SPECIFIC GRAVITY OF THE MIXTURE

Table F.1: Specific gravity dependence on temperature for the water – ethylene glycol mixture

Temperature (℃)	Specific Gravity -
-17.8	1.1
4.4	1.088
26.7	1.077
48.9	1.064

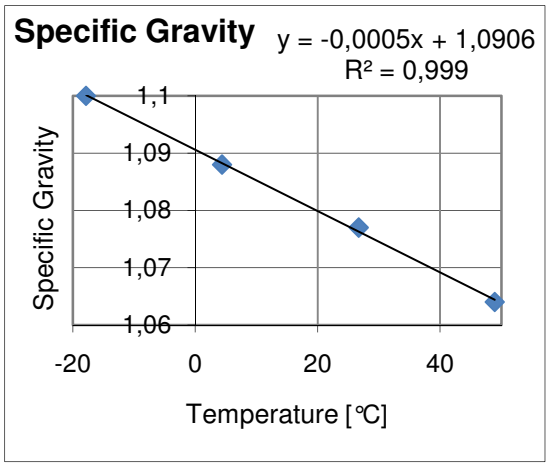

Figure F.1: Specific gravity versus temperature for the water – ethylene glycol mixture

F.2 SPECIFIC HEAT OF THE MIXTURE

Table F.2: Specific heat dependence on temperature for the water – ethylene glycol mixture

Temperature (℃)	Specific Heat (J/kgK)
-17.8	3265.704
4.4	3328.506
26.7	3412.242
48.9	3483.4176

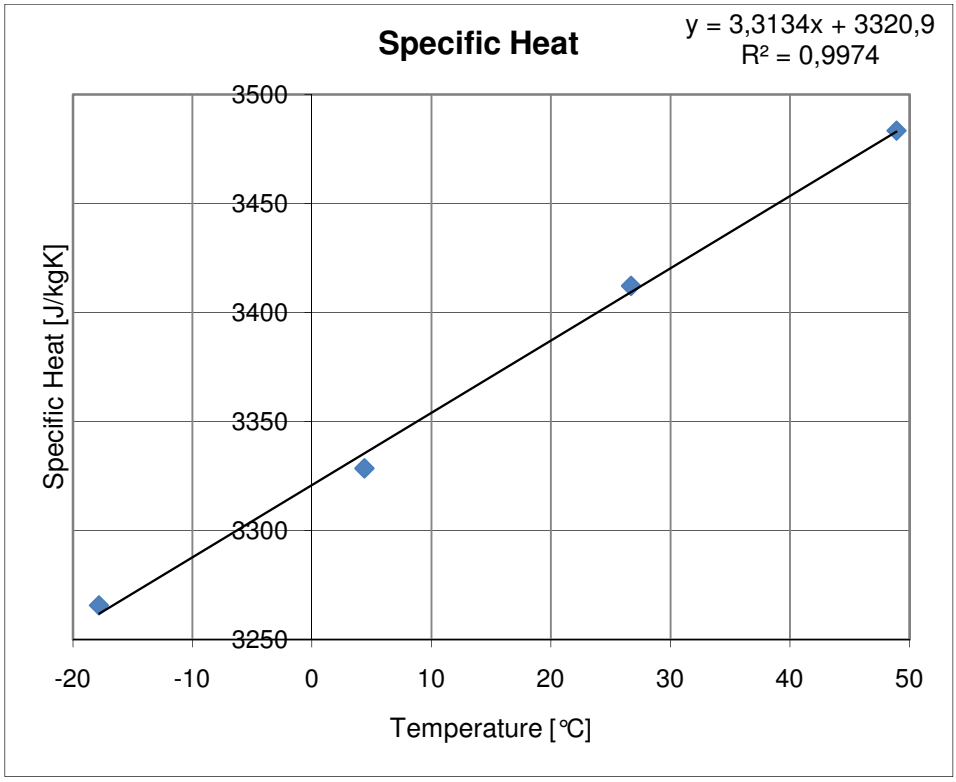

Figure F.2: Specific heat versus temperature for the water – ethylene glycol mixture

F.3 DYNAMIC VISCOSITY OF THE MIXTURE

Table F.3: Dynamic viscosity dependence on temperature for the water – ethylene glycol mixture

Temperature (℃)	Dynamic Viscosity (kg/ms)
-17.8	22
4.4	6.5
26.7	2.8
48.9	1.5

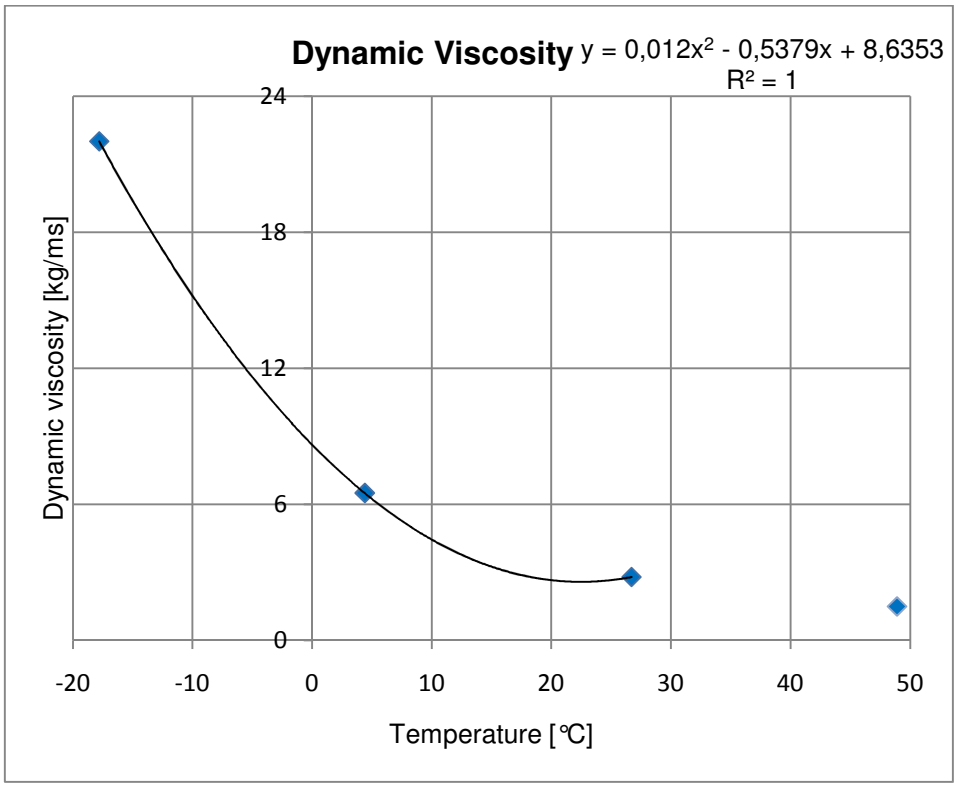

Figure F.3: Dynamic viscosity versus temperature for the water – ethylene glycol mixture

F.4 CONDUCTIVITY OF THE MIXTURE

Table F.4: Conductivity dependence on temperature for the water – ethylene glycol mixture

Temperature (℃)	Conductivity (W/mK)
-35	0.41
40	0.4
70	0.395

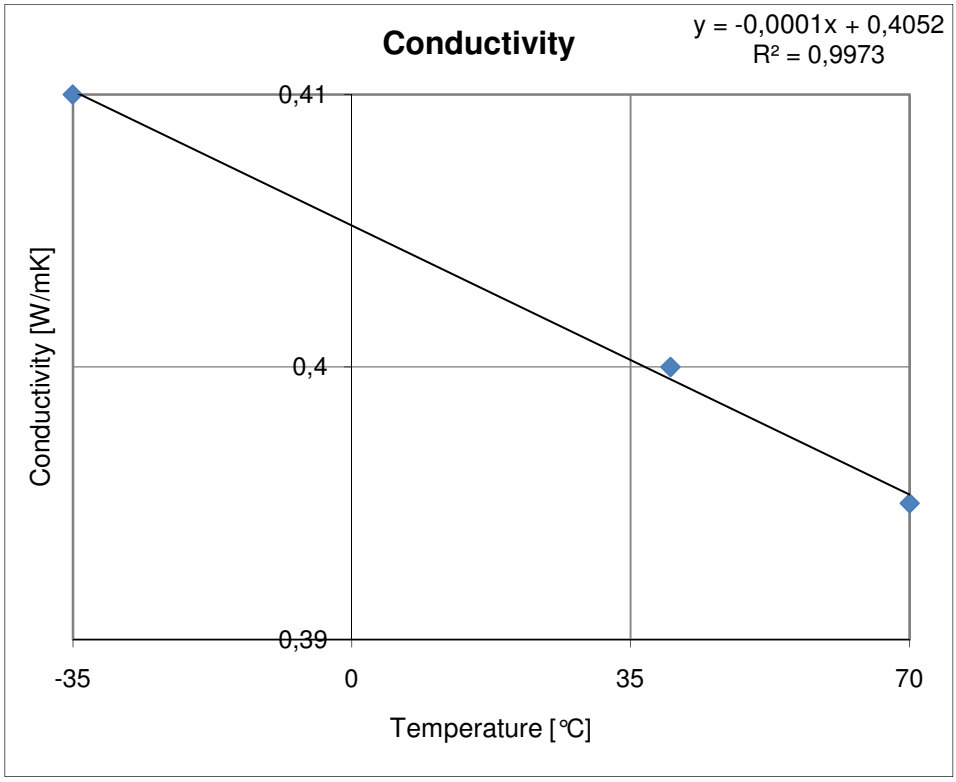

Figure F.4: Conductivity versus temperature for the water – ethylene glycol mixture

APPENDIX G

THE REFRIGERANT (R-134A) PROPERTIES

G.1 VISCOSITY (LIQUID) OF THE REFRIGERANT

Table G.1: Viscosity (liquid) dependence on saturation pressure for R-134a

Saturation pressure (bar)	Viscosity (liquid) (Pa.s)
0.728	0.000425
1.159	0.00037
1.765	0.000325
2.607	0.000288
3.721	0.000256
5.175	0.00023
7.02	0.000208
9.33	0.000189
12.16	0.000172
15.59	0.000158
19.71	0.000145

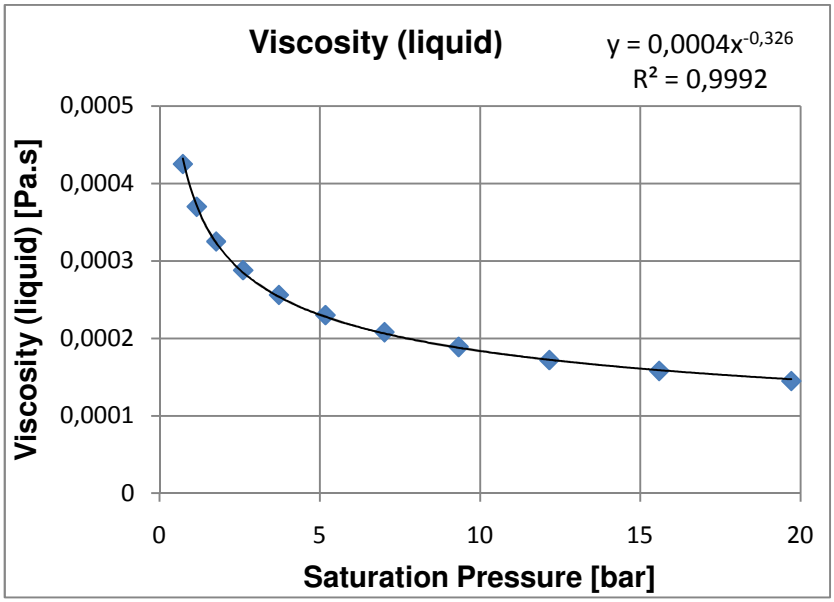

Figure G.1: Viscosity (liquid) versus saturation pressure for R-134a

G.2 VISCOSITY (VAPOR) OF THE REFRIGERANT

Table G.2: Viscosity (vapor) dependence on saturation pressure for R-134a

Saturation pressure (bar)	Viscosity (gas) (Pa.s)
0.728	0.0000095
1.159	0.0000099
1.765	0.0000104
2.607	0.0000108
3.721	0.0000112
5.175	0.0000117
7.02	0.0000121
9.33	0.0000125
12.16	0.0000129
15.59	0.0000133
19.71	0.0000137

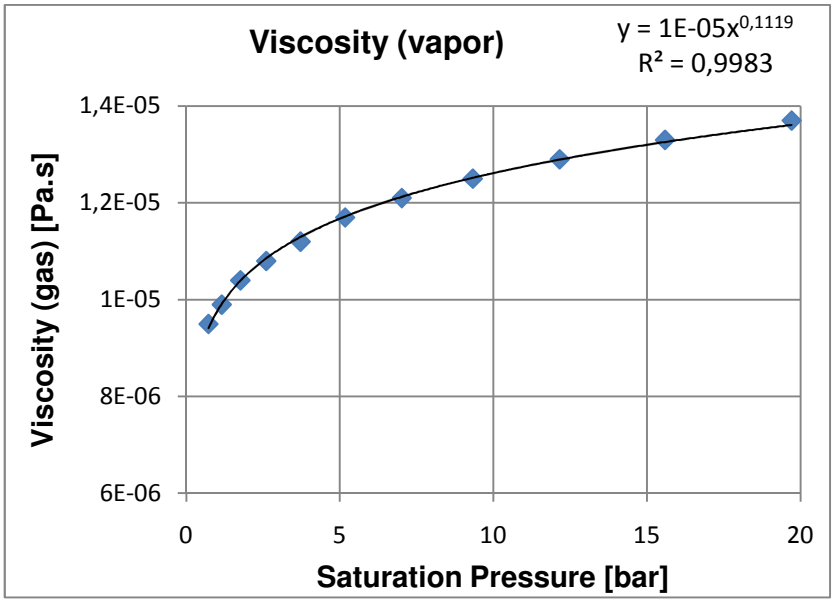

Figure G.2: Viscosity (vapor) versus saturation pressure for R-134a

G.3 CONDUCTIVITY (LIQUID) OF THE REFRIGERANT

Table G.3: Conductivity (liquid) dependence on saturation pressure for R-134a

Saturation pressure (bar)	Conductivity (liquid) (W(mK)
0.728	0.099
1.159	0.095
1.765	0.091
2.607	0.087
3.721	0.083
5.175	0.079
7.02	0.075
9.33	0.071
12.16	0.068
15.59	0.064
19.71	0.06

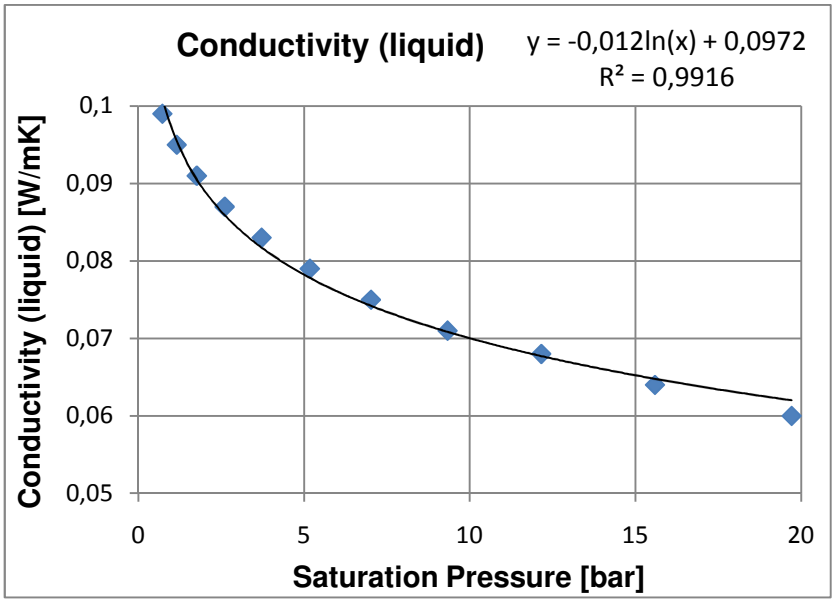

Figure G.3: Conductivity (liquid) versus saturation pressure for R-134a

G.4 CONDUCTIVITY (VAPOR) OF THE REFRIGERANT

Table G.4: Conductivity (vapor) dependence on saturation pressure for R-134a

Saturation pressure (bar)	Conductivity (gas) (W/mK)
0.728	0.008
1.159	0.008
1.765	0.008
2.607	0.009
3.721	0.009
5.175	0.01
7.02	0.01
9.33	0.01
12.16	0.011
15.59	0.011
19.71	0.012

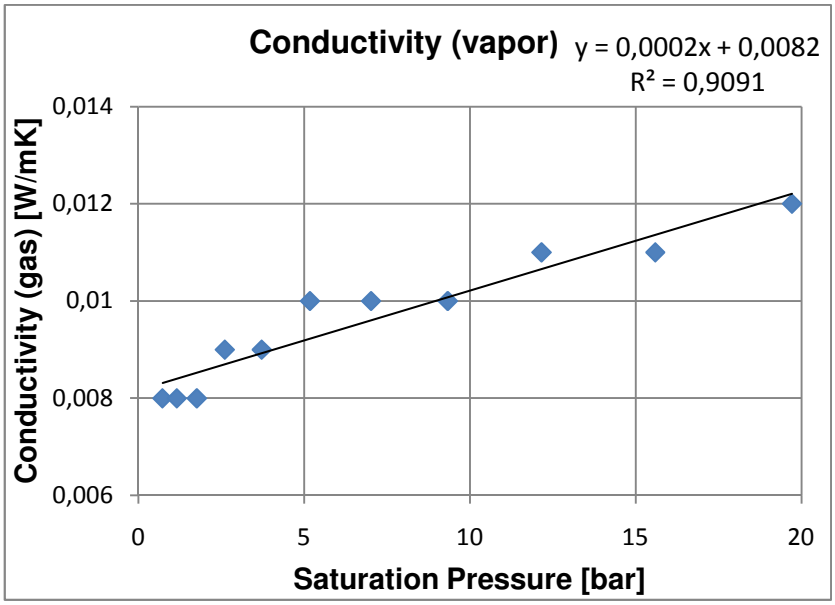

Figure G.4: Conductivity (vapor) versus saturation pressure for R-134a

G.5 PRANDTL NUMBER (LIQUID) OF THE REFRIGERANT

Table G.5: Pr (liquid) dependence on saturation pressure for R-134a

Saturation pressure (bar)	Pr (liquid) -
0.728	4.99
1.159	4.72
1.765	4.49
2.607	4.31
3.721	4.17
5.175	4.07
7.02	4.00
9.33	3.98

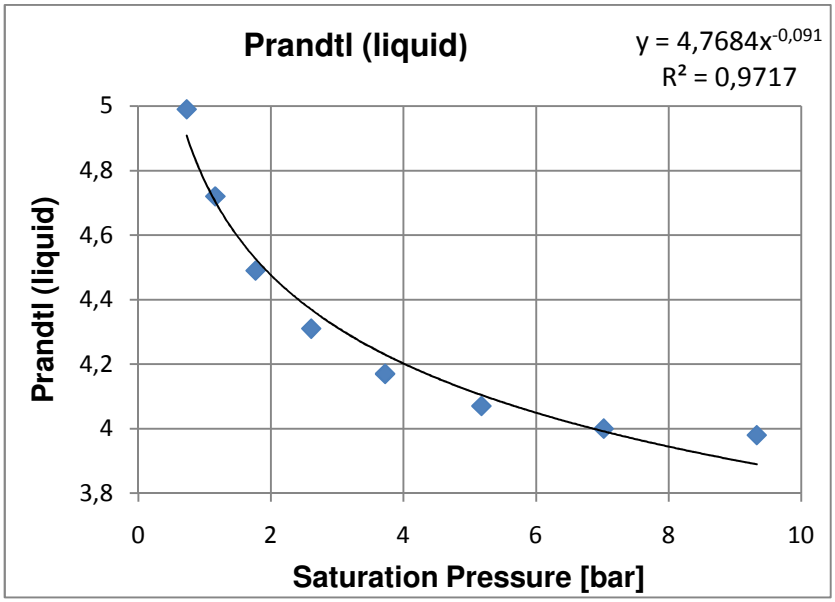

Figure G.5: Pr (liquid) versus saturation pressure for R-134a

G.6 PRANDTL NUMBER (VAPOR) OF THE REFRIGERANT

Table G.6: Pr (vapor) dependence on saturation pressure for R-134a

Saturation pressure	Pr (gas)
(bar)	-
0.728	0.9
1.159	0.96
1.765	1.02
2.607	1.08
3.721	1.14
5.175	1.2
7.02	1.27
9.33	1.34
12.16	1.57
15.59	1.44
19.71	1.74

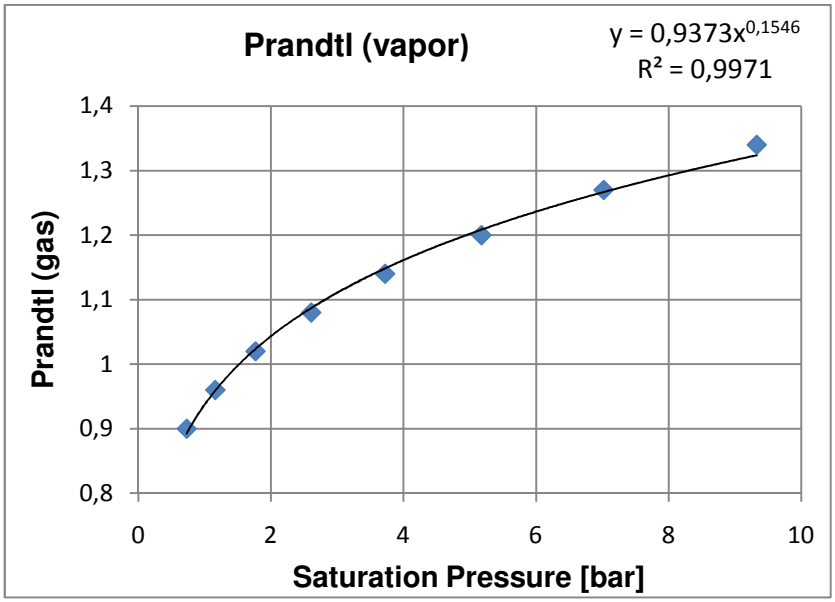

Figure G.6: Pr (vapor) versus saturation pressure for R-134a

G.7 SURFACE TENSION OF THE REFRIGERANT

Table G.7: Surface tension dependence on saturation pressure for R-134a

Saturation pressure (bar)	Surface tension (N/m)
1.159	0.0145
1.765	0.0131
2.607	0.0117
3.721	0.0103
5.175	0.009

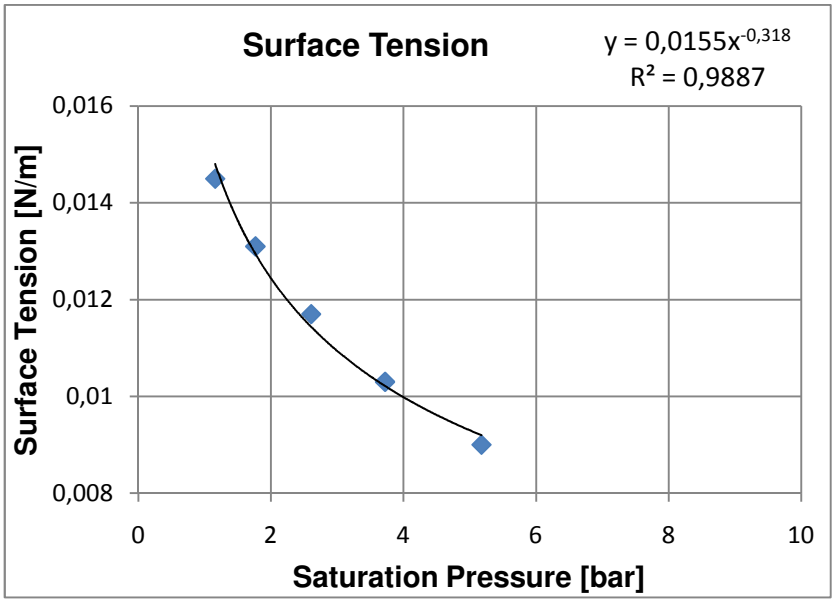

Figure G.7: Surface tension versus saturation pressure for R-134a

G.8 SPECIFIC HEAT (LIQUID) OF THE REFRIGERANT

Table G.8: Specific heat (liquid) dependence on saturation pressure for R-134a

Saturation pressure (bar)	Specific heat (liquid) (J/kgK)
0.728	1162
1.159	1212
1.765	1259
2.607	1306
3.721	1351
5.175	1397
7.02	1446
9.33	1497
12.16	1559
15.59	1638
19.71	1750

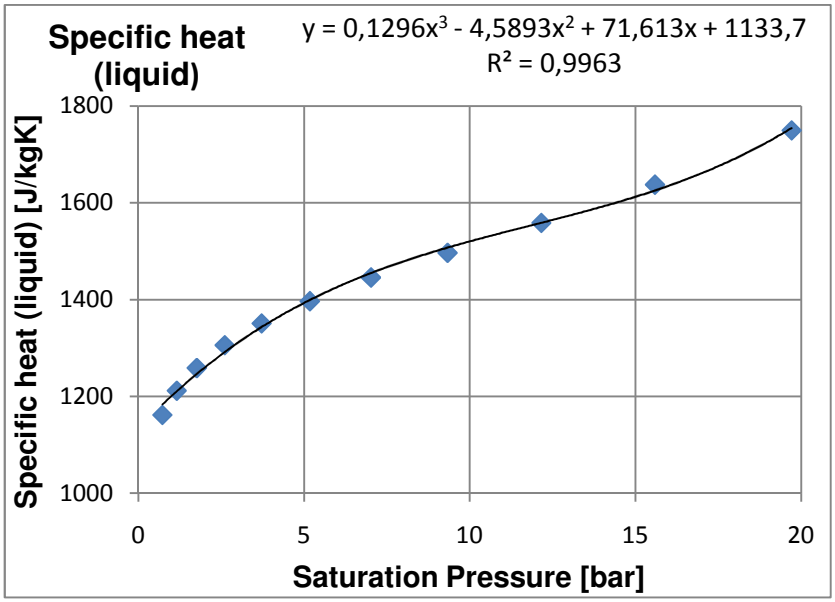

Figure G.8: Specific heat (liquid) versus saturation pressure for R-134a

APPENDIX H

THE RESULTS FOR A SAMPLE TWO-PHASE EXPERIMENT

H.1 THE GEOMETRY OF BOTH SIDES

Table H.1: The geometries of both sides

Refrigerant side geometry			**Water side geometry**		
Inner diameter	mm	1.65	Inner diameter	mm	3.175
Outer diameter	mm	3.175	Outer diameter	mm	10
Inner perimeter	mm	5.18	Inner perimeter	mm	9.97
Cross sectional area	mm^2	2.14	Outer perimeter	mm	31.42
Test length	mm	400	Cross sectional area	mm^2	70.62
Heat transfer area	mm^2	2073.45	Hydraulic diameter	mm	6.83
			Equivalent diameter	mm	28.32

H.2 TEST CONDITIONS FOR THE EXPERIMENT

Table H.2: Test conditions for the experiment

Refrigerant mass flow rate	g/s	0.505
Refrigerant inlet pressure	bar	7.32
Refrigerant flowmeter	℃	16.96
Refrigerant inlet temperature	℃	28.61
Refrigerant exit temperature	℃	28.09
Refrigerant Pressure drop	bar	0.05
Water inlet temperature	℃	33.83
Water exit temperature	℃	33.70
Water volumetric flow rate	l/min	1.65
Water mass flow rate	kg/s	0.030
Water mass flow rate	g/s	29.53
Test inlet wall temperature	℃	30.55
Test exit wall temperature	℃	30.71
Pre-heater power input	W	28.30
Pre-heater net power	W	24.05
Viscous Heating	W	9.06
Net heat transfer rate	W	22.24

H.3 REFRIGERANT EXPERIMENT STATES

Table H.3: Refrigerant experiment states

Flowmeter State (Pre-heater inlet)		
Refrigerant pressure	bar	7.32
Refrigerant temperature	℃	16.96
Refrigerant quality (%)	-	-
Refrigerant enthalpy (kJ/kg)	kJ/kg	223.23
Test Inlet (Pre-heater exit)		
Refrigerant pressure	bar	7.32
Refrigerant temperature	℃	28.24
Refrigerant quality (%)	-	18.09
Refrigerant enthalpy (kJ/kg)	kJ/kg	270.81
Test Exit		
Refrigerant pressure	bar	7.27
Refrigerant temperature	℃	28.02
Refrigerant quality (%)	-	43.40
Refrigerant enthalpy (kJ/kg)	kJ/kg	314.81

H.4 WATER SIDE PROPERTIES

Table H.4: Water side properties

Velocity	m/s	0.3894
Density	kg/m^3	1073.72
Viscosity	Pa.s	0.0042
Reynolds	-	687
Specific heat	J/kgK	3432.78
Conductivity	W/mK	0.402
Pr	-	35.49
Average temperature	℃	33.77
Mass flow rate	kg/s	0.0295

H.5 REFRIGERANT EXPERIMENTAL CALCULATIONS

Table H.5: Refrigerant experimental calculations

Net heat transfer rate	W	22.24
Heat flux	W/m^2	10726.16
Mass flux	kg/m^2s	236.40
Water average temperature	℃	33.77
Wall average temperature	℃	30.63
Water - wall temp. difference	℃	3.14
Refrigerant inlet temperature	℃	28.24
Refrigerant exit temperature	℃	28.02
Temp. Diff. Inlet	℃	-2.39
Temp. Diff. Exit	℃	-2.61
Log. Mean Temp. Diff.	℃	-2.50
U	W/m^2K	4293.24
h	W/m^2K	4318.26
Refrigerant average temp.	℃	28.13
Refrigerant saturation pres.	bar	7.30
Average quality (%)	-	30.75

H.6 CALCULATIONS OF THE CORRELATIONS IN THE LITERATURE

Table H.6: Calculations of correlations in the literature

CHEN					
ρ_{liquid}	kg/m³	1230.78	Mass flow rate	kg/s	5.05E-04
ρ_{vapor}	kg/m³	26.08	μ	Pa.s	1.52E-04
μ_{liquid}	Pa.s	2.091E-04	Refrigerant Re	-	2624
μ_{vapor}	Pa.s	1.249E-05	Re_{liquid}	-	1865
Xtt	-	0.45	$Re_{two\text{-}phase}$	-	8511
1/Xtt	-	2.22	Pe_{liquid}	-	7420.77
F	-	4.52	Pe_{liquid}*d/L	-	30.61
F_o	-	3.13	$h_{liquid\ only}$	W/m²K	163.59
k_{liquid}	W/mK	0.0737	$h_{convective\ boiling}$	W/m²K	511.89
k_{vapor}	W/mK	0.0097	θ_B	K	2.50
Pr_{liquid}	-	3.98	ΔP_v	J/m³	39809.22
Pr_{vapor}	-	1.27	S	-	0.91
σ	N/m	0.0077	$h_{vapor\ only}$	W/m²K	2398.88
$c_{p,liquid}$	J/kgK	1462.25	h	W/m²K	2910.77
GÜNGÖR			**BERTSCH**		
Re_{liquid}	-	1292	$h_{nucleate\ boiling}$	W/m²K	4088.31
E	-	5.28	Re_{liquid}	-	1865
h_{liquid}	W/m²K	163.59	Re_{vapor}	-	31228
S	-	0.88	$h_{convection,\ liquid}$	W/m²K	251.54
h_p	W/m²K	4088.34	$h_{convection,\ vapor}$	W/m²K	78.75
h_{TP}	W/m²K	4449.99	$h_{convection,\ boiling}$	W/m²K	198.41
			Co	-	0.491
			h	W/m²K	4137.56

H.7 EXPERIMENTAL RESULTS AND RESULTS OF THE CORRELATIONS IN LITERATURE

Table H.7: Experimental results and the results of the correlations in literature

Refrigerant mass flow rate	g/s	0.51
Mass flux	kg/m²s	236.40
Average quality (%)	-	30.75
h_{exp}	W/m²K	4318.26
$h_{Güngör}$	W/m²K	4449.99
$h_{Bertsch}$	W/m²K	4137.56
h_{Chen}	W/m²K	2910.769
Refrigerant pressure drop	bar	0.05